FINAL REPORT

Non-Leaching, Benign Antifouling Multilayer Polymer Coatings for Marine Applications

SERDP Project WP-1454

MARCH 2010

Christopher K. Ober
Cornell University

SERDP
DOD ▪ EPA ▪ DOE

Report Documentation Page

Form Approved
OMB No. 0704-0188

1. REPORT DATE	2. REPORT TYPE	3. DATES COVERED
MAR 2010	**N/A**	**-**

4. TITLE AND SUBTITLE
Non-Leaching, Benign Antifouling Multilayer Polymer Coatings for Marine Applications

5a. CONTRACT NUMBER
5b. GRANT NUMBER
5c. PROGRAM ELEMENT NUMBER

6. AUTHOR(S)

5d. PROJECT NUMBER
5e. TASK NUMBER
5f. WORK UNIT NUMBER

7. PERFORMING ORGANIZATION NAME(S) AND ADDRESS(ES)
Cornell University

8. PERFORMING ORGANIZATION REPORT NUMBER

9. SPONSORING/MONITORING AGENCY NAME(S) AND ADDRESS(ES)

10. SPONSOR/MONITOR'S ACRONYM(S)
11. SPONSOR/MONITOR'S REPORT NUMBER(S)

12. DISTRIBUTION/AVAILABILITY STATEMENT
Approved for public release, distribution unlimited

13. SUPPLEMENTARY NOTES
The original document contains color images.

14. ABSTRACT

The goal of this project has been to produce a non-toxic, metal-free, environmentally friendly elastomeric coating with superior fouling resistance and/or fouling release properties. This program is designed to ultimately provide feedback on the efficiency, uniformity and overall quality of coating formation and assesses the coatings performance in a marine environment. This work involves the production of fouling resistant and/or fouling release marine coatings from an environmentally benign multilayer film consisting of a SABC supported by a thick, soft elastomeric layer. The commercially available and relatively inexpensive poly(styrene)-blockpoly(ethylene/butylene)-block-polystyrene (SEBS) elastomeric layer provides the necessary corrosion protection, durability, and modulus for the coating system. The relatively thin SABC layer lends antifouling and/or fouling-release properties to the coating system through control of surface properties. To further our production of the bilayer coating system, a partnership between Cornell University and Kraton Polymers was formed. Kraton Polymers assisted us by designing and producing relatively large quantities of block copolymer precursors for SABC synthesis. Additionally, they compression molded thick sheets of extruded SEBS thermoplastic elastomer (TPE) onto aluminum test panels to act as the base layer for our coating system onto which the SABC was to be spray-coated for marine testing. Finally, Kraton also identified and provided a thermoplastic elastomer base layer to optimally match the SABC surface layer. Cornell meanwhile has focused on functionalization of the precursor polymers and other synthetic methods to form the SABC layer, characterizing the SABCs (both their bulk chemical properties and surface characteristics) once synthesized, fabricating the test coatings, and evaluating their antifouling and fouling-release behavior with the help of several collaborators who focus on marine biology. While we have now ended our formal partnership with Kraton due to changing business needs on their side, their previous contribution was necessary to push this research forward, and they are still assisting us in any technical method possible. For instance, they just supplied us with a large amount of a new, lower modulus TPE SEBS base layer which has already demonstrated some very encouraging fouling release characteristics with regards to soft fouling release

15. SUBJECT TERMS

16. SECURITY CLASSIFICATION OF:			17. LIMITATION OF ABSTRACT	18. NUMBER OF PAGES	19a. NAME OF RESPONSIBLE PERSON
a. REPORT	b. ABSTRACT	c. THIS PAGE			
unclassified	**unclassified**	**unclassified**	**SAR**	**132**	

Table of Contents

List of Figures

List of Tables

Acronyms

AFM	Atomic force microscopy
AIBN	2,2'-Azobis(2-methylpropionitrile)
ANOVA	Analysis of variance
ATRP	Atom transfer radical polymerization
b	block
BF_3•Et_2O	boron trifluoride diethyl etherate
BNL	Brookhaven National Labs
BF_3•Et_2O	boron trifluoride diethyl etherate
BSA	Bovine serum albumin
BSA-FITC	Fluorescein isothiocyanate labeled biovine serum albumin
CAN	Cerium ammonium nitrate
CCMR	Cornell Center for Materials Research
$CHCl_3$	chloroform
DCC	Dicylohexyl carbodiimide
DMAP	4-(dimethylamino)pyridine
DMAPA	N,N-dimethylamino propylamine
DMF	N,N-dimethyl formamide
DOW	Dow chemical company
DSC	Differential scanning calorimetry
E	Young's modulus
EGB	Entrance grid bias
FIT	Florida Institute of Technology
FT-IR	Fourier transform-infrared spectroscopy
GPC	gel permeation chromatography
GPS	(3-glycidoxypropyl)trimethoxysilane
IR	infrared
MA-SEBS	Maleic anhydride functionalized Poly(styrene-*block*-(ethylene/butylene)-*block*-styrene)
MBP	Methyl-2-bromo propionate
mCPBA	3-chloroperoxybenzoic acid
N	Normal (or Normality)
NaCl	Sodium chloride
NaOH	Sodium hydroxide
NBTC	Nanobiotechnology center
NEXAFS	near-edge X-ray absorption fine structure
NIST	National Institute of Standards and Technology
NMR	nuclear magnetic resonance spectroscopy
NMP	Nitroxidemediated polymerization
ONR	Office of Naval Research
PEG	poly(ethylene glycol)
PEY	partial electron yield

P(E/B)	poly(ethylene/butylene)
PDI	Polydispersity index
PDMS	Poly(dimethyl siloxane)
PDMSe	Poly(dimethyl siloxane)
PI	Polyisoprene
PLSD	Protected least Significant Difference
PMDETA	Pentamethyldiethylene triamine
PPG	Polypropylene glycol
PS	Polystyrene
PS-*b*-AA	Poly(styrene-*block*-acrylic acid)
PS-*b*-P(E/B)-*b*-PI	polystyrene-*block*-poly(ethylene/butylene)-*block*-polyisoprene
PTFE	poly(tetrafluoroethylene)
PVC	Poly(vinyl chloride)
QAC	Quarter ammonium compound
QTI	Intertek QTI laboratory
RFU	relative fluorescence units
rpm	rotations per minute
SABC	surface active block copolymer
SAG	surface active group
SBS	Poly(styrene-*block*-butadiene-*block*-styrene)
SEBS	Poly(styrene-*block*-(ethylene/butylene)-*block*-styrene)
SF	semifluorinated
SFM	Scanning force microscopy
SIS	Poly(styrene-*block*-isoprene-*block*-styrene)
SF	semifluorinated
SFM	scanning force microscopy
SQTC	semi quaternized
*t*BA	*tert*-butyl acrylate
TBT	tributyltin
TFT	α,α,α-trifluorotoluene
THF	tetrahydrofuran
TPE	thermoplastic elastomer
TPP	Triphenyl phosphine
TSB	Trypticase soy broth
WAXS	Wide-angle x-ray diffraction spectroscopy
w/v	weight per volume
XPS	X-ray photoelectron spectroscopy
υ	frequency
cm^{-1}	per centimeter (wave number)
ºC	Degree Celsius

Keywords:

Biofouling, foul release, surface active block copolymers (SABC), amphiphilic block copolymer, multilayer coatings, thermoplastic elastomer, spin coating, spray coating, surface rearrangement, contact angle, X-ray photoelectron spectroscopy (XPS), near edge X-ray absorption fine structure (NEXAFS), living polymerization, polymer modification.

Acknowledgements

The project was funded by United States Department of Defense's Strategic Environmental Research and Development Program (SERDP). We gratefully acknowledge the financial support of SERDP. Additional support was given by the Office of Naval Research which was used especially for the surface characterization of the polymers. We also acknowledge Brookhaven National Laboratory (BNL) where the NEXAFS surface characterization was performed. We also thank Prof. Edward Kramer at University of California Santa Barbara for his valuable inputs and also for the XPS characterization. We also acknowledge Kraton polymer who supplied the precursor polymer in the initial stage of this project. We gratefully acknowledge the Nanosurfaces Inc. for their support in making the large panels and the sea trial tests at the end of this project. We also acknowledge Cornell Nanoscale Science and Technology Facility (CNF), Nanobiotechnology Center (NBTC) and Cornell Center for Materials Research (CCMR) for helping us in the characterization of the synthesized polymers.

Abstract

The goal of this project has been to produce a non-toxic, metal-free, environmentally friendly elastomeric coating with superior fouling resistance and/or fouling release properties. This program is designed to ultimately provide feedback on the efficiency, uniformity and overall quality of coating formation and assesses the coatings performance in a marine environment. This work involves the production of fouling resistant and/or fouling release marine coatings from an environmentally benign multilayer film consisting of a SABC supported by a thick, soft elastomeric layer. The commercially available and relatively inexpensive poly(styrene)-*block*-poly(ethylene/butylene)-*block*-polystyrene (SEBS) elastomeric layer provides the necessary corrosion protection, durability, and modulus for the coating system. The relatively thin SABC layer lends antifouling and/or fouling-release properties to the coating system through control of surface properties.

To further our production of the bilayer coating system, a partnership between Cornell University and Kraton Polymers was formed. Kraton Polymers assisted us by designing and producing relatively large quantities of block copolymer precursors for SABC synthesis. Additionally, they compression molded thick sheets of extruded SEBS thermoplastic elastomer (TPE) onto aluminum test panels to act as the base layer for our coating system onto which the SABC was to be spray-coated for marine testing. Finally, Kraton also identified and provided a thermoplastic elastomer base layer to optimally match the SABC surface layer. Cornell meanwhile has focused on functionalization of the precursor polymers and other synthetic methods to form the SABC layer, characterizing the SABCs (both their bulk chemical properties and surface characteristics) once synthesized, fabricating the test coatings, and evaluating their anti-fouling and fouling-release behavior with the help of several collaborators who focus on marine biology. While we have now ended our formal partnership with Kraton due to changing business needs on their side, their previous contribution was necessary to push this research forward, and they are still assisting us in any technical method possible. For instance, they just supplied us with a large amount of a new, lower modulus TPE SEBS base layer which has already demonstrated some very encouraging fouling release characteristics with regards to "soft" fouling release.

To enable rapid and thorough evaluation of the coatings we produce, we have leveraged the abilities of the ONR anti-fouling coating program to characterize these coatings at the near-molecular level using scanning force microscopy (SFM) methods, near edge X-ray absorption fine structure (NEXAFS) measurements, and X-ray photoelectron spectroscopy (XPS) where appropriate. Additionally, abilities of the ONR program are being utilized to assess the fouling release character of the coatings. *Ulva* zoospore and sporeling and *Navicula* diatom settlement and growth and release testing is being conducted at the University of Birmingham, England by Professors James Callow and Maureen Callow. Leachate toxicity testing, barnacle larvae settlement and growth, force-gauge release testing, and field exposure testing on large scale test panels is being conducted at the California Polytechnic State University (CalPoly) by Professor Dean Wendt. Finally, large scale marine testing is also being performed at the Florida Institute

of Technology (FIT) by Professor Geoff Swain to give us test data from two very different marine sites. Additional testing at other facilities will be performed on an as-needed basis at other available testing sites. In the last phase of the project Nanosurfaces Inc. take over the sea-immersion tests. They licensed the IP from from Cornell and made the big panels needed for the sea immersion tests using the SABCs synthesized in their lab.

Objective

The objective of this project is to develop non-toxic, copper-free, environmentally benign, antifouling polymer coatings of controlled modulus and surface properties. The coating involved a multilayer approach using styrene-ethylene/butylene-styrene (SEBS) thermoplastic elastomer as a soft base layer. The functionalization of the surface was done by the coating of a functional SABC layer. A secondary objective was to determine whether low surface energy fluorinated coatings or hydrophilic poly(ethylene glycol)-based coatings provided the best fouling release behavior. To find out the optimal surface energy required for foulrelease applications polymers with different ratios of mixed hydrophobic/hydrophilic were also synthesized. For laboratory scale testing the functional polymeric coatings were tested with two fouling organisms (Ulva and Navicula) with extremely different fouling mechanisms as one release well from hydrophobic surfaces and the other release well from hydrophilic surfaces. These two organisms were kept as bench mark for the release properties of our functional surfaces. The objective here is to make surfaces which show good foul release for both of these foulants. The fouling release property of a surface was found to be dependent on the surface characteristics. The proof-of-principle of these multilayer systems was demonstrated and, with understanding of the key problems involved, improved systems for fouling release that eliminated the use of toxic organocopper antifoulants were developed. In brief the specific objectives of this project are: (1) synthesis and characterization of specific SABCs; (2) select an optimal, surface-active block polymer; (3) establish commercially viable approaches to synthesize antifouling coatings in large quantities; and (4) evaluate application processes for these coatings.

1.0 Background

Marine biofouling is a severe problem faced by all aspects of the nautical community, whether recreational, commercial, or defense oriented. It is caused by the accumulation and settlement of barnacles, macroalgae, microbial slimes, and other micro and macro scale organisms on man-made surfaces immersed in seawater (1-3). Marine biofouling can significantly increase drag, leading to startling consequences with regards to fuel consumption (4). Fouling has been estimated to raise drag by as much as 40 percent and fuel consumption by as much as 30 percent. This has been estimated to potentially lead to a powering penalty as great as 86 percent. Clearly, this demonstrates that marine biofouling is a significant, universal problem with regards to the transport of materials and resources. Additionally, any time spent by a seafaring vessel in dry-dock during cleaning of fouling material leads to inefficiency as it forces a vessel out of service. The approach of lowering the strength of adhesion between fouling organisms and the surface of marine vessels by use of environmentally friendly coatings holds promise to not only decrease the accumulation of organisms, but also aid in their removal (1-3). Furthermore, replacement technology for traditional tributyl tin and copper containing coatings is desperately needed (tributyl tin derived ablative coatings have been banned worldwide, and on-going environmental concerns exist concerning copper based ablative coatings) (5, 6). Additionally, the vast range of fouling organisms and environmental conditions throughout the world makes the task of developing a universal coating that resists fouling and/or self cleans in all cases extremely challenging, and novel non-toxic solutions to this problem are urgently needed.

Tin and copper containing metallic ablative coatings are rapidly being phased out due to non-specific toxicity in the environment. Current understanding of antifouling materials is that the most effective metal-free fouling control systems are low surface energy coatings, specifically silicone or fluoropolymer based systems. These materials minimize the adhesion strength between fouling organisms and the surface of a vessel (7, 8). For extended performance life, these coating systems must have controlled and stable surface energy and composition, exhibit elastomeric behavior, and adhere well to the substrate. To date, several nonmetallic fouling release coatings systems have been made commercially available, primarily those based on silicone polymers. Nevertheless, none of these coatings meet all of the desired performance characteristics listed previously. Many lack the toughness required to withstand the rigorous physical demands of a marine environment. Another issue is lack of sufficient and consistent self-cleaning properties—for instance, many of these coatings are not suitable for use on naval vessels which may spend a significant amount of time inactive in port or are highly susceptible to certain types of bioslimes. Finally, due to polymer restructuring or other degradation pathways, many of these coatings prematurely lose their desirable surface properties with time and exposure to a marine environment, requiring earlier than desirable reapplication.

It has been demonstrated that the adhesion strength of hard fouling organisms is proportional to $(\gamma E)^{(1/2)}$, where γ is the surface energy and E is the modulus of the surface (7, 8). Taking this into account, silicone elastomers are currently the only major commercial environmentally benign fouling release coatings available possessing both low modulus and surface energy. However, the efficacy of silicone polymers is lower

than that of biocide-containing antifouling paints, and regular mechanical cleaning (specifically scrubbing) of the coated surface is required. This greatly adds to operating expense as vessels must either be placed in dry-dock or cleaned somehow while operating. It would seem advantageous to use traditional fluorinated materials, such as polytetrafluoroethylene (PTFE/Teflon) to lower the surface energy of a coating and decrease the adhesion strength of biofouling organisms. Unfortunately, these materials are typically hard and brittle with high moduli and do not provide sufficient release of marine biofouling. Thermoplastic elastomers (TPEs) such as polystyrene-*block*-poly(ethylene/butylene)-*block*-polystyrene (SEBS) block copolymers offer desirable mechanical properties (relatively low modulus, E), but undesirable surface characteristics. Thus, a strategy to incorporate both of these previously described favorable properties, by layering SEBS TPE with surface-active block copolymers (SABCs), is expected to offer excellent fouling control. One minor caveat is that hydrophobic, heavily fluorinated surfaces often undergo rapid molecular reconstruction in polar environments, such as water. We tried using liquid crystalline fluorinated side chains to prevent the reconstruction in water.

We have also examined quaternized ammonium compounds (QACs) which are known to have extremely high resistance to bacterial fouling due to their ability to disrupt the bacterial cell wall. Furthermore, they have low environmental toxicity and good environmental stability. Since bacteria are instrumental in the early stages of the fouling process, we hoped that combining quaternized ammonium groups with our surface active groups would yield compounds with extremely favorable fouling resistance against many different organisms. A robust synthetic method to do so with our existing SABC precursors was identified and several SABCs were produced. Unfortunately, while these materials demonstrated some interesting antimicrobial results, they did not demonstrate particularly good antifouling properties in several biofouling assays.

Poly(ethylene glycol) (PEG) is commonly known by the biomaterials community to have robust fouling resistance. The polymer has many useful properties such as low protein absorption, good stability, low toxicity, and is in general, compatible with biological processes and the human body. For fouling-release applications, such materials by themselves are lacking in several critical properties such as desirable mechanical behavior, long-term stability, and ease of application. Unfortunately, this limits their use as coating materials. As with biomedical surfaces used in the body, the first event leading to biofouling in a marine environment is the adsorption of a conditioning film that includes proteins and other biomacromolecules. It is believed that the incorporation of PEG into a coating system would help limit protein adsorption, thereby reducing the adhesion of this conditioning film. Thus, PEG based surfaces were explored as an element of this project.

Additionally, we have identified several strategies to obtaining amphiphilic SABCs. One is based around functionalizing our SABC precursor with amphiphilic PEGylated fluoroalkyl groups that have also shown promising fouling resistance. The second strategy is synthesis of “mixed” amphiphilic SABC polymer having PEG and perfluoro chains attached to the precursor polymer. This strategy is advantageous that the

ratio between hydrophobic/hydrophilic functionality can be changed by simply changing the PEG and perfluor chains attached to the precursor. The third approach involved the synthesis of amphiphilic chains such as Brij and pluronic non-ionic surfactant attached to the precursor. Brij has PEG and hydrocarbon groups in a single chain as hydrophilic and hydrophobic groups. Pluronic has PEG and PPG in a single chain as hydrophilic and hydrophobic groups. Fourth approach is the synthesis of SABCs derived from simple hydrocarbon and PEG chains attached to the precursor with various ratios. This series is also a class of "mixed" amphiphilic SABCs.

Certain organisms preferentially foul hydrophobic surfaces while other organisms preferentially foul hydrophilic surfaces. One would initially think that these amphiphilic SABCs could end up giving us the "worst of both worlds" and act as a universal fouling surface. Based on our testing however, this is not the case, and it appears that we can obtain desirable behavior that is "the best of both worlds." Amphiphilic derived coatings have proven themselves resistant to fouling by organisms that preferentially attach to either hydrophobic or hydrophilic surfaces. Not a great deal is known yet about the amphiphilic coatings' interaction with biofouling organisms, but our initial hypothesis is that chemical ambiguity and the dynamic nature of the amphiphilic coatings' surface plays a large role in our success with these materials. These materials have been our most promising SABCs in dealing with biofouling.

2.0 Overall Technical Approach

2.1 Polymer Synthesis and Processing

SABCs for the initial stage of the project were prepared using polystyrene-*block*-polybutadiene-*block*-polystyrene (SBS) triblock copolymer provided by Kraton Polymers as a precursor material. Additional SABC synthetic work has focused on the use of two different polystyrene-*block*-polyisoprene-*block*-polystyrene (SIS) triblock copolymers, also provided to us by Kraton Polymers. Attachment of the semifluorinated (SF) side chains was primarily pursued through direct bromination of the precursor material followed by subsequent attachment of the semifluorinated side chain through a two phase substitution reaction. Meanwhile, attachment of poly(ethylene glycol) (PEG) groups to the precursor material has been pursued through epoxidation of the diene block followed by a subsequent etherification reaction.

Another set of SABCs were prepared from polystyrene-*block*-poly(acrylic acid) precursors at Cornell University through atom transfer radical polymerization (ATRP). These precursor polymers were readily functionalized with semifluorinated (SF), poly(ethylene glycol) (PEG) and amphiphilic side chains through DCC-coupling esterification reactions. Additional SABC synthetic work has focused on the use of two different precursor polystyrene-*block*-poly(ethylene/butylene)-*block*-poly(isoprene) (PS-*b*-P(E/B)-*b*-PI) ABC triblock copolymers synthesized by Kraton Polymers (one with a 10,000 g/mol isoprene block, the other with a 20,000 g/mol isoprene block). Attachment of SF, PEG, and amphiphilic side chains on this material has been pursued through selective epoxidation of the isoprene block followed by a subsequent catalyzed etherfication reaction using boron trifluoride diethyl etherate (BF_3•Et_2O). Additionally, amination followed by subsequent attachment through quaternization of the amine has been pursued as an alternative method of forming hydrolysis-free SABCs. Exploration of this chemistry was pursued due to the propensity of quaternized amine containing materials to be anti-microbial in combination with the possibility of this being an alternative attachment method of surface active groups (SAGs).

Based on the previous results, in the final stages of the project SABCs were prepared from only one polymer precursor. Synthetic work focused on the use of polystyrene-*block*-poly(ethylene/butylene)-*block*-poly(isoprene) (PS-*b*-P(E/B)-*b*-PI) ABC triblock copolymer precursor synthesized by Kraton Polymers with a 10,000 g/mol isoprene block. Attachment of Brij, Pluronic, hydrocarbon, SF, PEG, and amphiphilic side chains on this material has been pursued through selective epoxidation of the isoprene block followed by a subsequent catalyzed etherification using boron trifluoride diethyl etherate (BF_3•Et_2O). These amphiphilic SABCs formed from combining SF and PEG containing surface active groups (SAGs) demonstrated extremely promising biofouling results.

2.2 Preparation of Laboratory Biofouling Assays

A methodology to prepare multilayer coatings on substrates for small scale biofouling tests was developed. Glass slides are pretreated with (3-glycidopropyl)-

trimethoxysilane (GPS). After this, a layer of SEBS with grafted maleic anhydride is applied via spin coating. This is followed by the application of SEBS (without the maleic anhydride groups) via spin coating. Finally, a thin coating of the SABC is applied via spray-coating. Generally, the slides are annealed at 120° C after the application of each layer. The TPE SEBS layer assists the anchoring of the SABC coating to the substrate and provides the necessary bulk modulus properties to the coating. The lower SEBS layer contains domains of micellized polystyrene blocks of the SABC in the ethylene/butylene copolymer matrix. Furthermore, using this approach, only a small amount of the SABC was required for coating formation of a desirable thickness.

2.3 Preparation of Large Scale Test Panels

A methodology to prepare large scale (10" x 12") aluminum test panels for marine exposure testing was developed. The initial machining was done at Cornell with the aid of CCMR (Cornell Center for Materials Research). After initially trying to prepare panels solely in house at Cornell University, we realized that it would be to our advantage to leverage the industrial fabrication abilities of Kraton Polymers. Once the panels are machined to specifications, they are sent to Houston, Texas where they are epoxy coated by Coatings Engineers, a commercial coating house. This process was overseen by Kraton Polymers who then compression molded a thick layer (approximately 1 mm) of SEBS. Ultimately, the panels are shipped back to Cornell University where the final thin (approximately 1 micron) SABC layer is spray coated. This leads to the final step in which a thin layer of the SABC is spray coated on top of the SEBS base layer. On the final stages of the project we tried to prepare the large scale panel in Cornell itself. We initially faced the problem of shrinkage on the surface with soft MD6945 base which we overcame to make smooth surface.

2.4 Surface Characterization

The surface energy of the coatings was studied by determining the dynamic (advancing and receding) contact angles of water droplets on these surfaces. Furthermore, the surface morphology and chemical composition of the coatings was characterized using near edge x-ray absorption fine structure (NEXAFS) at the DOW/NIST U7A beamline at Brookhaven National Laboratory. Additional characterization was provided by Professor Ed Kramer at the University of California, Santa Barbara using x-ray photo electron spectroscopy (XPS). Scanning force microscopy was performed using a DI Dimension 3100 AFM in hard tapping mode.

2.5 Biofouling Assays

All SABCs containing PEG, semifluorinated, hydrocarbon, Brij, Pluronic and ethoxylated fluoroalkyl amphiphilic side chains were tested against *Ulva* sporelings and *Navicula* diatoms with the help of the Callows at the University of Birmingham, England.

A range of biofouling assays were conducted on SABCs. Barnacle cyprid larvae settlement and barnacle release testing were conducted by Professor Dean Wendt at Calpoly on SABCs produced at Cornell using the PS-*b*-PAA precursor. Leachate toxicity and barnacle settlement and adhesion testing have been explored for the samples by Dean Wendt's group at Calpoly, plus an initial batch of large scale test panels was tested using sea-water immersion by Geoff Swain's group at FIT. Only the amphiphilic samples were selected for full field-immersion study since the amphiphilic side chains performed the best across the range of lab-scale biofouling assays we looked at with our collaborators.

We have also tested some of the "mixed" amphiphilic SABCs for protein adsorption studies against BSA-FITC, collagen, fibrinogen and IgG.

3.0 Materials and Methods

The chemicals used for this project are listed in the table below:

Table 1: List of chemicals used

Chemical	Abbrevation	Supplier
3-chloroperoxybenzoic acid	mCPBA	Aldrich
potassium hydroxide	KOH	Aldrich
copper(I) bromide	CuBr	Aldrich
copper(II) bromide	$CuBr_2$	Aldrich
1,1,4,7,7- pentamethyldiethylenetriamine	PMDETA	Aldrich
methyl 2-bromopropionate	MBP	Aldrich
1,3-dicyclohexylcarbodiimide	DCC	Aldrich
4-(dimethylamino)pyridine	DMAP	Aldrich
poly(ethylene glycol) methyl ether	(Mn = 550); PEG550	Aldrich
Zonyl FSO-100	Zonyl	Aldrich
anhydrous pyridine	Py	Aldrich
triphenylphosphine	TPP	Aldrich
tributyl-tin hydride	Bu_3SnH	Aldrich
2,2-azobis(2-methylpropionitrile)	AIBN	Aldrich
carbon tetrabromide	CBr_4	Aldrich
potassium carbonate	K_2CO_3	Aldrich
9-decen-1-ol		Aldrich
1-methyl-2-pyrrolidone	NMP	Aldrich
iodomethane	CH_3I	Aldrich
imidazole		Aldrich
Styrene	St	Aldrich
tert-butyl acrylate	*t*BA	Aldrich
Calcium chloride	$CaCl_2$	Aldrich
Sodium hydroxide	NaOH	Aldrich
α,α,α-Trifluorotoluene	TFT	Aldrich
Perfluorooctyliodide		Fluka
bis(2-methoxyethoxy)aluminum hydride solution	Red-Al	Fluka
3-(Glycidoxypropyl)-trimethoxysilane	GPS	Gelest
Perfluorodecyliodide		SynQuest Fluorochemicals
1H, 1H, 2H, 2H-perfluorooctanol	F6H2	SynQuest Fluorochemicals
1H, 1H, 2H, 2H-perfluorodecanol	F8H2	SynQuest Fluorochemicals
1H, 1H, 2H, 2H-perfluorododecanol	F10H2	SynQuest Fluorochemicals

Styrene (Aldrich, 99%) was passed through a column of basic alumina to remove the 4-*tert*-butylcatechol inhibitor. *Tert*-butyl acrylate (*t*BA, Aldrich, 98%) containing 10-20 ppm of monomethyl ether hydroquinone as the inhibitor was extracted with 5% aqueous

NaOH and then washed with distilled water and distilled. The solvents used are dried using common laboratory procedures. All ohter chemicals were used as received. Kraton D-1102 SBS (Mn = 45000 g/mol, 30 weight % PS, 70 weight % PB) was generously provided by Kraton Polymers. Two additional proprietary SIS polymers (one 30 weight % PI, 70 weight % PS, the other 30 weight % PS, 70 weight % PI) were also provided by Kraton. Polystyrene-*block*-poly(ethylene/butylene)-*block*-polystyrene (SEBS) triblock thermoplastic elastomer (Kraton G1652M and MD6945) and SEBS grafted with maleic anhydride (MA-SEBS, Kraton FG1901X) were received from Kraton Polymers. Two proprietary polystyrene-*b*-poly(ethylene/butylene)-*b*-isoprene ABC triblock copolymers were synthesized as precursor polymers as part of the project by Kraton Polymers. The relative block weights were 8,000 g/mol PS, 25,000 g/mol P(E/B) and 10,000 and 20,000 g/mol isoprene (the length of the PI block was the only difference for each precursor).

3.1 Synthesis of Precursors

3.1.1 Synthesis of Semifluorinated Butyliodide (F8H4I)

The synthesis of this compound was performed as shown in figure 1. Perfluorooctyliodide (30.0 g, 55 mmol) and 3-buten-1-ol (4.75 g, 66 mmol) were mixed in a 100 mL round bottomed flask. AIBN (0.45 g, 2.75 mmol) was added and the reaction was performed for 2 hours at 80° C under a nitrogen atmosphere. The reaction was cooled to room temperature and semifluorinated iodobutanol (F8H4IOH) was recovered by crystallization in a toluene/hexane (1:4) mixture. Sodium bis(2-methoxyethoxy)aluminum hydride solution (Red-Al, 19.8 g, 98.0 mmol) was dissolved in 160 mL of ether in a 500 mL round bottom flask. F8H4IOH (30 g, 49 mmol) dissolved in 80 mL of ether was added and the reaction was performed for 3 hours at room temperature. The reaction was quenched with 200 mL of 2 M HCL solution and the aqueous phase was washed with 200 mL of brine, followed by drying with magnesium sulfate. The solution was concentrated under reduced pressure and the semifluorinated butanol (F8H4OH) was recovered by further drying under reduced pressure for 24 hours at room temperature. F8H4OH (22.5 g, 45.7 mmol), TPP (18 g, 68.6 mmol), and imidazole (4.67 g, 68.6 mmol) were dissolved in 200 mL of THF in a 500 mL round bottom flask. This mixture was cooled to -78° C and iodine (17.4 g, 68.6 mmol) was added. The reaction mixture was allowed to reach room temperature and maintained for an additional 2 hours under vigorous stirring. Ultimately, the reaction was quenched with 200 mL of water and 200 mL of ether was added. The organic layer was washed with brine, dried with magnesium sulfate, and concentrated. Triphenylphosphineoxide was precipitate din excess ether, and the product was further purified by passing through a short silica gel column. The final F8H4I product was recovered by drying under reduced pressure at room temperature.

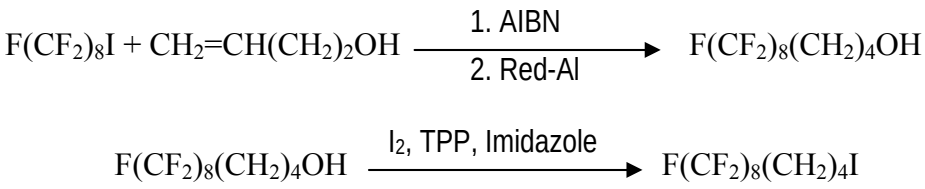

Figure 1: Synthesis of semifluorinated butyliodide (F8H4I).

3.1.2 Synthesis of 10-perfluorodecyl-1-decanol (F10H10OH)

The semifluorinated alcohol, 10-perfluorodecyl-1-decanol (F10H10OH) was performed by a radical coupling reaction. The reaction scheme is given in Figure 2. 9-decen-1-ol (14.07 g, 0.09 mol) and perfluorodecyliodide (38.76 g, 0.06 mol) were taken in a round bottom flask fitted with a condenser and septa. The reactants were purged with argon and the mixture was heated to 90° C while stirring. AIBN (300 mg) was added incrementally over a period of 45 minutes. After 5 hours, the reaction temperature was reduced to 80° C and 30 mL of anhydrous toluene was added, followed by additional AIBN (1.5 g) and tributyl tin hydride (52.38 g, 0.18 mol). The reaction mixture was stirred while heating at 80° C for 24 hours and then an additional 60 mL of anhydrous toluene was added to the reaction mixture, which was then allowed to cool to room temperature. The raw F10H10OH product crystallized out of solution as a white solid and was collected by filtration and subsequently recrystallized from hot toluene three times to remove residual starting products and tributyl tin impurities. Finally, the purified F10H10OH was dried under reduced pressure at room temperature for 48 hours. The proton NMR and IR characterization showed the characteristic functional groups as summarized below.

^{1}H NMR for F10H10OH (300 MHz, $CDCl_3$, δ): 3.63 (q, 2H, HO**CH_2**CH_2-), 2.07 (m, 2H, -CH_2**CH_2**CF_2-), 1.58 (m, 2H, -CF_2CH_2**CH_2**CH_2-); 1.30 (br s, 12H, -CF_2-CH_2-CH_2-**$(CH_2)_6$**- and 1H, –**H**OCH_2-). IR (dry film) υ_{max} (cm^{-1}): 3250 (O-H stretching); 2925, 2850 (C-H stretching); 1470, 1452 (C-H bending); 1330-1095 (C-F stretching); 1055 (C-O stretch).

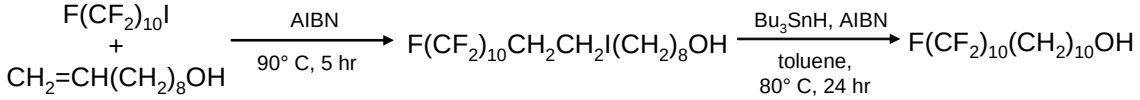

Figure 2. Synthesis of semifluorinated 10-perfluorodecyl-1-decanol (F10H10OH).

3.1.3 Synthesis of Perfluorooctyl Hexylbromide (F8H6Br)

F8H6OH (22.5 g, 43.3 mmol) and CBr_4 (23 g, 69.3 mmol) was dissolved in 100 mL of anhydrous THF in a 500 mL round bottom flask. The mixture was cooled to -5 ºC. Triphenyl phosphine (TPP, 18.1 g, 69.3 mmol) was then added and the reaction was performed for 1 hour at -5 °C, followed by an additional 8 hours at room temperature. The THF was then evaporated under reduced pressure and 200 mL diethyl ether was added to the crude product. The TPP oxide byproduct was separated by filtration, and the

F8H6Br product was further purified by passing the reaction solution through a short slica gel column.

3.1.4 Bromination of SBS Copolymer

A typical process for polymer bromination is given here. SBS (10.0 g, 0.16 mol) was dissolved in 500 mL THF in a 1000 mL round bottom flask at room temperature. Bromine (27 mL) was added via an addition funnel slowly over a period of 4 hours under stirring, and the reaction was maintained for 3 additional hours. The solution was poured into a large amount of sodium carbonate saturated aqueous solution slowly to precipitate the polymer. The polymer was collected via filtration, and dissolved in THF again. The THF solution was then reprecipitated (again in saturated aqueous sodium carbonate solution) to remove residual bromine. The white product was dried at reduced pressure at 40º C for 12 hours.

3.1.5 Epoxidation of SBS (and SIS) Copolymer

For a typical reaction, SBS (10.0 g, 0.16 mol) and 200 mL dichloromethane were mixed in a 500 mL flask at room temperature to form a homogenous solution. MCPBA (32.0 g, 0.19 mol) was added to the flask. The flask was sealed with a rubber septum, and the reaction was allowed to proceed for approximately 8 hours at room temperature. The solution was concentrated and the epoxidized polymer was precipitated into 600 mL of methanol and filtered. The polymer was rinsed repeatedly with 200 mL of methanol, and then dissolved in a suitable reaction solvent (THF, dioxane, TFT, etc.) and stored in solution for further steps. An analogous reaction was also used to epoxidize SIS copolymers.

3.1.6 Preparation of PS-*b*-PAA Precursor Polymers

The following reaction was used to produce a scaled up sample of PS_{38K}-*b*-PAA_{3K} 38400:3100 block weight ratio) precursor polymer. A mixture of 9 mL of acetone, *t*BA (30.8 g, 240 mmol), and PMDETA (0.24 mmol), deoxygenated by purging with argon, was added to CuBr (0.24 mmol) and $CuBr_2$ (0.12 mmol) in a round bottom flask. After complex formation, which was evident from the change in appearance of the solution from colorless to clear and light green, MBP (4.8 mmol) was added using a syringe, and the monomer was polymerized for 6 hours at 60° C. After cooling the reaction mixture to room temperature, 150 mL of acetone was added, and the polymer solution was treated with neutral alumina to remove the copper salts. Acetone was removed by evaporation, and the polymer was further purified by dissolving in diethyl ether and precipitating in a methanol/water mixture (1:1 volume/volume) at 0° C. After collecting the polymer by filtration and drying, this process was repeated to further remove residual *t*BA. Ultimately, the P*t*BA was dried under vacuum, yielding 17.75 g of a flakey white powder. Characterization by gel permeation chromatography (GPC) and ^{1}H NMR analysis indicated a polymer molecular weight on the order of 5500 g/mol, with a polydispersity index of 1.10.

Bromine terminated P*t*BA$_{5.5K}$ (14 g, 2.7 mmol) and CuBr (6.65 mmol) were taken in a round-bottomed flask. Deoxygenated styrene (69.25 g, 665 mmol) was added to the reactor and stirred until the polymer dissolved. PMDETA (6.65 mmol) was injected to form a complex with CuBr. Polymerization at 100° C for 60 minute results in a viscous liquid that was dissolved in THF after cooling to room temperature. The solution was treated with neutral alumina to remove copper salts, concentrated by evaporation of the solvent, and precipitated in excess methanol. After reprecipitation in methanol, the polymer was collected by filtration and dried under vacuum at room temperature. Characterization by GPC and ^{1}H NMR analysis indicated a total polymer molecular weight on the order of 43900 g/mol (5500:38400 P*t*BA$_{5.5K}$:PS$_{38K}$) with a polydispersity index of 1.17.

Preparation of the final PS$_{38K}$-*b*-PAA$_{3K}$ precursor polymer from PS$_{38K}$-*b*-P*t*BA$_{5.5K}$ was done through deprotection of the *t*BA groups. In a typical reaction, two milliliters of concentrated hydrochloric acid solution (12 N) was added to a 10% weight/volume solution of PS$_{38K}$-*b*-P*t*BA$_{5.5K}$ in 1,4-dioxane and the solution was refluxed for about 6 hours. The polymer was recovered by cooling the dioxane solution and precipitating it in an ice/water mixture. Complete hydrolysis of the *tert*-butyl acrylate was confirmed by ^{1}H NMR spectroscopy.

3.1.7 Epoxidation of PS-*b*-P(E/B)-*b*-PI Precursor Polymers

In a typical epoxidation reaction, proprietary PS-*b*-P(E/B)-*b*-PI Kraton Polymer (K3 (PI=10k) , 5 g, 14.5 mmol of reactive isoprene sites) was dissolved in 200 mL of dichloromethane (cyclohexane was used in the later stages as it is a good solvent for the rubbery block) in a round bottomed flask. Upon dissolution, MCPBA (3.9 g, 17.4 mmol) was added to the reaction and the contents were allowed to vigorously stir for 5 hours. At this time, the polymer was precipitated in methanol, collected, and reprecipitated to remove residual MCPBA. The white, rubbery product was dried at room temperature under reduced pressure to remove residual solvent. The reaction was confirmed by ^{1}H NMR spectroscopy which indicated the disappearance of the proton signatures associated with the unsaturated alkene groups of the isoprene and the appearance of oxirane ring protons (associated with the epoxide ring).

3.1.8 Amination of PS-*b*-P(E/B)-*b*-PI Precursors

Epoxidized proprietary PS-*b*-P(E/B)-*b*-PI Kraton Polymer (PI=10k, 1.00 g, 5 mmol of reactive epoxy sites) was dissolved in 50 mL of NMP in a 300 mL round bottomed flask. The mixture was heated to 90° C. DMAPA (25.4 g, 250 mmol) was added, and the amination was refluxed for 48 hours at 200° C. The aminated polymers were precipitated in excess distilled water, filtered, dissolved in 50 mL of NMP, reprecipitated in excess distilled water, filtered, and dried under reduced pressure at room temperature for 48 hours.

3.2 Synthesis of SABCs from Precursors

3.2.1 Attachment of Semifluorinated Side Chains to Brominated SBS Copolymer

In a typical polymer side chain attachment to brominated SBS (SBS-Br), SBS-Br (2.0 g) was dissolved in 200 mL chloroform. F8H2 (5 g), 200 mg 18-crown-6 and 5 g potassium hydroxide in 100 mL water were added. The biphase system was refluxed for 72 hours under nitrogen atmosphere while undergoing mechanical agitation. The chloroform was evaporated away, and the polymer was precipitated in methanol, filtered, and then redissolved in THF. The THF solution was poured into methanol slowly to precipitate the polymer. When a dry sample was needed for characterization, the polymer was dried under reduced pressure at 50 ºC for 12 hours.

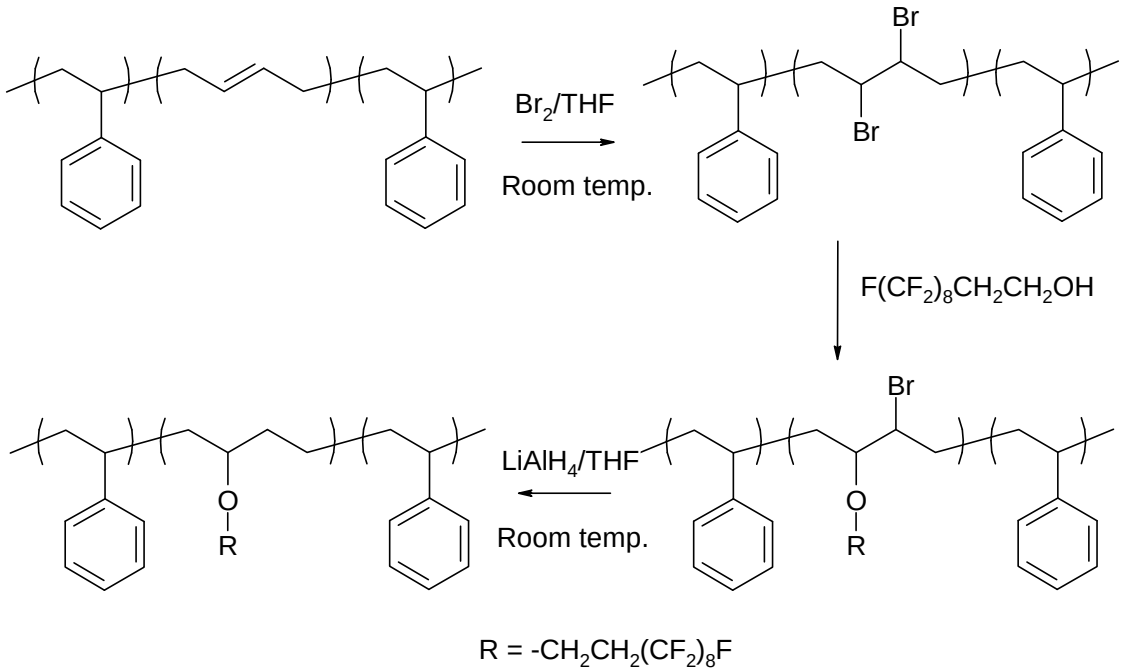

Figure 3: Bromination and subsequent attachment of SF side chains to SBS copolymers to form SF SABCs.

3.2.2 Attachment of SF and PEG Side Chains to Epoxidized SIS Copolymers

In a typical reaction, epoxidized SIS (2.0 g) was dissolved in 40 mL of dichloromethane. In a separate flask, F8H2 (20 g), and cerium ammonium nitrate (CAN) (0.285 g) were dissolved in roughly 400 mL of dichloromethane. The SIS dichloromethane solution was added drop-wise at a rate of 5 mL per 2 hours while the system was refluxed at 50 ºC. The system was heated for a total of 72 hours under a nitrogen atmosphere while undergoing vigorous stirring. The dichloromethane was then mostly evaporated away to concentrate the reaction mixture and the polymer was precipitated in methanol. The precipitate was filtered, redissolved in dichloromethane,

concentrated, and then reprecipitated to remove residual CAN and F8H2. The polymer was dried under reduced pressure at 50 ºC for 12 hours.

3.2.3 Esterification Attachment of SAGs to PS-*b*-PAA Precursor Polymers

The synthsis of this polymer was performed as shown in figure 4. The following reaction was used to produce scaled up PS_{38K}-*b*-PAA_{3k}-Amp SABCs. PS_{38K}-*b*-PAA_{3k} (10 g) was dissolved in 50 mL of anhydrous pyridine (20% weight/volume). In a separate flask, DCC (61.1 mmol), DMAP (7.7 mmol), and Zonyl FSO-100 (28 g) were dissolved in 300 mL of anhydrous THF. The THF solution was then added drop-wise to the polymer containing pyridine solution and mixed vigorously at room temperature for 96 hours. The reaction solution was filtered to remove DCC byproduct, and concentrated under reduced pressure. The polymer was recovered by precipitation and reprecipitation in methanol at 0° C. Esterfication of PEG side chains was performed in a similar fashion, but the final PEGylated block copolymer was precipitated in water at 0° C containing NaCl. In the case of the semifluorinated alcohol, anhydrous TFT was added after about 1 day of reaction in pyridine and THF and precipitation was performed in methanol.

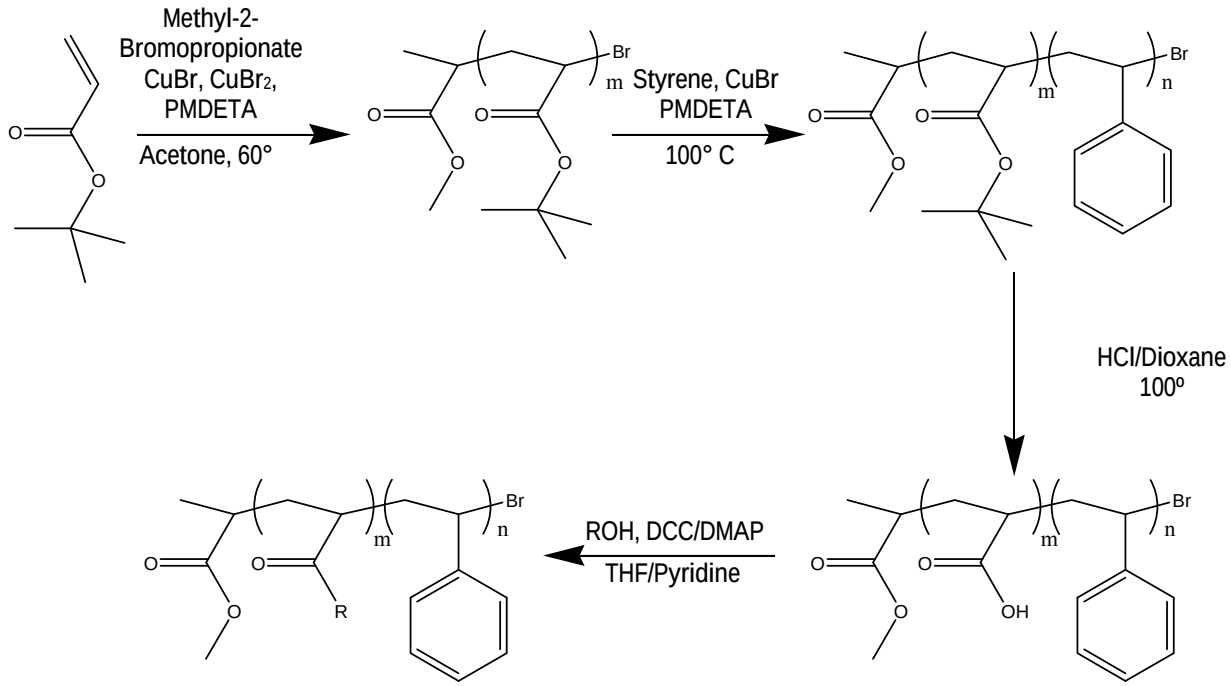

Figure 4: Reaction schematic for production of PS-b-PAA derived SABC polymers. ROH = $HOCH_2CH_2(CF_2)_7CF_3$, $HO(CH_2CH_2O)_xOCH_3$, $H(OCH_2CH_2)_y(CF_2CF_2)_zF$

3.2.4 Etherification Attachment of SAGs to PS-*b*-P(E/B)-*b*-PI Precursors

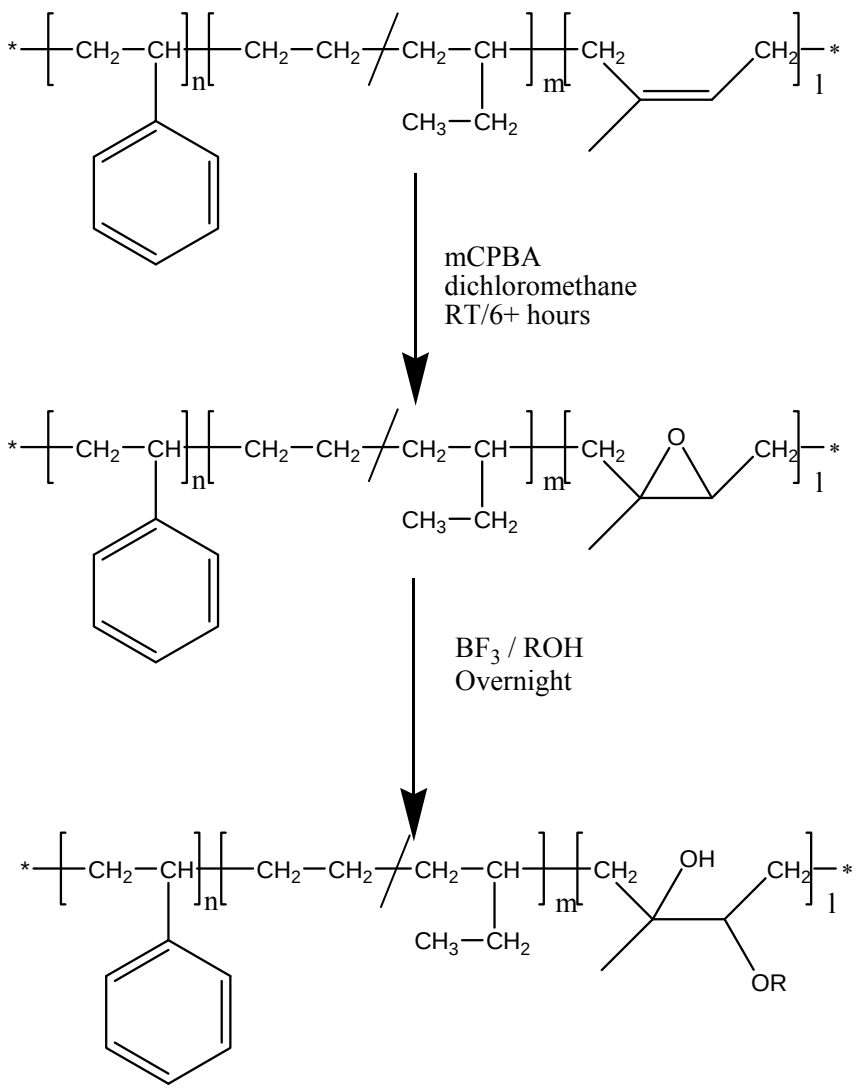

Figure 5: Reaction schematic for production of PS-*b*-P(E/B)-*b*-PI derived SABC polymers. ROH = $HOCH_2CH_2(CF_2)_7CF_3$, $HO(CH_2CH_2O)_xOCH_3$, $H(OCH_2CH_2)_y(CF_2CF_2)_zF$. ROH = $C_mH_{2n+1}(O\ CH_2CH_2)_nOH$, $C_mH_{2n-1}(OCH_2CH_2)_nOH$ (Brij surfactants) and $HO(CH_2CH_2O)_x(CH_2CH(CH_3)O)_y(CH_2CH_2O)_zH$, $HO(CH_2CH(CH_3)O)_a(CH_2CH_2O)_b(CH_2CH(CH_3)O)_cH$ (Protected and non-protected Pluronic surfactants).

The following procedure (scheme is shown in figure 5) was used to prepare small scale ether-linked SABCs based on PS-*b*-P(E/B)-*b*-PI precursors. It has been scaled up to five times its original amounts successfully. Epoxidized K3 (1.05 g, 2.9 mmol of reactive epoxy sites), and either 7.98 g PEG550, 11.01 g Zonyl FSO-100, or 6.73 g F8H2 (29 mmol) were dissolved in anhydrous chloroform. The mixture was degassed by purging with Ar and then dried overnight under molecular sieves. BF_3•Et_2O (1.16 mmol) was

syringed into the mixture and the reaction was carried out for roughly 24 hours. The reaction was then quenched with aqueous NaOH and concentrated by evaporation. Polymers containing Zonyl and F8H2 side chains were precipitated twice in methanol from chloroform. Meanwhile, polymers functionalized with PEG550 were precipitated twice in an ice/water mixture. Rates of conversion by etherification were found to be on the order of 40% or higher.

Amphiphilic mixed surfaces combining F10H10 and PEG550 side groups were also produced in an analogous manner using PS_{8K}-*b*-$P(E/B)_{25K}$-*b*-PI_{20K} SABC precursor polymers. In these reactions, the feed ratio of F10H10 and PEG550 was controlled in distinct proportions (1:4, 2:3, 3:2, and 4:1 F10H10:PEG550 were used) to produce SABCs of various mixed compositions. For these reactions, overall attachment was found to generally be between 20% and 30% relative to epoxidized isoprene groups. Similarly for other "mixed" amphiphilic series the reactions were preformed with different feed ratios of hydrophobic and hydrophilic compounds. All the reactions have been scaled up to six times this original amount successfully to produce larger scale samples used in seawater immersion field testing. The similar procedure is used for all the SABCs of this type using Brij, Pluronic, hydrocarbon and PEG. Thus a series of amphiphilic and "mixed" amphiphilic SABCs were synthesized.

3.2.5 Etherification Attachment of Amphiphilic Brij Non-Ionic Surfactants

To produce ether-linked amphiphilic side chain surface active block copolymers, 2.1 g of epoxidized PS_{8K}-*b*-$P(E/B)_{25K}$-*b*-PI_{10K} (5.8 mmol of epoxide) was taken in a round bottom flask in conjunction with a three times molar excess (17.4 mmol) of the Brij surfactant alcohol. The reactants were purged with argon, and subsequently dissolved in ca. ~ 150 mL of anhydrous chloroform. Activated molecular sieves were added to the reaction mixture and it was allowed to sit for ca. ~ 12 h to optimize the up-take of water. Etherification was performed through the addition of boron trifluoride diethyl etherate catalyst (0.345 g, 2.4 mmol) followed by vigorous stirring at room temperature for at least 72 hours. Following the reaction, 6.25 N sodium hydroxide was added to quench any residual boron catalyst and the reaction mixture was concentrated under reduced pressure using a rotary evaporator. The resultant SABC was precipitated into methanol and the yellow rubbery product was collected by filtration and subsequently reprecipitated twice from chloroform to remove additional residual amphiphilic surface active side-chain alcohol. Finally, the finished sample was dried under reduced pressure at room temperature for 48 hours to fully remove residual solvent. The overall reaction scheme is depicted in figure 5. The proton NMR and IR characterization showed the characteriestic functional groups as summarized below.

^{1}H NMR for PS_{8K}-*b*-$P(E/B)_{25K}$-*b*-PI_{10K} functionalized with Brij surfactant side chains (300 MHz, $CDCl_3$, δ): 6.58, 7.10, (5H, styrene), 3.65 (br s, 40H, -(O$\mathbf{CH_2CH_2}$)$_{10}$-), 3.43 (t, 2H, –-(OCH_2CH_2)$_{10}$$\mathbf{CH_2}$($CH_2$)$_{17}$-); 0.82, 1.06, 1.23, 1.82 ($\mathbf{CH_3(CH_2)_{16}}$$CH_2$- of Brij 76 side chain, and back-bone). IR (dry film) υ_{max} (cm $^{-1}$): 3480 (O-H stretching); 2930, 2855 (C-H stretching); 1460, 1380 (C-H bending); 1115 (C-O stretching); 765, 700 (C-H bending, aromatic).

3.2.6 Etherification Attachment of Amphiphilic Pluronic Non-Ionic Surfactants

To produce ether-linked amphiphilic side chain surface active block copolymers, 2.1 g of epoxidized PS_{8K}-*b*-$P(E/B)_{25K}$-*b*-PI_{10K} (5.8 mmol of epoxide) was taken in a round bottom flask in conjunction with a three times molar excess (17.4 mmol) of the pluronic surfactant alcohol. The reactants were purged with argon, and subsequently dissolved in ca. ~ 150 mL of anhydrous chloroform. Activated molecular sieves were added to the reaction mixture and it was allowed to sit for ca. ~ 12 h to optimize the up-take of water. Etherification was performed through the addition of boron trifluoride diethyl etherate catalyst (0.345 g, 2.4 mmol) followed by vigorous stirring at room temperature for at least 72 hours. Following the reaction, 6.25 N sodium hydroxide was added to quench any residual boron catalyst and the reaction mixture was concentrated under reduced pressure using a rotary evaporator. The resultant SABC was precipitated into methanol and the white rubbery product was collected by filtration and subsequently reprecipitated twice from chloroform to remove additional residual amphiphilic surface active side-chain alcohol. Finally, the finished sample was dried under reduced pressure at room temperature for 48 hours to fully remove residual solvent. The overall reaction scheme is depicted in figure 5. The proton NMR characterization showed the characteriestic functional groups as summarized below.

^{1}H NMR for PS_{8K}-*b*-$P(E/B)_{25K}$-*b*-PI_{10K} functionalized with pluronic surfactant side chains (300 MHz, $CDCl_3$, δ): 6.54, 7.06, (5H, styrene); 3.61, 3.52 (br s, Protons of PEG and PPG), 3.37 (br, s, -CH_3 of PPG); 0.77-0.82, 1.02-1.60 (back-bone).

3.2.7 Etherification Attachment of "Mixed" Hydrophobic and Hydrophilic SABCs

To produce ether-linked side chain surface active block copolymers, 2.1 g of epoxidized PS_{8K}-*b*-$P(E/B)_{25K}$-*b*-PI_{10K} (5.8 mmol of epoxide) was taken in a round bottom flask in conjunction with a three times molar excess (17.4 mmol) of side-chain precursor alcohol (1-Octadecanol and/or PEG550). Five different mixtures of 1-Octadecanol relative to PEG550 were used in the feed to produce a range of different SABCs: 100% 1-Octadecanol /0% PEG550, 75% 1-Octadecanol/25% PEG550, 50% 1-Octadecanol/50% PEG550, 25% 1-Octadecanol/75% PEG550 and 0% 1-Octadecanol/100% PEG550. The reactants were purged with argon, and subsequently dissolved in ca. ~ 150 mL of anhydrous chloroform. Activated molecular sieves were added to the reaction mixture and it was allowed to sit for ca. ~ 12 h. Etherification was performed through the addition of boron trifluoride diethyl etherate catalyst (0.345 g, 2.4 mmol) followed by vigorous stirring at room temperature for at least 72 hours. Following the reaction, 6.25 N sodium hydroxide was added to quench any residual boron catalyst and the reaction mixture was concentrated under reduced pressure using a rotary evaporator. The resultant surface active triblock copolymers were precipitated into methanol. The SABCs were collected by filtration and subsequently reprecipitated twice from chloroform to remove additional residual surface active side-chain alcohol precursors. Finally, the finished samples were dried under reduced pressure at room temperature for 48 hours to fully remove residual solvent. The modification to the previously reported synthetic scheme is depicted in Figure 5. The proton NMR and IR characterization showed the characteriestic functional groups as summarized below.

^{1}H NMR for PS_{8K}-*b*-$P(E/B)_{25K}$-*b*-PI_{10K} functionalized with PEG550 side chains (300 MHz, $CDCl_3$, δ): 6.56, 7.08, (5H, styrene), 3.63 (br s, 4H –O**CH_2CH_2**O-); 3.38 (s, 3H, -O**CH_3**); 2.24 (s, 1H, -**OH**); 0.83, 1.06, 1.24, 1.80 (back-bone). IR (dry film) υ_{max} (cm $^{-1}$): 3350 (O-H stretching); 2935, 2865 (C-H stretching); 1455, 1375 (C-H bending); 1120 (C-O stretching); 700 (C-H bending, aromatic).

^{1}H NMR for PS_{8K}-*b*-$P(E/B)_{25K}$-*b*-PI_{10K} functionalized with 1-Octadecanol side chains (300 MHz, $CDCl_3$, δ): 6.57, 7.07, (5H, styrene), 3.50 (br m, 2H –O**CH_2**CH_2-); 0.5-1.85 (-OCH_2**$(CH_2)_{17}$**, back-bone).

3.2.8 Quaternization of Aminated PS-*b*-P(E/B)-*b*-PI with F8H4I

The synthetic scheme for this polymer is shown in figure 6. Aminated PS-*b*-P(E/B)-*b*-PI K4 (0.5 g, 1.02 mmol) was dissolved in 20 mL of DMF in a 100 mL round bottom flask. The mixture was heated to 90° C. The solution was purged with nitrogen for 30 minutes to degas, and F8H4I (1.8 g, 3.06 mmol) and potassium carbonate (0.14 g, 1.02 mmol) were added. The flask was sealed with a rubber septum and the quaternization was performed for 48 hours at 90° C under nitrogen atmosphere. The residual amine groups were further quaternized with iodomethane (0.14 g, 1.02 mmol) for 12 hours at 60° C. Roughly four-fifths of the DMF was removed by evaporation. The quaternized polymers were precipitated in excess diethyl ether, filtered, dissolved in 5 mL of DMF, reprecipitated in an excess of diethyl ether, filtered, and dried under reduced pressure at room temperature for 48 hours. ^{1}H NMR of quaternized polymers provided evidence of successful quaternization.

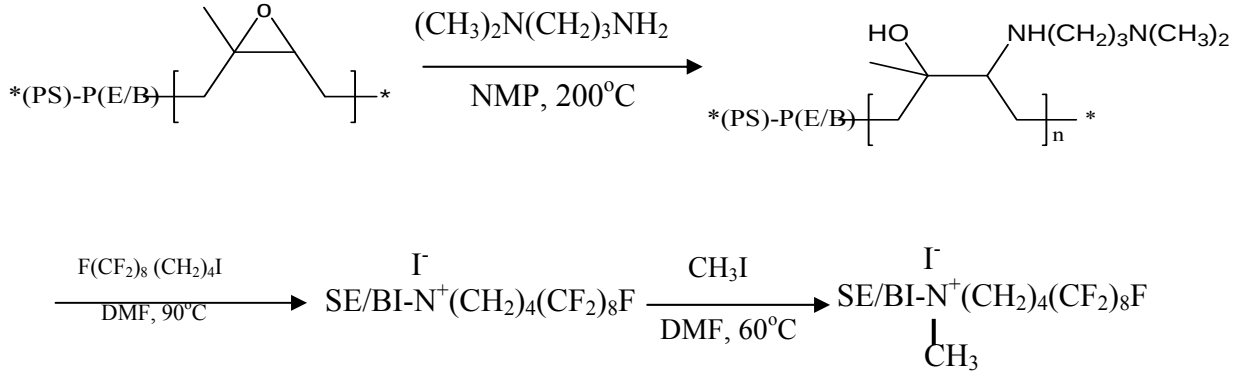

Figure 6: Synthesis of quaternized PS-*b*-P(E/B)-*b*-PI-F8H4I (SE/BI = PS-*b*-P(E/B)-*b*-PI).

3.2.9 Quaternization of Aminated PS-b-P(E/B)-b-PI with F8H6Br and H6Br

The synthesis was done as shown by the scheme in figure 7. Aminated PS_{8K}-*b*-$P(E/B)_{25K}$-*b*-PI_{20K} (0.4 g, 5.95 mmol of reactive amino and amine groups) was dissolved in 20 mL of DMF in a 100 mL round bottom flask at 90º C. F8H6Br (10.4 g, 17.9 mmol) and potassium carbonate (1.38 g, 10 mmol) were added to the reaction mixture. The flask was sealed with a rubber septum and the quaternization reaction was performed for 48 hours at 90º C under nitrogen atmosphere. The residual amine groups were further

quaternized with excess H6Br for 24 hours at 90 ºC. Following completion of the second quaternization, about 80 % of DMF was removed using a rotary evaporator under reduced pressure. The semifluorinated quaternized SABCs were precipitated in excess diethyl ether, filtered, dissolved in 5 mL of DMF, re-precipitated in excess diethyl ether, filtered, and dried under reduced pressure at room temperature for 48 hours. ^{1}H NMR and elemental analysis of the quaternized SABCs provided evidence of successful quaternization.

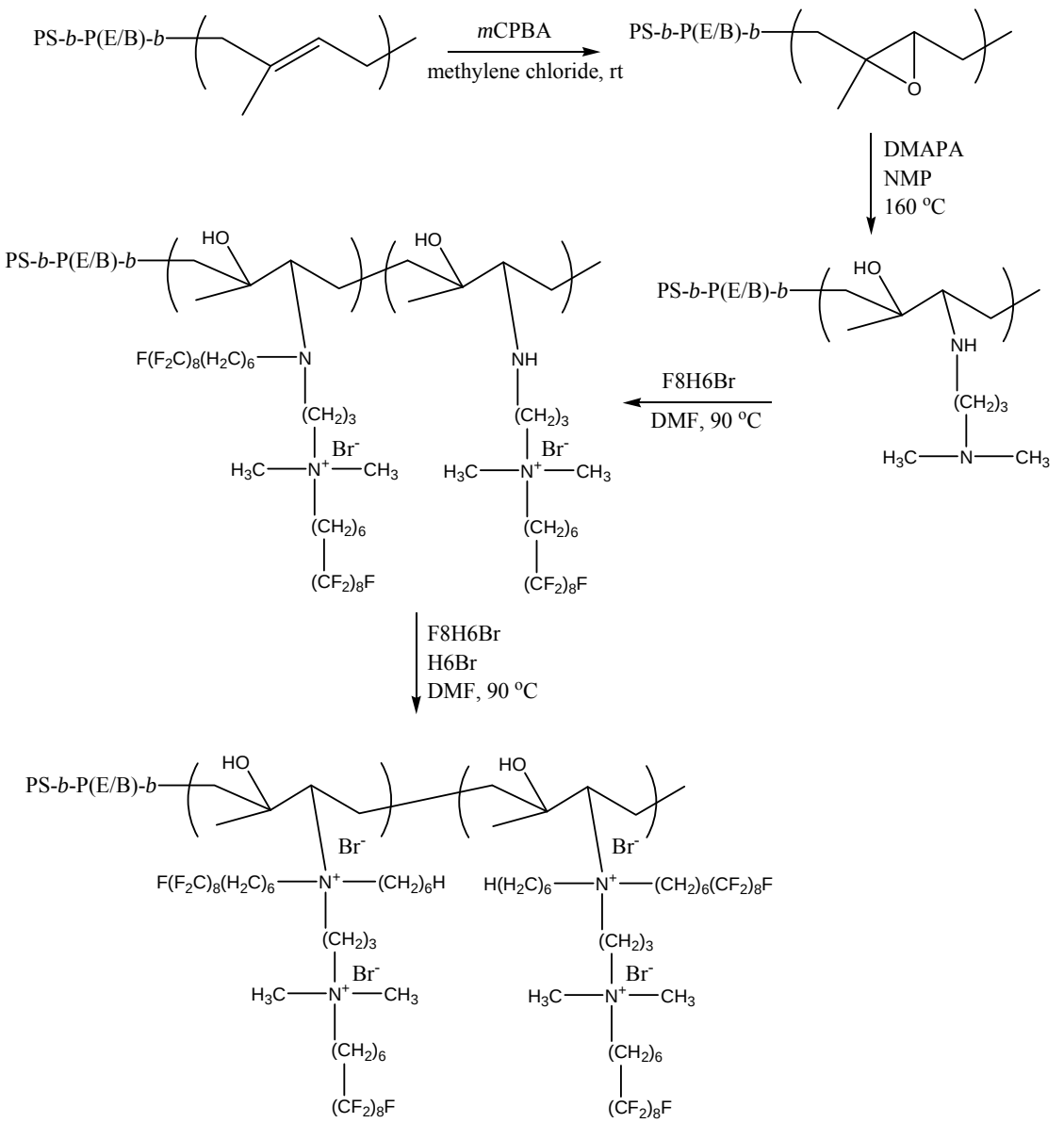

Figure 7: Schematic depicting synthesis of semifluorinated quaternized PS_{8K}-*b*-$P(E/B)_{25K}$-*b*-PI_{20K}.

The proton NMR and IR characterization showed the characteriestic functional groups as summarized below.

^{1}H NMR for PS_{8K}-*b*-$P(E/B)_{25K}$-*b*-PI_{10K} functionalized with PEG550 side chains (300 MHz, $CDCl_3$, δ): 6.56, 7.08, (5H, styrene), 3.63 (br s, 4H –O**CH_2CH_2**O-); 3.38 (s, 3H, -O**CH_3**); 2.24 (s, 1H, -**OH**); 0.83, 1.06, 1.24, 1.80 (back-bone). IR (dry film) υ_{max} (cm $^{-1}$): 3350 (O-H stretching); 2935, 2865 (C-H stretching); 1455, 1375 (C-H bending); 1120 (C-O stretching); 700 (C-H bending, aromatic). Elemental analysis: C (76.1 %), H (11.7 %).

^{1}H NMR for PS_{8K}-*b*-$P(E/B)_{25K}$-*b*-PI_{10K} functionalized with F10H10 side chains (300 MHz, $CDCl_3$, δ): 6.57, 7.07, (5H, styrene), 3.50 (br m, 2H –O**CH_2**CH_2-); 2.40 (br s, 2H –CH_2**CH_2**CF_2-); 0.82, 1.04, 1.24, 1.57, 2.03 (back-bone, -OCH_2**$(CH_2)_8$**CH_2CF_2). IR (dry film) υ_{max} (cm $^{-1}$): 3480 (O-H stretching); 2930, 2860 (C-H stretching); 1460, 1380 (C-H bending); 1220 (C-F stretching); 1090 (C-O stretching); 700 (C-H bending, aromatic). Elemental analysis: C (67.5%), H (9.4%), F (18.3%). Surface active block copolymers incorporating both types of side chain were found to have a blend of peaks that correlated to the amount of incorporation of each moiety.

3.3 Bulk Characterization of SABCs

3.3.1 Instrument details

NMR spectra were recorded on a Varian Gemini 400 MHz spectrometer. Infrared spectra were obtained using a Mattson on a 2020 Galaxy Series FTIR spectrometer. Wide-angle x-ray diffraction spectroscopy (WAXS) was performed on a SCINTAG θ/2θ diffractometer. The Ni-filtered Cu X-Ray tube (Kα = 1.5418) was operated at 45 kV and 40 mA. DSC was performed on a TA Q100, and the sample was heated to 150º C to remove thermal history, and then was cooled to -100º C at a rate of 10º C/minute. The sample was heated at a rate of 10º C/minute to 150º C, and the report data is from the second heating. Elemental analysis of the content of bromine and fluorine was performed by QTI.

3.3.2 Stress-Strain Analysis of SEBS Base Layers

Samples of the Kraton G1652 and Kraton MD6945 SEBS thermoplastic elastomers were pressed at 100 °C between teflon paper to 0.5 mm thickness and then cut into dog bones. The samples were then monotonically stretched to fracture using an Instron (Norwood, MA) 1123 testing machine. All stress-strain curves were recorded at room temperature. Elastic modulus values were estimated for each sample by examining the slope of the stress-strain curve in the elastic deformation region.

3.4 Formulation of SF Multilayer Coatings

3.4.1 For SABCs Prepared From Kraton Polymers K3 and K4

Glass slides were cleaned in hot piranha solution (concentrated sulfuric acid and 30 wt% hydrogen peroxide solution, 7:3 volume/volume), rinsed with distilled water, and blown dry using nitrogen. A 2% (w/v) solution of (3-glycidoxypropyl)-trimethoxysilane (GPS) in 95% ethanol (pH adjusted between 4.5 and 5 using acetic acid) was prepared by

adding the silane to the ethanol solution and stirring for 5 minutes. The slides were then soaked in this solution for at least 1 hour, rinsed with ethanol, and heated in an oven at 110° C for a minimum of 10 minutes. The GPS-functionalized glass slides were spin-coated with a toluene solution containing 5% (w/v) of MA-SEBS, and 2% (w/v) SEBS, and annealed in a vacuum-oven at 120° C for 12 hours. The styrene content of both SEBS and MA-SEBS was 30 wt%, and the latter had 1.4-2.0 wt % of grafted maleic anhydride. A noncatylzed epoxy-anhydride curing mechanism results in covalent attachment of the SEBS to the glass surface. The surfaces were further spin-coated three times with 12% (w/v) solution of SEBS in toluene (2500 rpm) followed by vacuum annealing at 120° C for 12 hours.

3.4.2 For Diblock Copolymer SABCs Prepared From PS-*b*-PAA

Poly(glycidyl methacrylate) was prepared by free radical polymerization of 35 g of glycidyl methacrylate in 150 mL of methyl ethyl ketone using AIBN (0.3695 g, 2.25 mmol) as initiator at 60º C. 10 mL of this polymer solution was diluted with 20 mL of ethyl methyl ketone, and blended with a solution containing 5% w/v each of SEBS (Kraton G1652) and SEBS with grafted maleic anhydride (Kraton FG1901x) in toluene. The GPS functionalized glass slides were coated with the blend, air dried and then coated again with a 10% w/v solution of SEBS. After drying at room temperature in a fume-hood, the slides were annealed at 125º C under vacuum for 2 hours. A 13 weight % solution of SEBS in toluene was spun coat successively two times, followed by a 12 hour drying under reduced pressure at 120º C.

3.4.3 Application of SABCs to the Base Layers

A schematic representation of the multilayers is shown in figure 8. In general, the SABCs were applied to the base layers by spray coating method using a 3 % w/v solution in appropriate solvents using a Badger model 250 airbrush (shown in figure 9) at 50 psi using nitrogen gas to obtain a SABC surface density of 1.5-2 mg/cm^2. PS-b-PAA-Amp and PS-b-PAA-PEG550 were spray coated from toluene solution and the PS-*b*-PAA-F8H2 polymer was applied using a 3.0% (w/v) solution in TFT. The K4 PS-*b*-P(E/B)-*b*-PI-F8H4I was applied using a 3.0% (w/v) solution in toluene. Finally the surfaces were subjected to a two-step annealing which involves annealing at 60 ºC for 24 h and 120 ºC for another 24 h under vacuum.

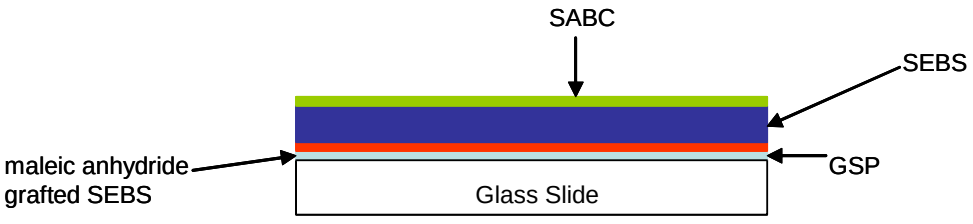

Figure 8: Schematic of the multilayer coatings prepared for small scale testing of our SABCs.

Functional polymer thin films on silicon wafer was performed by spin coating of the polymer solution on plain silicon wafer.

Figure 9: Device used for spray coating SABC on small scale test samples—Badger Model 250, single-action, external-mix, siphon-feed airbrush.

3.4.4 Fabrication of SABC Multilayer Coatings On Aluminum Test Panels

A six step process for fabricating multilayer coatings on 10" x 12" aluminum test panels was developed. First of all, the panels were machined in house at Cornell University by CCMR (Cornell Center for Materials Research). They were then shipped to Kraton Polymers in Houston, TX. Kraton handled the transport of the panels to Coating Engineerings, a commercial coating company. Here the panels were sandblasted and then spray-coated with a 25 micron layer of Amerlock 400 marine epoxy. At this point, the panels were quickly transported back to Kraton Polymer's facilities and coated ca. ~ 1 micron of MA-SEBS (Kraton FG1901X). Then, they were melt-pressed with 1 mm of SEBS (Kraton G1652) thermoplastic elastomer. Finally, the panels were shipped back to Cornell University where they were spray coated with a thin layer of SABC, roughly 1 micron in thickness. Preparation in these final steps is analogous to that used for mutilayer glass slides. The schematic depicting the panel fabrication technique previously used is depicted in figure 10.

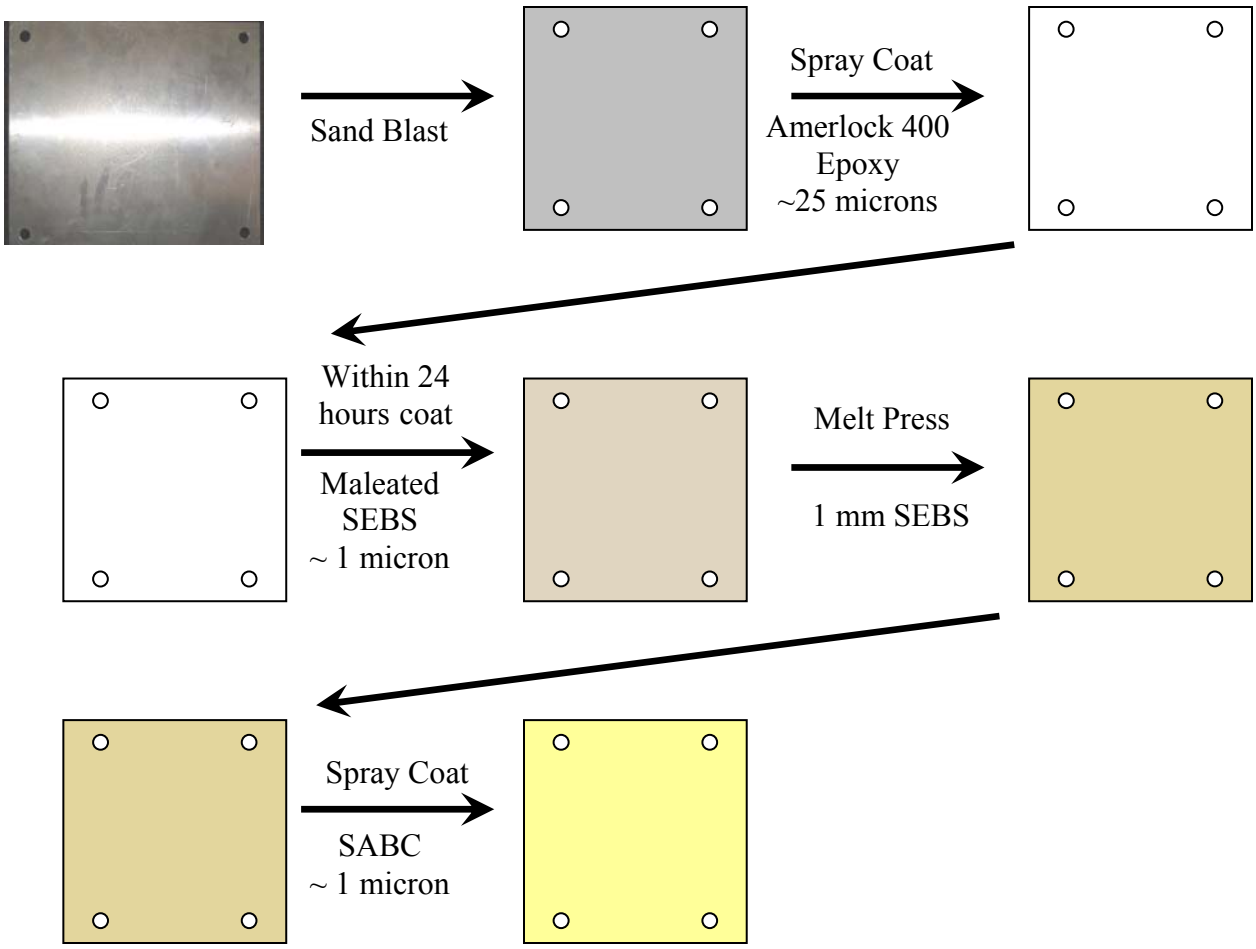

Figure 10. Schematic of the fabrication of large scale multi-layer coating test panels previously utilized.

Since Kraton Polymers left the project, an updated methodology has been developed. The panels are still being machined in house at Cornell University, however we are now doing the fabrication using the molds that Kraton previously produced. The panels are sandblasted to both clean them and increase surface roughness and subsequently dip coated in an ethanol solution of GPS, which imparts epoxy functionality to the native aluminum oxide layer on the panel. At this point they are spray coated with MA-SEBS from cyclohexane and subsequently compression molded with ca. ~ 1 mm of SEBS (the new, softer TPE base layer, Kraton MD6945). The final SABC application is as before by spray coating.

3.5 Surface Characterization of SABC Coatings

Surfaces for NEXAFS (near-edge X-ray absorption fine-structure) spectroscopy, XPS (X-ray photo electron spectroscopy) and dynamic water contact angle measurements were prepared on silicon wafers by spin-coating 3% (w/v) solutions of the SABCs in TFT. Multi-layer coatings on glass slides (through the same process used to prepare samples

for biofouling assays) were also analyzed in some cases. Surfaces were annealed for a minimum of 12 hours at 120° C under vacuum.

Contact angles were measured using a VCA Optima XE goniometer. These measurements were performed by depositing a roughly 2 μL droplet of water on the surface and then withdrawing it. The process can be recorded using a CCD camera taking 30 frames per second. Image analysis software is then used to calculate the advancing and receding contact angles based on the shape of the water droplet.

XPS measurements were performed using a Kratos Axis Ultra Spectrometer (Kratos Analytical, Manchester, UK) with a monochromatic Al Kα X-ray source (1486.6 eV) operating at 225 W under 1.0×10^{-8} torr. Charge compensation was carried out by injection of low-energy electrons into the magnetic lens of the electron spectrometer. The pass energy of the analyzer was set at 40 eV for high-resolution spectra and 80 eV for survey scans, with energy resolutions of 0.05 and 1 eV, respectively. The spectra were analyzed using CasaXPS v.2.3.12Dev4 software. The C-C peak at 285 eV was used as the reference for binding energy calibration.

NEXAFS experiments were carried out on the U7A NIST/Dow materials characterization end-station at the National Synchrotron Light Source at Brookhaven National Laboratory (BNL). The X-ray beam was elliptically polarized (polarization factor = 0.85), with the electric field vector dominantly in the plane of the storage ring. The photon flux was about $1x10^{11}$ photons per second at a typical storage ring current of 500 mA. A spherical grating monochromator was used to obtain monochromatic soft X-rays at an energy resolution of 0.2 eV. The C 1s NEXAFS spectra were acquired for incident photon energy in the range 270–320 eV. The angle of incidence of the X-ray beam, measured from the sample surface, was 50°. The partial-electron-yield (PEY) signal was collected using a channeltron electron multiplier with an adjustable entrance grid bias (EGB). Data was reported for a grid bias of -150 V. The channeltron PEY detector was positioned in the equatorial plane of the sample chamber and at an angle of 36° relative to the incoming X-ray beam. The PEY C 1s spectra were normalized by subtracting a linear pre-edge baseline and setting the edge jump to unity at 320 eV. The photon energy was calibrated by adjusting the peak position of the lowest π* phenyl resonance from polystyrene to 285.5 eV.

Intermittent contact mode (tapping mode) AFM images were obtained in water employing a MFP 3D microscope from Asylum Research, Santa Barbara, CA, USA and NBTC at Cornell University. V-shaped silicon nitride cantilevers purchased from Veeco (MLCT-AUNM) with spring constants in the range of ~ 0.5 N/m were used for the measurement.

BSA protein force adhesion measurements were obtained using a commercial AFM microscope (Asylum Research, molecular force probe MFP-3D Santa Barbara, CA). Bovine serum albumin (BSA) coated AFM tips (Novascan Technologies, Inc.) were used for all measurements exhibiting a nominal spring constant of ~50 pN/nm. Prior to measurements, the spring constant was determined using the thermal noise method (9). The resulting force-extension curves were analyzed with custom analysis software (Igor Pro, Wavemetrics). All experiments were carried out in deionized water (MilliQ 18 Ω) at room temperature.

A small number of force plots are obtained per tip as the AFM tips can get contaminated by the polymer which would affect the results. A total of 60 force plots were obtained for each AFM tip (20 for glass, 20 for PS-*b*-PAA-Amp and 20 for PDMS in the order mentioned). The results (histograms) are a summary of three BSA coated AFM tips used for the measurements.

4.0 Biofouling Tests

4.1 Leachate Toxicity Test on SABC Coatings

Leachate toxicity testing was performed by the Wendt Group at California Polytechnic State University. The experiment consisted of soaking the test-coatings (on glass slides) and glass-slide controls in 100mL of filtered seawater for 6 days. At 72 hour intervals, the seawater was replaced. 100 brine shrimp nauplii (shown in figure 11) were then exposed to this leachate, and their survival was monitored for two days. The mortality of the brine shrimp subjected to the experimental coating's leachate was compared to the mortality of the control solutions. This allowed us to gain insight into any possible physiological effects of chemicals leached into the seawater by the experimental coatings and confirm that they were indeed non-toxic—an important goal for this project.

Figure 11: Brine shrimp nauplii used in the leachate toxicity testing.

4.2 Biofouling Assay – Settlement of *Ulva* Spores and Release of *Ulva* Sporelings

James and Maureen Callow at the University of Birmingham, England provided testing of several of our series of SABC coatings for performance against *Ulva* spores and sporelings (shown in figure 12) (10, 11). Glass test slides for biofouling tests of the green alga *Ulva* were soaked in a 30 mL tank of recirculating deionized water at ~ 20 ^{o}C for 3 days. The slides were then placed in dishes containing artificial seawater 1 h prior to the start of the experiments. Fertile plants of *Ulva linza* were collected from Wembury Beach, England (50^{o}18' N; 4^{o}02' W). 10 mL of zoospore suspension (1×10^{6} spores per mL), prepared as described previously (10), was placed into 9 compartments of polystyrene culture dishes (Greiner Bio-One)—each containing a glass microscope test slide. The test slides were incubated in the dark at ~ 20 ^{o}C for 1 h and then washed in

seawater to remove zoospores that had not attached. The density of zoospores attached to the surfaces of 3 replicates was estimated as described in Hoipkemeier-Wilson *et al* (11). Glass slides coated with PDMSe and polystyrene-*b*-poly (ethylene-*ran*-butylene)-*b*-polystyrene (SEBS) were used as standards. The PDMSe surfaces were prepared as described previously.

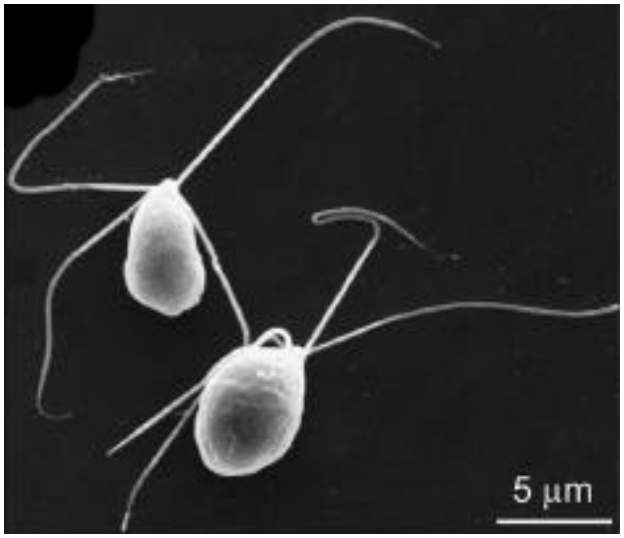

Figure 12: Micrograph of *Ulva* sporelings [10].

A water jet was used to measure strength of attachment of the sporelings. One of each of the six replicate slides was subjected to a single impact pressure by the water jet. A series of water pressures were used and the proportion of biomass removed was estimated using a fluorescence plate reader.

4.3 Biofouling Assay – Barnacle Settlement and Growth on SABC Coatings

Barnacle settlement and growth testing was also conducted by the Wendt group at California Polytechnic State University on several of our SABC coating series. Photograph of barnacle cypris larvae is shown in figure 13. The settlement assay consisted of placing a 0.4 mL drop of seawater containing 20-40 barnacle cypris larvae on the experimental coatings. The larvae were then allowed to settle for 72 hours, or until the settlement rate on glass and polystyrene control surfaces reached 50%. At this time, the number of barnacles that had settled on each surface was counted, and the settlement rate on the experimental coatings was compared with the settlement rates of the controls. Barnacles are then cultivated to a mature size (over two to four months) at which point their adhesion strength is determined by force gauge release testing (an individual barnacle is pushed with a force probe to measure its detachment force). This assay is used to determine anticipated hard-fouling release properties of our coating system.

Figure 13: Photograph of barnacle cypris larvae used in settlement and growth testing.

4.4 Biofouling Assay – Barnacle Grow Out and Release Testing on SABC Coatings

After settling on the glass slides as described previously, barnacle cyprid larvae are cultivated for two to four months until they mature to the appropriate size for force gauge removal testing. During removal force testing, the barnacle is first photographed. Digital image analysis is used to calculate the area of the barnacle's basal plate. The glass slide is then clamped into a force-gauge apparatus which consists of a force gauge mounted on a motorized test stand and a custom chamber that houses the slide immersed in seawater. This allows the shear force necessary to remove the barnacles to be measured in situ. The barnacles are removed with the force gauge, and maximum applied force is recorded. The critical removal stress (N/mm^2) is calculated and compared against other coatings, as well as control groups. If the barnacle's basal plate is partially removed, the remaining basal plate is photographed and the exact percentage remaining after testing is calculated with digital image analysis.

4.5 Biofouling Assay –Immersion Panel Testing of PS-*b*-PAA-Amp at Calpoly

10" x 12" large scale multi-layer coated aluminum test panels were prepared using the methodology previously detailed. PS-*b*-PAA-Amp was selected as the most desirable SABC to scale up from the PS-*b*-PAA derived SABCs due to its good performance in lab biofouling assays relative to soft fouling settlement and release (*Ulva* and *Navicula*) and barnacle settlement. Three test panels were prepared and annealed at 60° C for 72 hours. Additionally, a SEBS panel (no SABC top coat) was sent to Calpoly to act as a control. The samples were immersed in Calpoly's estuarine site at Morro Bay and the biofouling community present on the panels was monitored for roughly a six month period (the panels were photographed at regular intervals and the images were analyzed using image analysis software to determine what species of fouling were present). Barnacle force gauge release testing was conducted in a method analogous to that described above and water jet testing was also performed at four months into testing

to see what critical water pressure was needed to remove the fouling (we added this assay to our initial plan, thus why it was only performed once).

4.6 Biofouling Assay – Immersion Panel testing of PS-*b*-PAA-Amp at FIT

10" x 12" large scale multi-layer coated aluminum test panels with PS-*b*-PAA-Amp as the SABC were also sent to FIT for field exposure testing at their marine site. Similarly, a SEBS control panel was sent along for testing. The four panels were exposed at the Florida Institute of Technology static immersion site in the Indian River Lagoon on August 10, 2007. All panels were held ~1 meter below the surface. Panels were placed back to back on a frame. The panels were placed such that two panels faced north and two faced south. After 1 month, the frames were removed from the water and digital photos were taken of the frames and the individual panels. The panels were exposed for a second month during which time they became heavily fouled. Barnacle adhesion was then tested by applying shear force with a force gauge.

4.7 Antibacterial Assay – Cell Growth on SF Quaternized PS_{8K}-*b*-$P(E/B)_{25K}$-*b*-PI_{20K}

Bacterial cell growth assays were conducted on semifluorinated quaternized PS_{8K}-*b*-$P(E/B)_{25K}$-*b*-PI_{20K} SABCs to test for antimicrobial character. 100 μL of *Staphylococcus aureus (S. aureus)* was incubated in Trypticase Soy Broth (TSB, 5 mL; per liter: 3 g of soy meal peptone, 17 g of casein peptone, 2.5 g of glucose, 5 g of NaCl, and 2.5 g of dipotassium hydrogen phosphate) at 37 °C for 4 h. The cells were centrifuged at 5000 rpm for 1 min using a microcentrifuge (Eppendorf 5415C), and the precipitate was resuspended in 1 mL of sterile filtered water.

Cobetia marina (C. marina) (ATTC 25374) was grown overnight in broth from a single isolated colony from a plate. Difco marina broth and Difco marine agar were used for growth. The cells were inoculated into fresh marine broth (100 uL into 4.9 ml) and grown for 5 hours. Then, 1 mL of exponential culture was placed in an Eppendorf tube, spun down at max speed for a clinical centrifuge and resuspended in 1 mL of sterile water.

4.8 Antibacterial Assay – Colony Counts on SF Quaternized PS-*b*-P(E/B)-*b*-PI

Bacterial colony count assays were conducted on semifluorinated quaternized PS_{8K}-*b*-$P(E/B)_{25K}$-*b*-PI_{20K} SABCs to further test for antimicrobial character. Aqueous suspensions of *S. aureus* with concentrations of ~10^6 cells/mL were sprayed on the test surfaces, dried in air for 2 min and placed in sterile Petri dishes. They were covered by Molten agar-containing TSB (1.5 % w/v of agar), allowed to solidify and then incubated at 37º C overnight. The number of bacterial colonies was counted using a colony counter.

4.9 Live/Dead Baclight Bacterial Viability on SF Quaternized PS-*b*-P(E/B)-*b*-PI

Finally, Live/Dead Baclight bacterial viability analysis was also conducted on semifluorinated quaternized PS_{8K}-*b*-$P(E/B)_{25K}$-*b*-PI_{20K} SABCs. A Live/Dead Bacterial Viability Kit was obtained from Molecular Probes, Inc. Equal volumes of SYTO 9 and propidium iodide were mixed thoroughly in a microcentrifuge tube. The BacLight dye mixture (30 μL) was added to 1 mL of the cell suspension, which was then sprayed on the test surfaces. Immediately after the spraying, the test surfaces were covered with glass coverslips, sealed with finger nail polish to avoid desiccation, and incubated in the dark for 15 min. Phase-contrast and fluorescence microscopy were performed, within 1hr after spraying, using an Olympus BX61 epifluorescence microscope with a 100× UPlanApo (N.A.135) objective. The microscope was equipped with filter cubes for viewing SYTO 9 and PI fluorescence. Glass microscope slides were used as controls.

4.10 Protein Adsorption Testing on Mixed Amphiphilic PS-*b*-P(E/B)-*b*-PI SABCs

Figure 14 depicts the methodology used for protein adsorption testing of bovine serum albumin (BSA) on mixed amphiphilic surfaces derived from PS_{8K}-*b*-$P(E/B)_{25K}$-*b*-PI_{20K} SABCs. A drop of artificial sea water containing 100 μg BSA per mL of water was placed on a silicon wafer coated with the SABC. The droplet was left in contact with the surface for 1 hour and then fluorescence microscopy of the four different mixed amphiphilic samples was performed and compared relative to a SEBS control.

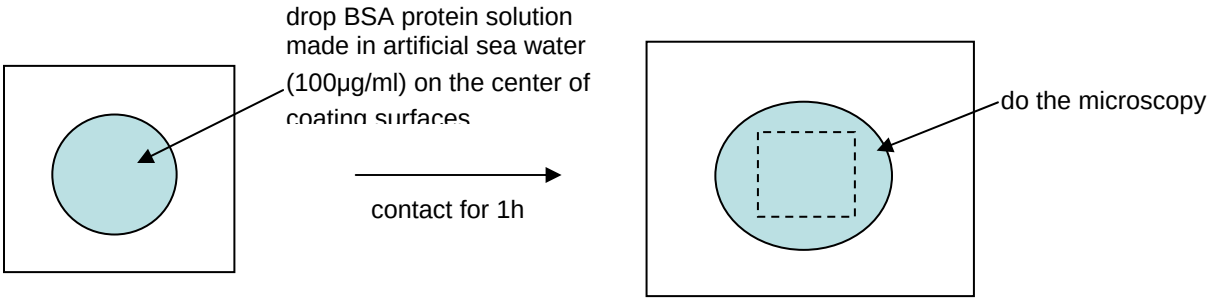

Figure 14. Schematic depicting methodology for carrying out protein adsorption testing on mixed amphiphilic surfaces of PS_{8K}-*b*-$P(E/B)_{25K}$-*b*-PI_{20K} SABCs.

5.0 Accomplishments and Results

5.1 Synthesis and Characterization

5.1.1 Synthesis and Characterization of Semifluorinated SABCs Prepared from SBS

A series of SABCs were synthesized using bromination and subsequent substitution onto SBS precursor polymer. The reaction was followed on a step by step basis using ^{1}H NMR and FTIR when appropriate. NMR indicated roughly a 97%

conversion of the SBS precursor polymer to brominated SBS (Figure 15). FTIR analysis of the reaction products after attachment of the semifluorinated side chain showed the presence of C-F bonding, supporting the reaction having occurred. Quantitative analysis was performed on the finished SABC materials to determine the degree of conversion in attaching the semifluorinated side chains (Table 2).

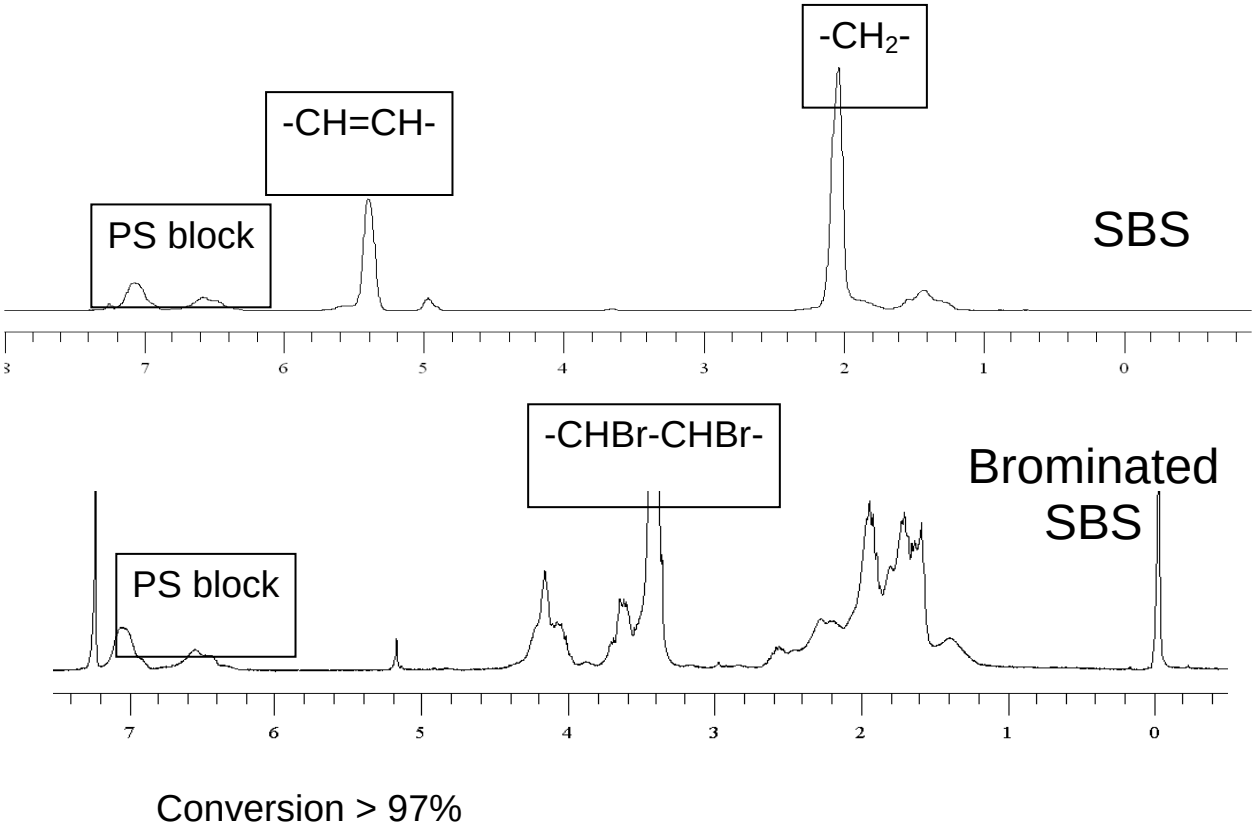

Figure 15: NMR Spectra showing the conversion of SBS precursor polymer into brominated SBS.

Table 2: Quantitative analysis results of weight percent fluorine contained in SBS-Br-F8H2 and SBS-Br-F10H2 polymers synthesized. SBS-Br-F8H2 and SBS-Br-F10H2 represent theoretical 100% side chain attachment weight percents.

Sample	Br %	F %
SBS-Br	65	0
SBS-Br-F8H2	12.8	51.8
SBS-Br-F8H2-12	32.1	12.1
SBS-Br-F8H2-47	15.4	47.2
SBS-H-F8H2-20	7.8	20.1
SBS-Br-F10H2	11.0	69.2
SBS-Br-F10H2-10	44.1	10.1
SBS-Br-F10H2-52	9.5	52.1

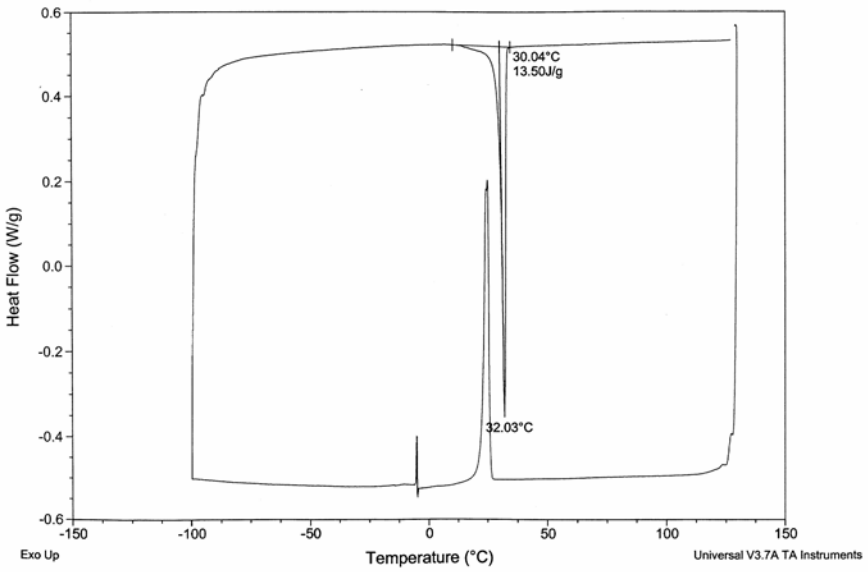

Figure 16: Differential scanning calorimetry of SBS-Br-F8H2 polymer. The polymer was taken through a heating and cooling cycle at a temperature ramp rate of 10 °C/minute.

Subsequent characterization and testing was performed on SBS-Br-F8H2-47 (which will simply be referred to as SBS-Br-F8H2) since this product was obtained from a successful scale up. DSC analysis of this sample showed the presence of a liquid crystalline transition at roughly 32° C (Figure 16).

5.1.2 Diblock SABCs Synthesis and Characterization

A diblock copolymer, PS-*b*-PAA, was used as a precursor for the synthesis of SABC. PS_{38K}-*b*-PAA_{3K} derived samples were primarily characterized by ^{1}H NMR. FT IR was used at times to support NMR data, but ^{1}H NMR was the predominant method of choice to quantify side chain attachment. This was done by integrating the known intensity of aromatic protons of PS at 6.6 and 7.1 δ versus specific protons in the side chain. For PS_{38K}-*b*-PAA_{3K}-Amp, side chain attachment was found to be on the order of 80%. A similar degree of attachment was seen for the PEG550 and F8H2 functionalized samples.

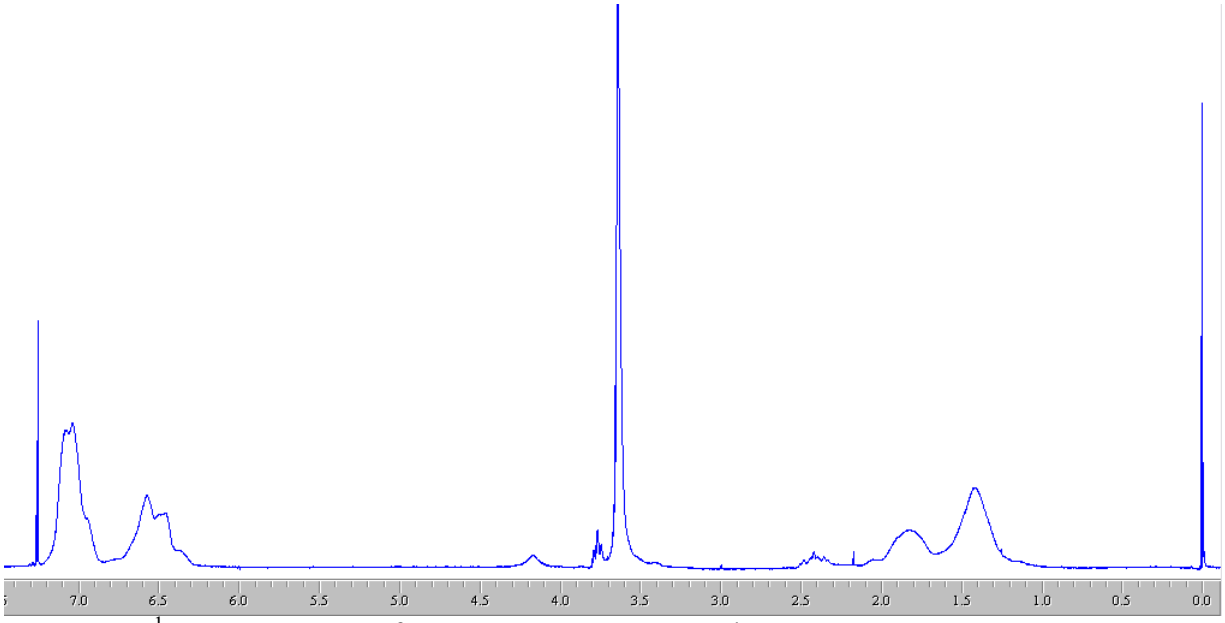

Figure 17: ^{1}H NMR spectra of PS_{38K}-*b*-PAA_{3K}-Amp. polymer.

The peak values of ^{1}H NMR in figure 17 can be assigned as follows: 6.6 and 7.1 (5H, styrene); 4.18 (br s, 2H, -$COOCH_2$-); 3.77 (t, 2H, -$COOCH_2CH_2$-); 3.64 (br s, -OCH_2CH_2O-); 2.42 (m, 2H, -CH_2CF_2-); 1.85, 1.43 (back-bone).

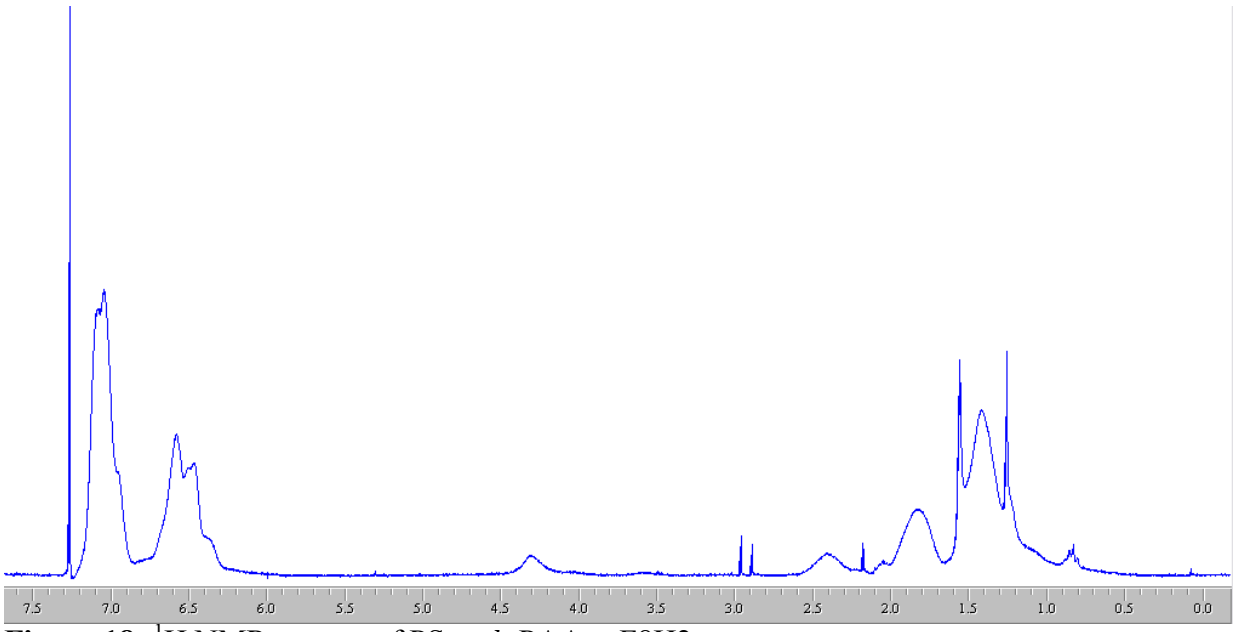

Figure 18: ^{1}H NMR spectra of PS_{38K}-*b*-PAA_{3K}-F8H2.

The peak values of ^{1}H NMR (figure 18) are assigned as follows: 6.6 and 7.1 (5H, styrene); 4.31 (br s, 2H, -$COOCH_2$-);2.42 (br s, -CH_2CF_2-), 1.86, 1.45 (back-bone).

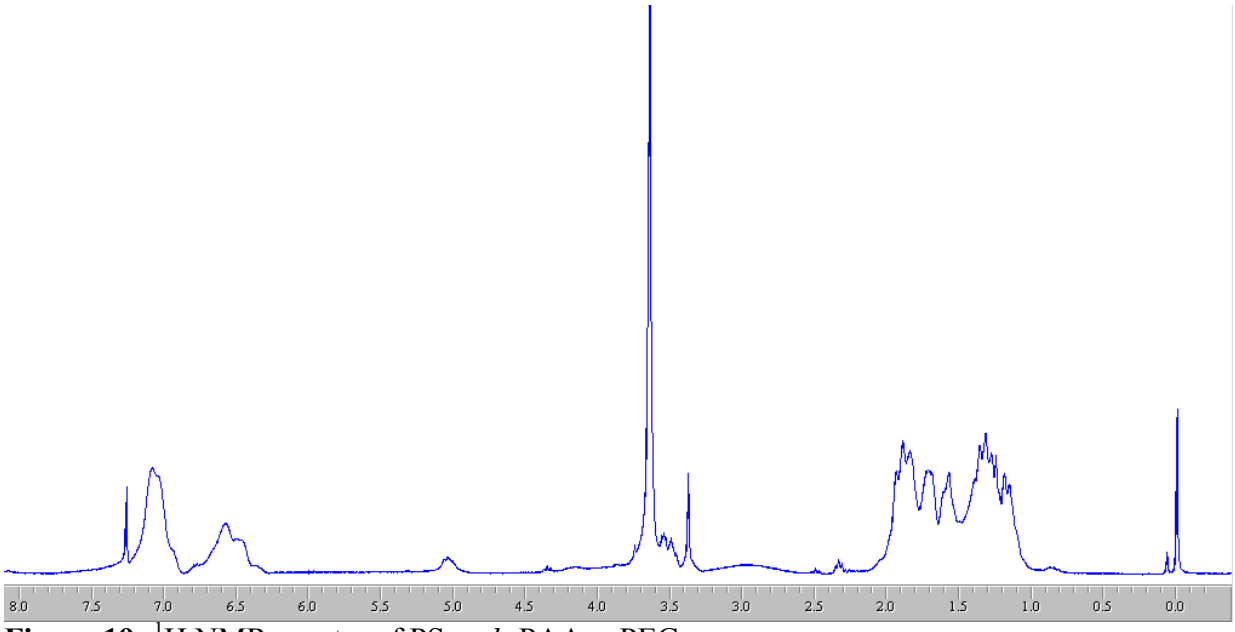

Figure 19: ^{1}H NMR spectra of PS_{38K}-*b*-PAA_{3K}-PEG.

The peak values of ^{1}H NMR (figure 19) are assigned as follows: 6.6 and 7.1 (5H, styrene); 4.18 (br s, 2H, -$COOCH_2$-); 3.65 (br s, -OCH_2CH_2O-); 3.46 (s, -OCH_3); 1.79, 1.39 (back-bone).

^{1}H NMR spectroscopy of K3 PS-*b*-P(E/B)-*b*-PI-Amp polymers was also performed to quantify attachment of side chains. The attachment was on the order of 50% has been demonstrated as found by the NMR shown in figure 20.

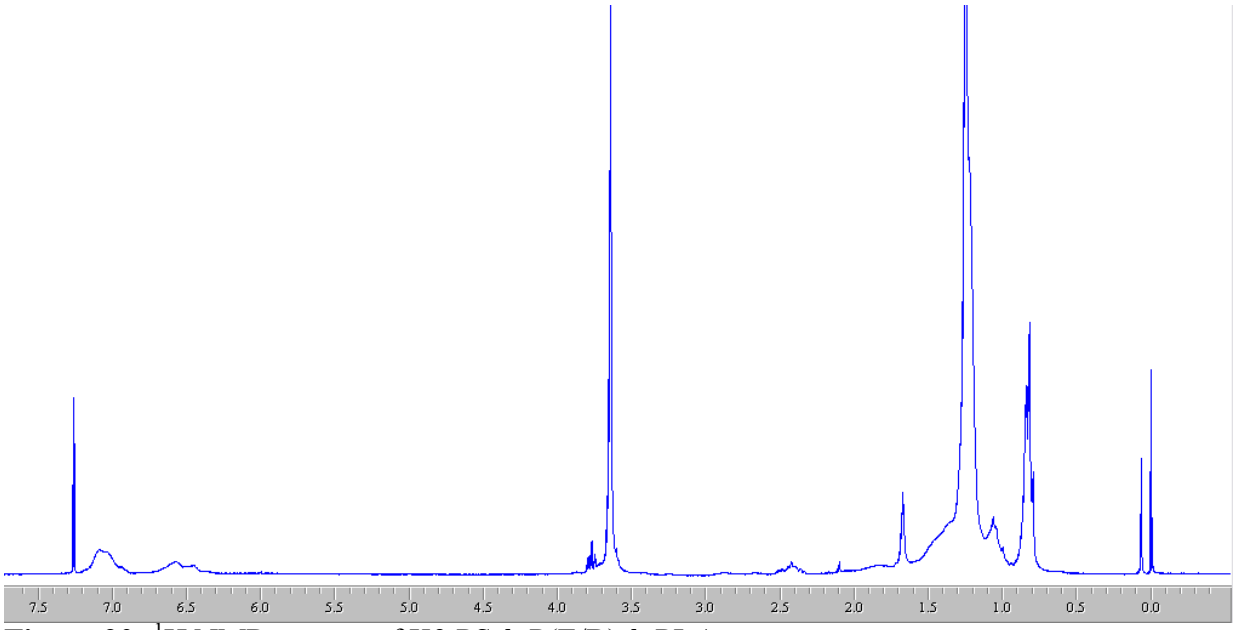

Figure 20: ^{1}H NMR spectra of K3 PS-*b*-P(E/B)-*b*-PI-Amp.

The δ values of ^{1}H NMR in figure 20 can be assigned as follows: 6.6 and 7.1 (5H, styrene); 3.65 (br s, -OCH_2CH_2O-); 1.65, 1.25, 0.82 (back-bone).

5.1.3 Triblock PS-*b*-P(E/B)-*b*-PI SABCs: Synthesis and Characterization

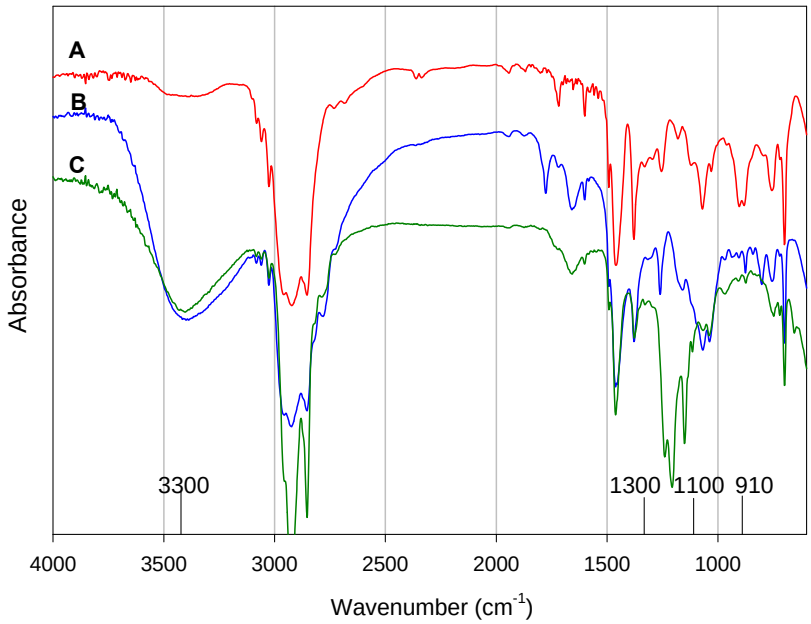

Figure 21: FT-IR spectra of (A) epoxidized K4 PS-*b*-P(E/B)-*b*-PI, (B) aminated K4 PS-*b*-P(E/B)-*b*-PI, and (C) quaternized K4 PS-*b*-P(E/B)-*b*-PI-F8H4I.

Figure 21 shows the FT-IR spectra of modified K4 PS-*b*-P(E/B)-*b*-PI-F8H4I polymers. Before the amination was performed, the specific peak of epoxy was observed at circa 910 cm^{-1} (Figure 21A). The epoxy peak disappeared after a 48 hour amination with

DMAPA at 200°C and the strong stretching vibration at circa 3300 cm^{-1} of amine and hydroxyl gained greatly in intensity (Figure 21B). The appearance of C-F peaks between 1100 and 1300 cm-1 (Figure 21C) demonstrated the attachment of F8H4I fluorinated groups by quaternization of aminated PS-*b*-P(E/B)-*b*-PI. Elemental analysis performed by QTI demonstrated 18.1 wt % of fluorine in the finished polymer.

Table 3 summarizes percent attachment of side chains relative to epoxidized isoprene and also gives advancing and receding water contact angle measurements. In general, the high advancing angle (122°) of PS_{8K}-*b*-$P(E/B)_{25K}$-*b*-PI_{10K}-F10H10 suggests the presence of the semifluorinated side chains at the surface. The higher than expected advancing contact angle (87°) of PS_{8K}-*b*-$P(E/B)_{25K}$-*b*-PI_{10K}-PEG550 demonstrates the segregation of the PS block to the surface of the sample. Finally, the large contact angle hysteresis (107° to 26°) of the PS_{8K}-*b*-$P(E/B)_{25K}$-*b*-PI_{10K}-Amp confirms its amphiphilic nature.

Table 3. Table depicting the attachment percentages and advancing and receding water contact angle measurements for amphiphilic PS_{8K}-*b*-$P(E/B)_{25K}$-*b*-PI_{10K}-Amp, hydrophilic PS_{8K}-*b*-$P(E/B)_{25K}$-*b*-PI_{10K}-PEG550, and hydrophobic PS_{8K}-*b*-$P(E/B)_{25K}$-*b*-PI_{10K}-F10H10.

SABC	% Attachment Relative to Isoprene	Contact Angles Adv. (°), Rec. (°)
PS-b-P(E/B)-b-PI-Amp	46	107±2, 26±2
PS-b-P(E/B)-b-PI-PEG550	47	87±2, 28±2
PS-b-P(E/B)-b-PI-F10H10	50	122±2, 53±3

5.1.4 Semi Fluorinated Quaternized PS-*b*-P(E/B)-*b*-PI Synthesis and Characterization

Figure 22 shows the IR spectra of PS_{8K}-*b*-$P(E/B)_{25K}$-*b*-PI_{20K}, epoxidized PS_{8K}-*b*-$P(E/B)_{25K}$-*b*-PI_{20K}, aminated PS_{8K}-*b*-$P(E/B)_{25K}$-*b*-PI_{20K}, and semifluorinated quaternized PS_{8K}-*b*-$P(E/B)_{25K}$-*b*-PI_{20K} (SQTC-F8H6Br-H6Br). All IR spectra show the C-H bending vibrations associated with the styrene phenyl ring at 700 cm^{-1}. After the epoxidation reaction, an absorption peak at 875-900 cm^{-1}, indicating the presence of the epoxy groups was observed (Figure 22B). This epoxy peak disappeared after the 48 h amination with DMAPA at 160 ºC, whereas the strong stretching vibration of amine and hydroxyl were present around 3300-3600 cm^{-1} (Figure 22C) implying that the epoxy groups were consumed by the amination. Using elemental analysis, it was determined that the aminated PS-*b*-P(E/B)-*b*-PI contained 5.7 % nitrogen content, corresponding to 59.6 % of amination based on the 245 epoxy groups present in the epoxidized PS_{8K}-*b*-$P(E/B)_{25K}$-*b*-PI_{20K}. The quaternization reaction with F8H6Br and H6Br resulted in the appearance of fluorine peaks at 1100-1300 cm^{-1} (Figure 22D) indicating successful attachment of fluorine groups.

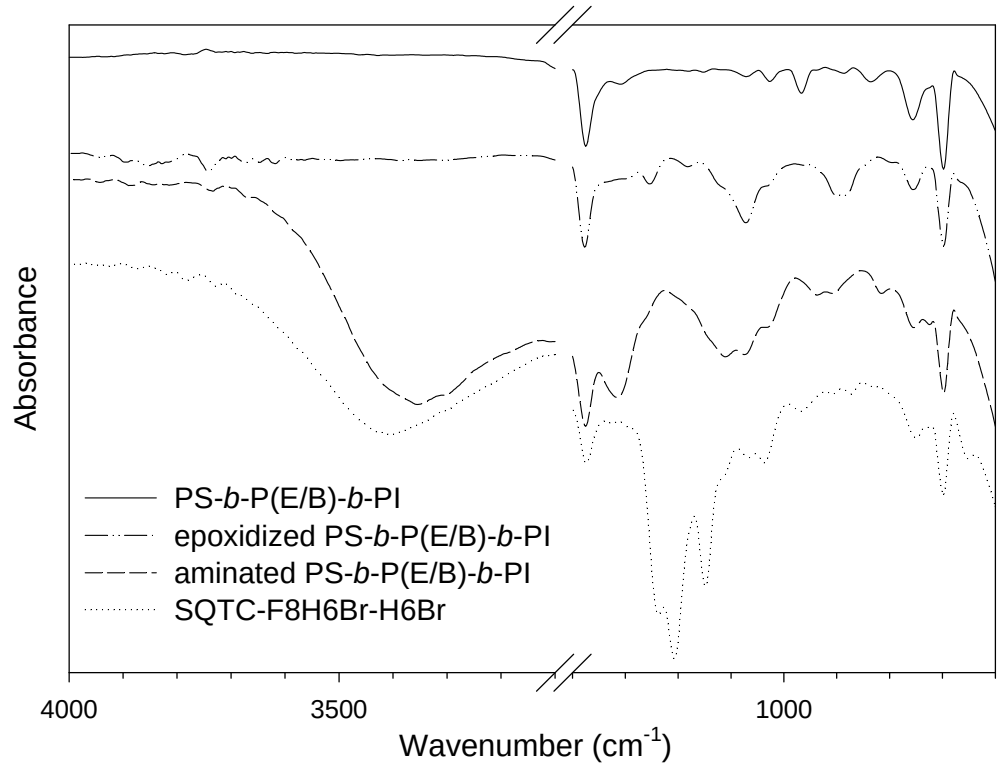

Figure 22. FT-IR spectra of (A) PS_{8K}-*b*-$P(E/B)_{25K}$-*b*-PI_{20K}, (B) epoxidized PS_{8K}-*b*-$P(E/B)_{25K}$-*b*-PI_{20K}, (C) aminated PS_{8K}-*b*-$P(E/B)_{25K}$-*b*-PI_{20K}, and (D) semifluorinated quaternized PS_{8K}-*b*-$P(E/B)_{25K}$-*b*-PI_{20K}, SQTC-F8H6Br-H6Br.

5.1.5 Mixed Amphiphilic PS-*b*-P(E/B)-*b*-PI SABCs: Synthesis and Characterization

Table 4 demonstrates the relative feed ratios of F10H10OH and PEG550 alcohols used in the catalyzed etherification reactions of PS_{8K}-*b*-$P(E/B)_{25K}$-*b*-PI_{20K} to produce mixed amphiphilic SABCs. Attachment of the F10H10 surface active group was determined by elemental analysis. The percent weight of fluorine was found and then estimated attachment was determined by back calculating this value relative to what it would have been if 100% of the epoxy sites in the epoxidized PS_{8K}-*b*-$P(E/B)_{25K}$-*b*-PI_{20K} precursor had been functionalized with F10H10OH. Attachment of PEG550 meanwhile was determined by integration of the characteristic ^{1}H NMR peaks for -OCH_2CH_2O- relative to those associated with the aromatic ring of the polystyrene block. Total attachment of side groups for these reactions was found to be on the order of 20 to 30% relative to epoxy. Dynamic water contact angle results are also listed and demonstrate the steadily decreasing hydrophobicity as one moved from 80% F10H10OH to 20% F10H10OH in the feed. Significant contact angle hysteresis was experienced for all four samples.

Figure 23 shows the IR spectra of mixed amphiphilic PS_{8K}-*b*-$P(E/B)_{25K}$-*b*-PI_{20K} SABCs produced by varying the feed ratio of F10H10OH and PEG550 alcohols during

catalyzed etherification reactions. All IR spectra show the characteristic C-H bending vibrations associated with the styrene phenyl ring at 700 cm^{-1}. Of particular note is the differing intensity of the C-F peaks at ca. 1250 cm^{-1} versus the R-O-R peaks at ca. 1100 cm^{-1}. A clear increase in relative intensity of these peaks relative to the feed ratio used in each of the four reactions can be readily identified.

Table 4. Relative feed ratios of mixed amphiphilic derived SABCs produced from catalyzed etherification reactions of PS_{8K}-*b*-$P(E/B)_{25K}$-*b*-PI_{20K} are given along with the attachment results of both the F10H10OH and PEG550 alcohols. Finally, advancing and receding dynamic water contact angle results are given in the final column.

Feed Ratio		Attachment		Contact Angles	
PEG550	F10H10	PEG550	F10H10	Adv. (°)	Rec. (°)
20 %	80 %	6.50 %	17.20 %	128 ± 4	67 ± 4
40 %	60 %	13.30 %	8.86 %	124 ± 2	54 ± 2
60 %	40 %	18.10 %	5.30 %	118 ± 4	48 ± 3
80 %	20 %	27.50 %	2.50 %	103 ± 5	28 ± 3

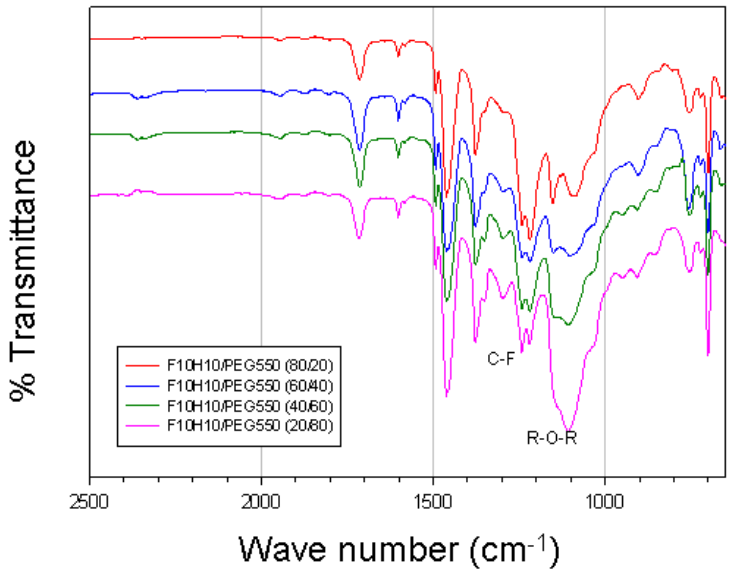

Figure 23. FT-IR spectra of mixed amphiphilic derived SABCs produced from catalyzed etherification reactions of PS_{8K}-*b*-$P(E/B)_{25K}$-*b*-PI_{20K}. Feed ratio of F10H10OH versus PEG550 alcohol is indicated by key. Primary points of interest are the C-F peak ca. 1250 cm^{-1} and the R-O-R peak at ca. 1100 cm^{-1}.

5.1.6 Synthesis and Characterization of PS_{8k}-*b*-$P(E/B)_{25k}$-*b*-PI_{10k} Functionalized with Ethoxylated Fluoroalkyl Surfactant Side Chains

This SABC synthesis is very similar to that of PS_{8k}-*b*-$P(E/B)_{25k}$-*b*-PI_{20k}. The synthesis of the ether-linked side chain SABC with pendent ethoxylated fluoroalkyl groups was followed using both infrared spectroscopy and ^1H NMR spectroscopy. Following the epoxidation reaction, ^1H NMR spectroscopy clearly showed that there was no longer evidence of any protons associated with unsaturated alkene groups on the polymer back-bone, and a significant peak at ca. ~ 2.7 ppm appeared indicating the presence of protons adjacent to the newly formed oxirane rings on the polyisoprene back-bone. Additionally, infrared spectroscopy clearly showed the appearance of a C-O-C stretching peak at roughly 880 cm^{-1} associated with the epoxide ring. This indicated that most of the residual unsaturated alkene groups were successfully converted to their epoxidized form. Subsequent catalytic ring-opening using ethoxylated fluoroalkyl alcohol led to the disappearance of the epoxide proton peak in the ^1H NMR spectra. Further analysis of the ^1H NMR spectra showed the appearance of peaks at ca. ~ 2.4, 3.6 and 3.8 ppm for the Zonyl functionalized sample demonstrating successful attachment of the side groups. These findings were supported by infrared spectroscopy which demonstrated the appearance of a strong C-O stretching peak at ca. ~ 1125 cm^{-1} indicating formation of ether and alcohol groups from ring opening of the epoxy in conjunction with a strong C-F stretching peak at ca ~ 1220 cm^{-1} suggesting the presence of the semifluorinated amphiphilic side chain moieties.

The percentage of attachment of ethoxylated fluoroalkyl side chain was estimated by ^1H NMR integration. Specifically, this was done by comparing the total amount of aromatic protons (associated with the PS block) in the ^1H NMR spectra with the number of protons associated with the PEGylated section of the amphiphilic side chain. The number of repeat units associated with the PEGylated section of the attached Zonyl ethoxylated fluoroalkyl side chains were checked in an analogous fashion to and confirmed to be similar to those previously reported. This analysis suggested attachment of side chains on the order of ca. ~ 45% relative to epoxy functionality. Using GPC, the polydispersity of the sample was found to increase from 1.06 for the PS-*b*-P(E/B)-*b*-PI precursors to ca. ~ 1.12 for its epoxidized form. Finished, substituted SABC samples containing ethoxylated fluoroalkyl side chains were found to have PDI values of ca. ~ 1.3. This rise in polydispersity combined with the observation of complete reaction of the epoxide despite less than 100% attachment suggested that some of the epoxide was most likely lost to intermolecular cross linking reactions. Additionally, intramolecular reactions in combination with epoxide ring-opening by any residual water molecules left in the reaction mixture may have contributed to this lowered observed attachment. Since this work spanned several batches of polymers, chemical characterization for each batch was done independently. Nevertheless, chemical analysis demonstrated very similar results from batch to batch. Thus values given here are representative of the several samples tested.

5.1.7 Synthesis and Characterization of PS_{8k}-*b*-$P(E/B)_{25k}$-*b*-PI_{10k} Functionalized with PEG 550 and F10H10OH Mixture

The synthesis (as in Figure 5) of a series of amphiphilic SABCs containing mixed discrete hydrophobic semifluorinated side-chains and hydrophilic PEGylated side chains was closely followed using both infrared spectroscopy and ^{1}H NMR. Following the epoxidation reaction, ^{1}H NMR studies clearly showed that there was no longer evidence of any alkene protons, and a significant peak at ca. ~ 2.7 ppm appeared indicating the presence of protons adjacent to the newly formed oxirane rings on the PI backbone. Additionally, infrared spectroscopy clearly showed the appearance of a C-O-C stretching peak at roughly 880 cm^{-1} associated with the epoxide ring. This indicated that all of the residual unsaturated alkene groups were successfully converted to their epoxidized form. Subsequent catalytic ring-opening using F10H10OH and/or PEG550 alcohols led to the disappearance of the epoxide peak in the ^{1}H NMR spectra. Further analysis of the ^{1}H NMR spectra demonstrated the appearance of peaks at ca. ~ 3.3 and 3.6 ppm for the PEG550 functionalized sample in conjunction with the appearance of a peak at ca. ~ 3.5 ppm for the F10H10OH functionalized sample demonstrated successful attachment of the side groups. These findings were supported by infrared spectroscopy which demonstrated the appearance of a strong C-O stretching peak at 1120 cm^{-1} for samples functionalized with PEG550 and a strong C-F stretching peak at 1200 cm^{-1} for samples functionalized with F10H10OH. For mixed samples functionalized with both moieties, peak intensity generally varied with the amount of incorporation of the side chain.

Table 5. The percentage of attachment of PEG550 and F10H10OH and fluorine content for both series of SABCs produced from different molar ratios of F10H10OH and PEG550 in the reaction feed.

PS_{8K}-*b*-$P(E/B)_{25K}$-*b*-PI_{10K} Precursor						
Feed % F10H10	Feed % PEG550	Attach % F10H10	Attach % PEG550	Overall Attachment	Weight % F	Nomenclature
0	100	0	33	33	0	PS_{8K}-b-$P(E/B)_{25K}$-b-PI_{10K}-0F-33P
20	80	22	27	49	8.4	PS_{8K}-b-$P(E/B)_{25K}$-b-PI_{10K}-22F-27P
40	60	19	28	47	6.9	PS_{8K}-b-$P(E/B)_{25K}$-b-PI_{10K}-19F-28P
50	50	24	24	48	9.2	PS_{8K}-b-$P(E/B)_{25K}$-b-PI_{10K}-24F-24P
60	40	28	19	47	10.4	PS_{8K}-b-$P(E/B)_{25K}$-b-PI_{10K}-28F-19P
80	20	41	13	54	15.2	PS_{8K}-b-$P(E/B)_{25K}$-b-PI_{10K}-41F-13P
100	0	50	0	50	18.3	PS_{8K}-b-$P(E/B)_{25K}$-b-PI_{10K}-50F-0P

Table 5 demonstrates the percentage of attachment of PEG550 and F10H10OH for each different molar feed ratio for the PS-*b*-P(E/B)-*b*-PI precursor. The percentage of PEG550 and F10H10OH successfully attached was calculated by ^{1}H NMR integration and elemental analysis of fluorine, respectively. Specifically, the percent attachment of PEG550 was obtained by comparing the total amount of aromatic protons (associated with the PS block) in the ^{1}H NMR spectra with the number of protons associated with the PEG side chain. Meanwhile, the weight percent of fluorine obtained by elemental analysis allowed the determination of F10H10OH attachment by comparing this value to that which would have been obtained assuming 100% attachment. The attachment of both

PEG550 and F10H10OH generally depended on the molar ratios in the feed, and the overall attachment relative to epoxidized isoprene was generally between 33 and 54% for the PS_{8K}-*b*-$P(E/B)_{25K}$-*b*-PI_{10K} precursor. Using GPC, the polydispersity of the samples was found to increase from 1.06 for both of the PS-*b*-P(E/B)-*b*-PI precursors to ca. ~ 1.12 for their epoxidized forms. Finished, substituted SABC samples containing F10H10 and/or PEG550 side chains generally had a polydispersity between 1.2 and 1.3.

5.1.8 Synthesis and Characterization of PS-*b*-P(E/B)-*b*-PI Functionalized with Brij Non-Ionic Surfactant Side Chains

This synthesis is also similar to that of the fluorinated/PEG SABC with Brij being used instead of F10H10OH/PEG. The synthesis of the ether-linked side chain SABC with Brij non-ionic surfactant was followed by using infrared spectroscopy and ^{1}H NMR spectroscopy. Following the epoxidation reaction, ^{1}H NMR spectroscopy clearly showed that there was no longer evidence of any protons associated with unsaturated alkene groups on the polymer back-bone, and a significant peak at ca. ~ 2.7 ppm appeared indicating the presence of protons adjacent to the newly formed oxirane rings on the polyisoprene back-bone. Additionally, infrared spectroscopy clearly showed the appearance of a C-O-C stretching peak at roughly 880 cm^{-1} associated with the epoxide ring. This indicated that most of the residual unsaturated alkene groups were successfully converted to their epoxidized form. Subsequent catalytic ring-opening using Brij non-ionic surfactant alcohol led to the disappearance of the epoxide peak in the ^{1}H NMR spectra. Further analysis of the ^{1}H NMR spectra demonstrated the appearance of peaks at ca. ~ 3.6 and 3.4 ppm indicating the presence of oligoethylene glycol groups for the Brij functionalized sample, indicating successful attachment of the amphiphilic side chain. These findings were supported by infrared spectroscopy which demonstrated the appearance of a strong O-H stretching peak between 3300 and 3500 cm^{-1}, formed during ring-opening of the epoxy, and a C-O stretching peak at ca ~ 1115 cm^{-1}, formed from the etherification attachment of side chains.

Table 6. Attachment, PDI, and elemental analysis of the triblock copolymer with grafted amphiphilic side chains.

Compounds	ROH (SABC)	Attachment (%)	PDI	Elemental Analysis		
				C%	H%	O%
PEG.BE	$C_4H_9(OCH_2CH_2)_nOH$, n~4	40.0	1.55	77.70	11.62	10.68
Brij 30	$C_{12}H_{25}(OCH_2CH_2)_4OH$	36.53	1.48	78.67	11.75	9.58
Brij 72	$C_{18}H_{37}(OCH_2CH_2)_nOH$, n~2	45.71	1.29	78.97	11.93	9.10
Brij 76	$C_{18}H_{37}(OCH_2CH_2)_nOH$, n~10	37.63	1.24	76.43	11.57	12.00
Brij 78	$C_{18}H_{37}(OCH_2CH_2)_nOH$, n~20	28.46	1.16	73.52	11.24	15.24
Brij 97	$C_{18}H_{35}(OCH_2CH_2)_nOH$, n~10	35.48	1.68	74.67	11.32	14.85

The percent attachment of the Brij side chain was estimated by ^{1}H NMR integration. Specifically, this was done by comparing the total amount of aromatic protons (associated with the PS block) in the ^{1}H NMR spectra with the number of protons associated with the PEGylated section of the amphiphilic side chain. The attachment was found to be between 25 - 45% relative to epoxy functionality. Using GPC, the polydispersity of the polymer was found to increase from 1.06 for the PS-*b*-P(E/B)-*b*-PI precursors to ca. ~ 1.12 for its epoxidized form. Finished, substituted SABC samples containing Brij side chains were found to have PDI values from 1.16 to 1.68 (Table 6).

5.1.9 Synthesis and Characterization of PS-*b*-P(E/B)-*b*-PI Functionalized with Pluronic Non-Ionic Surfactant Side Chains

The synthesis of the ether-linked side chain SABC with Pluronic non-ionic surfactant was followed using ^{1}H NMR spectroscopy. Following the epoxidation reaction, ^{1}H NMR spectroscopy clearly showed that there was no longer evidence of any protons associated with unsaturated alkene groups on the polymer back-bone, and a significant peak at ca. ~ 2.7 ppm appeared indicating the presence of protons adjacent to the newly formed oxirane rings on the polyisoprene back-bone. Subsequent catalytic ring-opening using Pluronic non-ionic surfactant alcohol led to the disappearance of the epoxide peak in the ^{1}H NMR spectra. Further analysis of the ^{1}H NMR spectra demonstrated the appearance of peaks at ca. ~ 3.6 and 3.4 ppm indicating the presence of oligoethylene glycol groups for the Pluronic functionalized sample, indicating successful attachment of the amphiphilic side chain. The percent attachment of the Pluronic side chain was estimated by ^{1}H NMR integration. Specifically, this was done by comparing the total amount of aromatic protons (associated with the PS block) in the ^{1}H NMR spectra with the number of protons associated with the PEGylated section of the amphiphilic side chain. The attachment of side chains was found to be of the order of ca. ~ 30% relative to epoxy functionality.

5.1.10 Polymer Synthesis and Characterization of PS-*b*-P(E/B)-*b*-PI Functionalized with "Mixed" Hydrophobic and Hydrophilic Side Chains

The synthesis of a series of amphiphilic SABCs containing mixed hydrophobic alkyl side-chains and hydrophilic PEGylated side chains was closely followed using ^{1}H NMR spectroscopy. Following the epoxidation reaction, ^{1}H NMR studies clearly showed that there was no longer evidence of any alkene protons, and a significant peak at ca. ~ 2.7 ppm appeared indicating the presence of protons adjacent to the newly formed oxirane rings on the PI backbone. Subsequent catalytic ring-opening using 1-Octadecanol and/or PEG550 alcohols led to the disappearance of the epoxide peak in the ^{1}H NMR spectra. Further analysis of the ^{1}H NMR spectra demonstrated the appearance of peaks at ca. ~ 3.3 and 3.6 ppm for the PEG550 functionalized sample in conjunction with the appearance of a peak at ca. ~ 3.5 ppm for the 1-Octadecanol functionalized sample demonstrated successful attachment of the side groups.

5.1.11 Determination of Elastic Modulus for SEBS Base Layers

Since there are two types of SEBS polymers available it was decided to test their elastic modulus and to find whether the difference in elastic modulus, if any, can be used as an advantage for biofouling release. Figure 24 shows the measured stress-strain curves for the Kraton G1652 and Kraton MD6945 SEBS thermoplastic elastomers. Kraton G1652 was found to have a measured elastic modulus (E) of ca. ~ 18 MPa while the measured value of E for Kraton MD6945 was an order of magnitude less, ca. ~ 1.2 MPa. This demonstrates that MD6945 has a modulus much closer to that of PDMS, which is dependent on degree of polymerization and crosslinking, but is reported to be between 1.4-3.0 MPa for the commercial PDMS elastomers RTV11 and Intersleek.

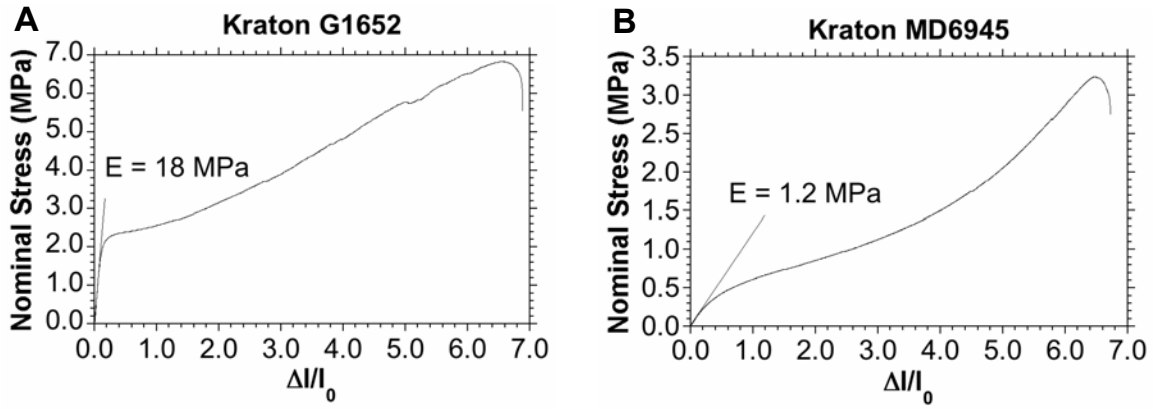

Figure 24. Measured stress-strain curves for SEBS thermoplastic elastomers A) Kraton G1652 and B) Kraton MD6945. Young's Modulus (E) values are estimated from the slope of the stress-strain curve during elastic deformation.

All the initial experiments were performed with G1652 base layer and later when Kraton supplied the soft elastomer, MD6945, it was used as the base layer.

5.2 Surface Characterization Results of Multilayer Coatings

5.2.1 Surface Characterization of Semifluorinated SABCs Prepared from SBS

Figure 25 shows the NEXAFS spectra of surfaces prepared by spray-coating the SBS-Br-F8H2 polymer directly on a silicon substrate followed by annealing in vacuum at two different temperatures. Also shown in the figure is the NEXAFS spectrum of the surface that was not annealed. The $\sigma^*_{C\text{-}F}$ resonance at 293 eV photon energy indicated the presence of the fluorinated block within approximately 3 nm of the the surface. NEXAFS spectra of spray-coated bilayer coatings (on a SEBS substrate) showed similar features (Figure 26).

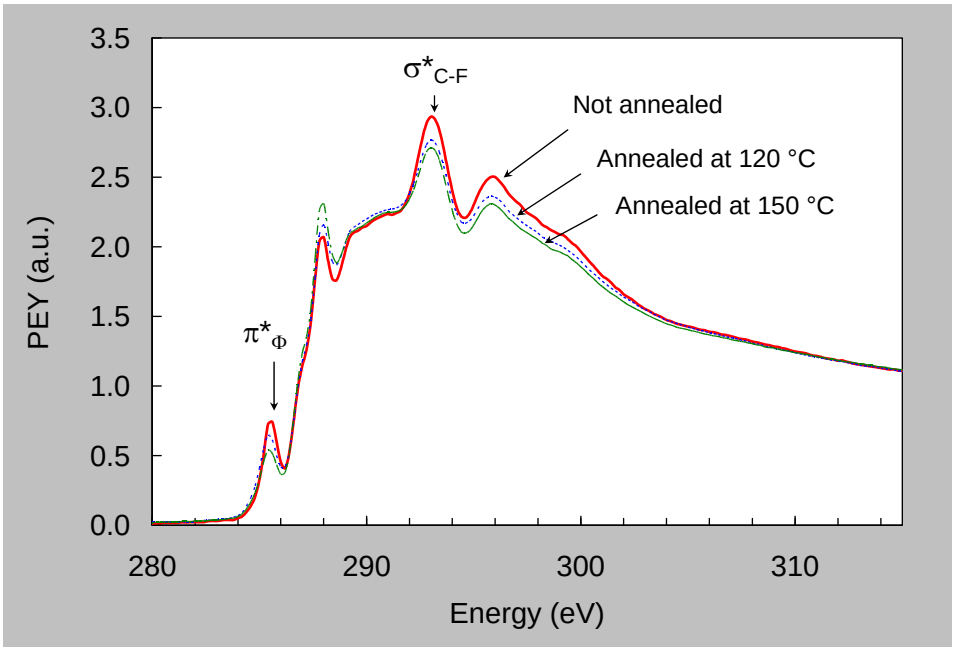

Figure 25: NEXAFS spectra of SBS-Br-F8H2 polymer spray-coated on silicon wafer and annealed at two different temperatures: 120° C and 150° C. The peak at 293 eV corresponding to C 1s $\rightarrow \sigma^*_{C\text{-}F}$ resonance is characteristic of a fluorinated surface. All spectra were acquired at X-ray incidence angle of 55°.

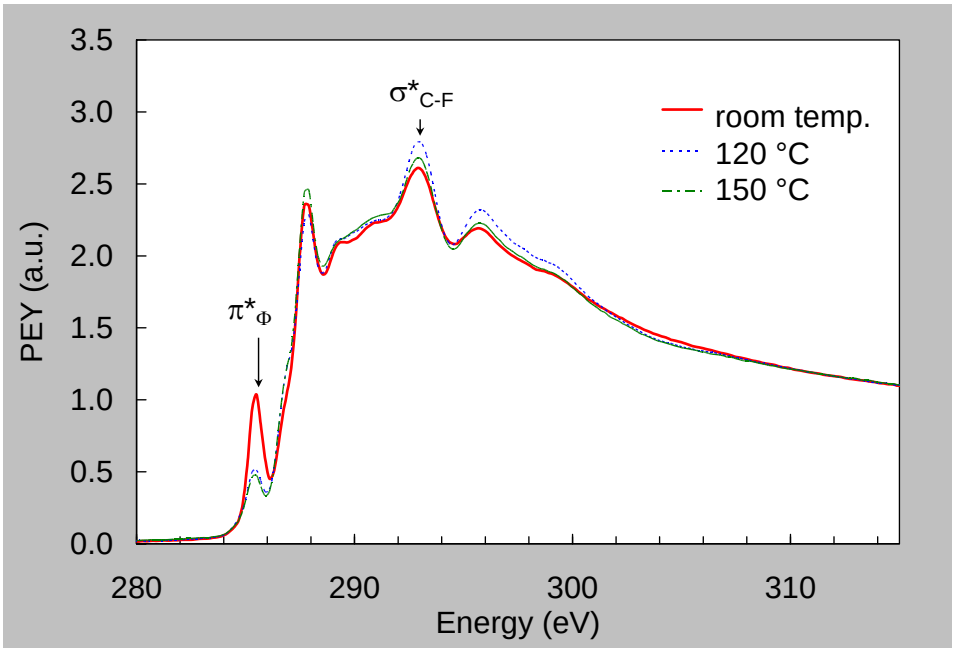

Figure 26: NEXAFS spectra of SBS-Br-F8H2 polymer spray-coated on a SEBS substrate and annealed at two different temperatures: 120 °C and 150 °C. The peak at 293 eV corresponding to C 1s → $\sigma^*_{C\text{-}F}$ resonance is characteristic of a fluorinated surface.

The XPS spectra of the spin-coated and spray-coated surfaces, shown in Figures 27 and 28, respectively, also indicated the presence of CF_2 and CF_3 groups within a few nanometers of the top of the surface.

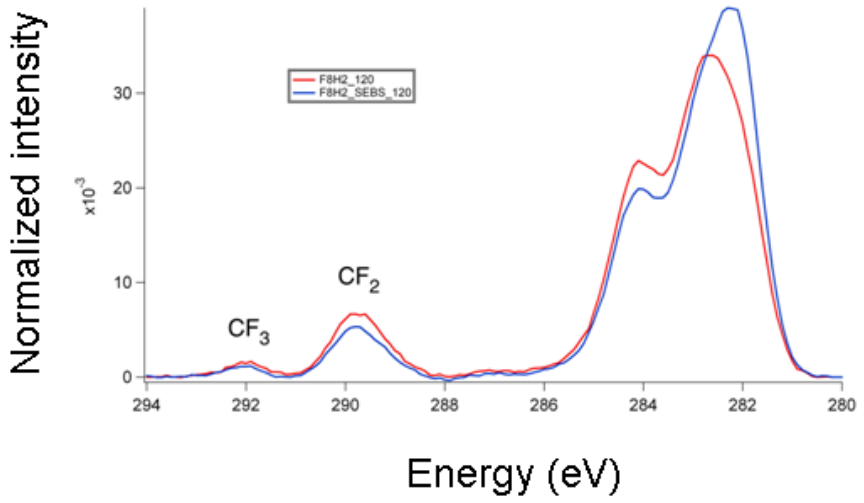

Figure 27: SBS-Br-F8H2 polymer spin-coated on silicon and SEBS substrates and annealed at 120 °C.

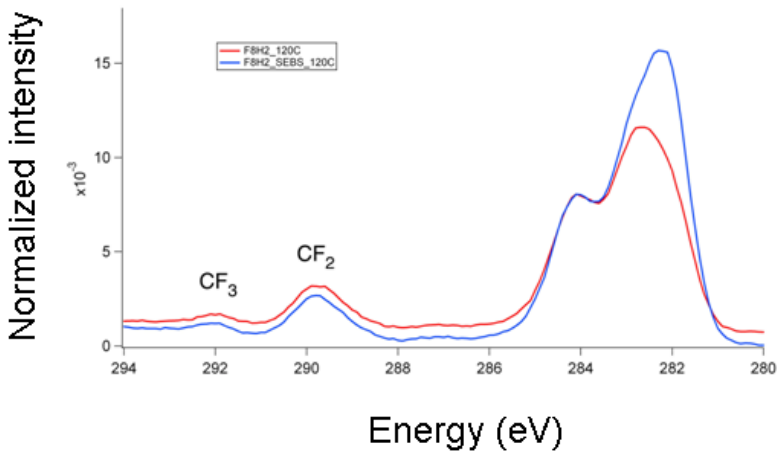

Figure 28: SBS-Br-F8H2 polymer spray-coated on silicon and SEBS substrates and annealed at 120 °C.

The NEXAFS spectrum for this polymer is shown in figure 29. An unexpected lowering of the $\sigma^*_{C\text{-}F}$ resonance (with a corresponding increase in the π^*_{Φ} resonance) was observed on annealing the surfaces at high temperatures under high vacuum (~ 10^{-8} torr). This is possibly due to incomplete conversion of the brominated butadiene block. Because of higher surface-energy, the residual C-Br bonds could drag the entire butadiene block (to which the fluorinated side-chains are attached) into the bulk, causing the surface to be primarily occupied by the lower energy PS block. Furthermore, inefficient attachment of the fluorinated side-chains, resulting in their removal from the surface under high-vacuum and high temperature, is another potential reason for the observed change in surface composition upon annealing. Due to this the process was repeated to increase the percent attachment and other types of SABCs were developed.

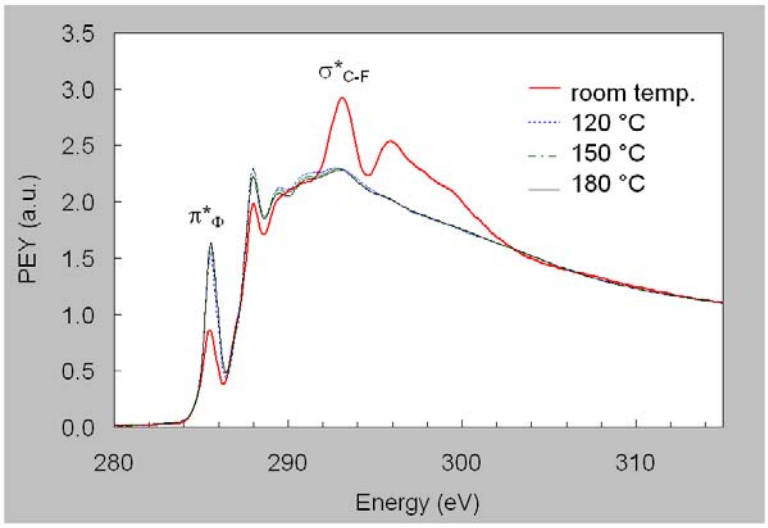

Figure 29: The NEXAFS spectra of a SBS-Br-F8H2 polymer spin-coated on silicon wafer and annealed under high-vacuum at temperatures of 120° C, 150° C and 180° C.

5.2.2 Surface Characterization of SABCs derived from PS-*b*-PAA

Contact angle analysis on spin coated surfaces of PS_{38K}-*b*-PAA_{3K}-Amp on silicon found $\theta_{w,adv}$ = 86±2° and $\theta_{w,rec}$ = 41±2°. This was similar to previously observed contact angles for amphiphilic surfaces and suggests rapid surface reorganization in the presence of water. PS_{38K}-*b*-PAA_{3K}-F8H2 meanwhile exhibited $\theta_{w,adv}$ = 121±1° and $\theta_{w,rec}$ = 71±1°, suggesting a hydrophobic, fluorinated surface. Typical contact angles for K3 PS-*b*-P(E/B)-*b*-PI-Amp are on the order of $\theta_{w,adv}$ = 99±1° and $\theta_{w,rec}$ = 25±3°.

Figure 30 shows the C 1s partial electron yield NEXAFS spectra of the block copolymer surfaces spin-coated on silicon. The $PS_{38k}PAA_{3k}$-F8H2 surface exhibited the characteristic C 1s → $\sigma^*_{C\text{-}F}$ peak, arising from the C atoms of the perfluorooctyl groups of the side chains. The surfaces with PEG and amphiphilic PEGylated fluoroalkyl (Zonyl) side-groups showed NEXAFS spectra similar to those we have previously seen as part of our related ONR project. It should be noted that although all three surface-active polymers were prepared from the same PS_{38k}-*b*-PAA_{3k} precursor, and had the same PS block molecular weight, the intensity of the C 1s → π^*_{Φ} peak at 285.5 eV was the lowest for the $PS_{38k}PAA_{3k}$-F8H2 surface and the highest for the $PS_{38k}PAA_{3k}$-PEG550 surface. This can be attributed to surface segregation of the low-surface-energy fluorinated block in the former, displacing the higher surface energy PS block from the surface. The $PS_{38k}PAA_{3k}$-Zonyl surface also showed a similar surface-segregation of the fluoroalkyl groups, resulting in a lower π^*_{Φ} signal compared to the $PS_{38k}PAA_{3k}$-PEG550 surface. Because the surface energy of PEG is slightly higher than that of PS, we expect a preferential presence of PS at the surface of $PS_{38k}PAA_{3k}$-PEG550.

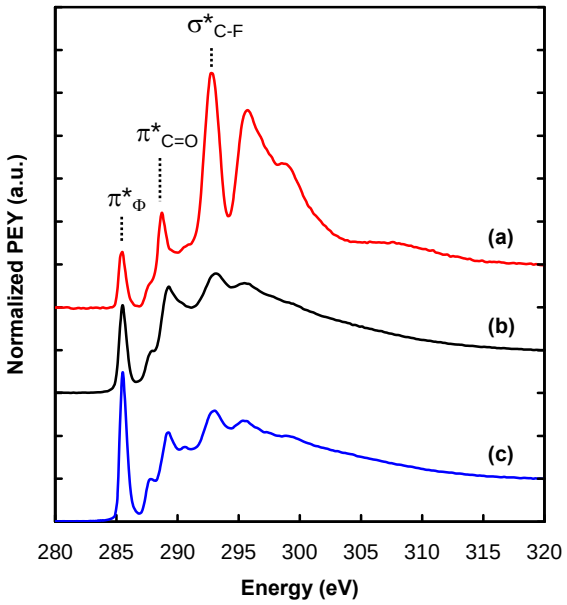

Figure 30. C 1s NEXAFS spectra of (a) PS_{38k}-*b*-PAA_{3k}-F8H2, (b) PS_{38k}-*b*-PAA_{3k}-Ampl, and (c) PS_{38k}-*b*-PAA_{3k}-PEG550 block copolymers.

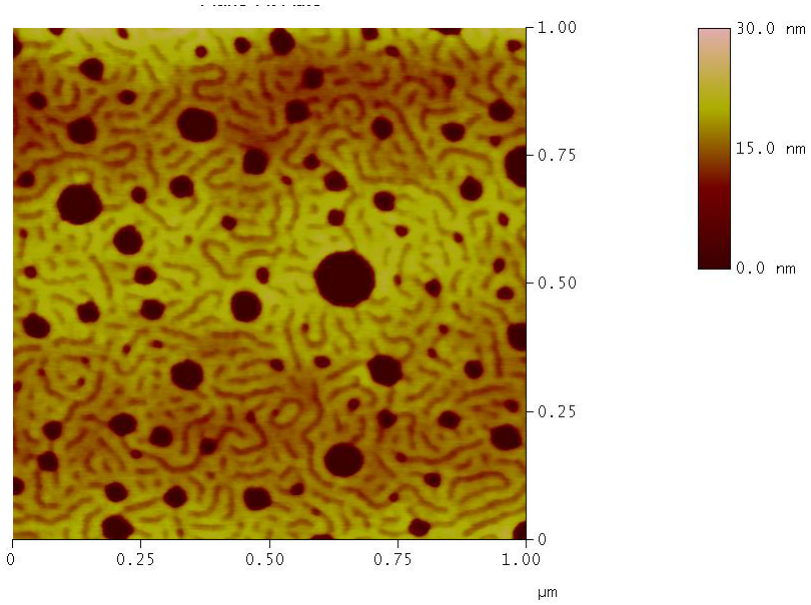

Figure 31: SFM height image of PS_{38K}-*b*-PAA_{3K}-Amp recorded in tapping mode.

Experiments using scanning force microscopy (SFM) were also conducted on several SABCs spin coated on silicon wafers. Interesting, lying cylinder-like morphology was seen for the amphiphilic side chain containing PS_{38K}-b-PAA_{3K}-Amp SABC. Complete surface coverage was evident. The dark areas in both the height and phase images (Figures 31 and 32) are most likely an artifact from sample preparation.

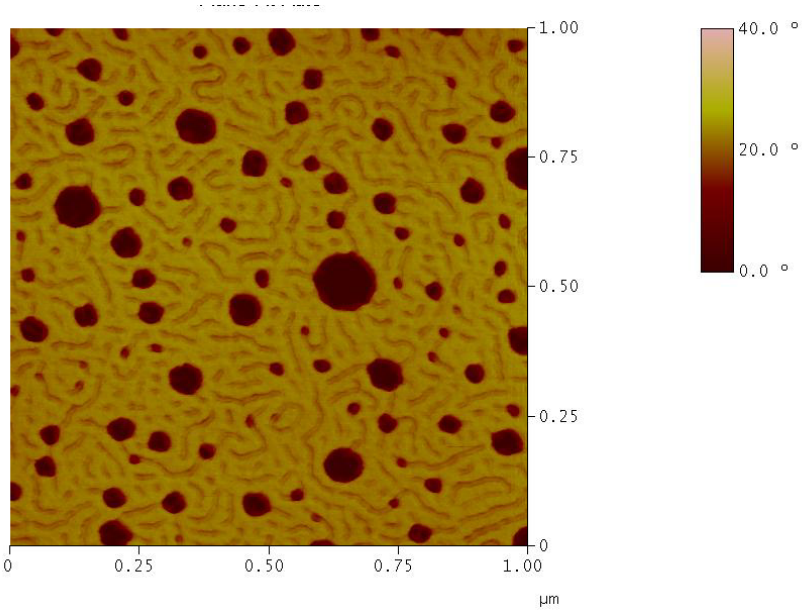

Figure 32: SFM phase image of PS_{38K}-*b*-PAA_{3K}-Amp recorded in tapping mode.

In addition to atomic force microscopy analysis of PS-*b*-PAA-Amp in an air environment we were able to obtain underwater AFM images of our sample by working

with Gil Walker at the University of Toronto (who is part of the ONR antifouling coatings program). This helps to see if and how the surface microstructure changed when exposed to an aqueous environment. We also devised an experiment with them to examine the adhesion force of bovine serum albumin (BSA) to our SABC surface (relative to glass and PDMS controls) using functionalized AFM tips.

A phase image (Figure 33) taken in tapping mode under water clearly provide evidence of a regular cylindrical or spherical microstructure. When a line scan was taken of a small section of the image (Figure 34), the domain size of the surface microstructure was found to be on the order of 35 nm.

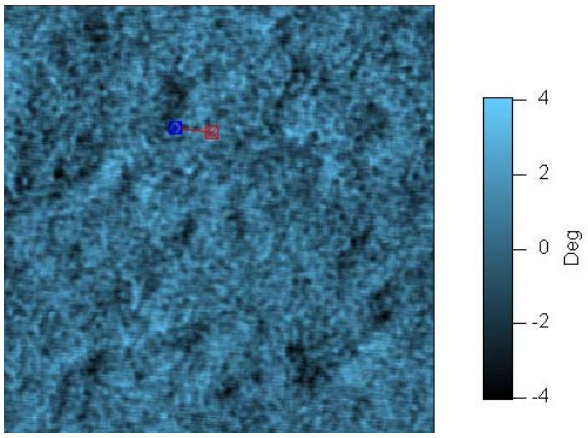

Figure 33. AFM phase image taken in tapping mode in an aqueous environment. Evidence of a regular cylindrical or spherical microstructure at the surface is readily apparent.

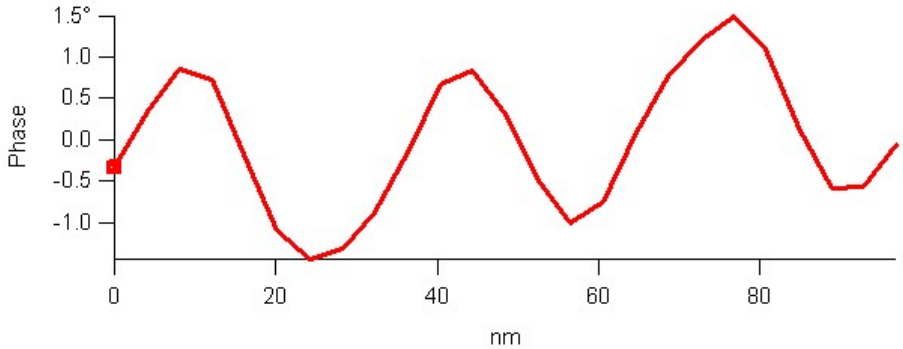

Figure 34. Line scan trace from the phase image above supporting a regular microstructure with domains on the order of 35 nm in size.

BSA protein force adhesion experiments using functionalized AFM tips yielded very interesting results. For glass, the adhesion force of BSA protein to the surface was found to be 0.26 ± 0.1 nN (Figure 35). For PDMS meanwhile, the adhesion force of BSA protein to the surface was found to be 3.5 ± 0.7 nN (Figure 36). Our PS-b-PAA-Amp SABC surface however actually had 58% of the counts demonstrate no adhesion force at

all (Figure 37), suggesting that the BSA protein was interacting extremely weakly with the surface.

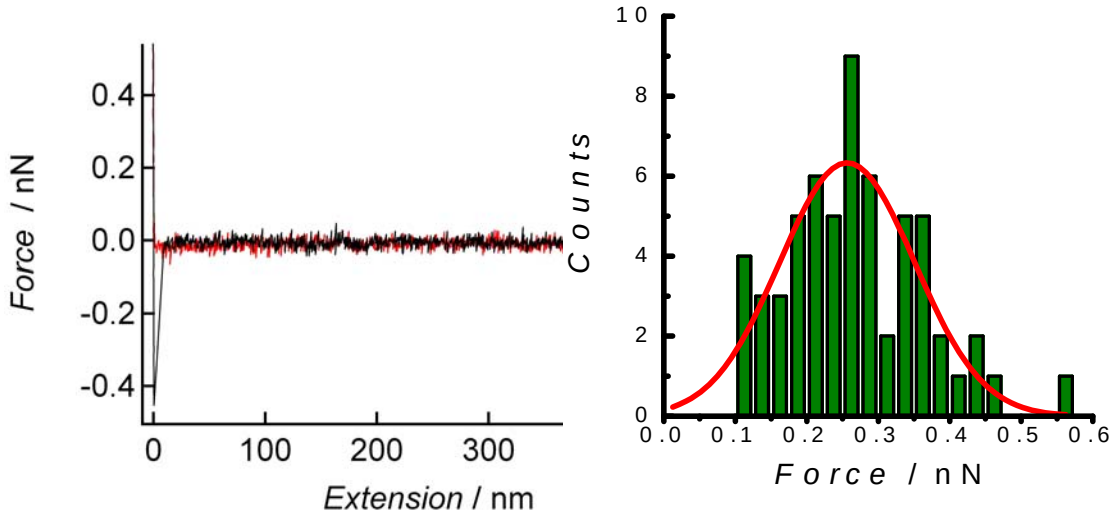

Figure 35. BSA protein adhesion force results for glass (the force of adhesion was found to be 0.26 ± 0.1 nN).

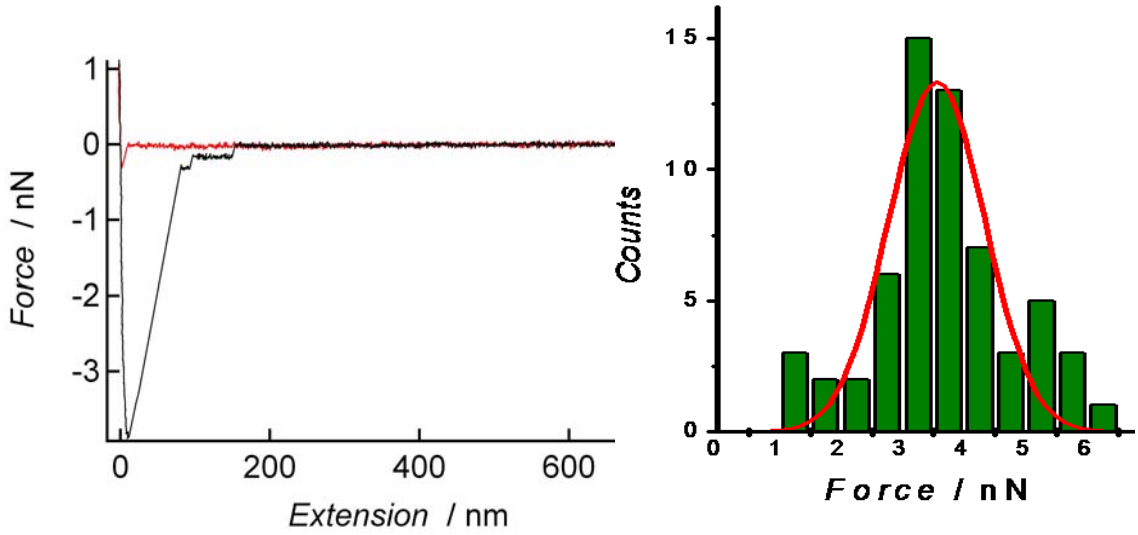

Figure 36. BSA protein adhesion force results for PDMS (the force of adhesion was found to be 3.5 ± 0.7 nN).

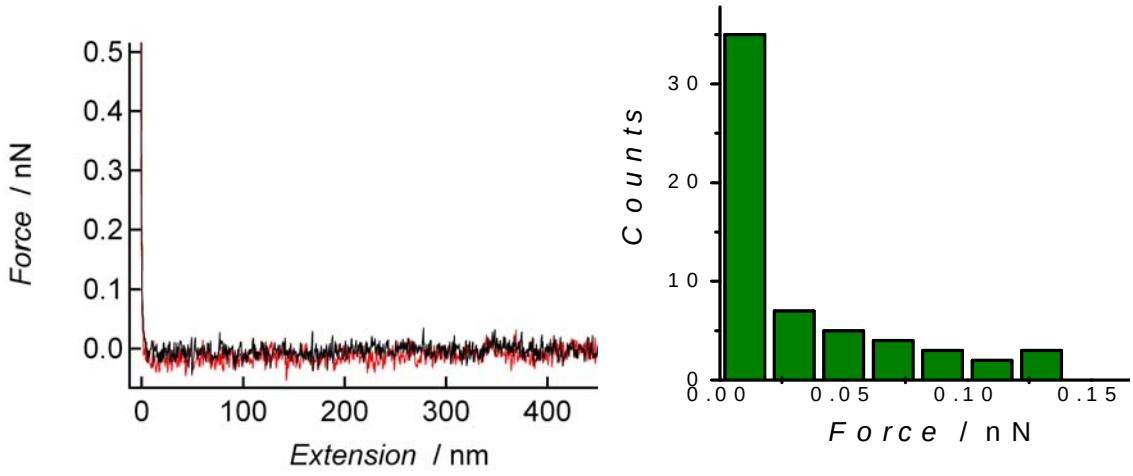

Figure 37. BSA protein adhesion force results for PS-*b*-PAA-Amp SABC (the force of adhesion was found to be 3.5 ± 0.7 nN).

A series of NEXAFS spectroscopy experiments was also conducted on ether-linked SABCs derived from K3 PS-*b*-P(E/B)-*b*-PI. All spectra were obtained at 50° X-ray incidence and -150 V entrance grid bias of an "in-plane" electron detector. Normalization of the O 1s and F 1s spectra was based on the C 1s spectrum. Figure 38 depicts a NEXAFS spectrum of a surface of K3 PS-*b*-P(E/B)-*b*-PI-Amp-40. The spectrum shows the expected O 1s and F 1s edges, arising from the amphiphilic side chains, in addition to the C 1s edge.

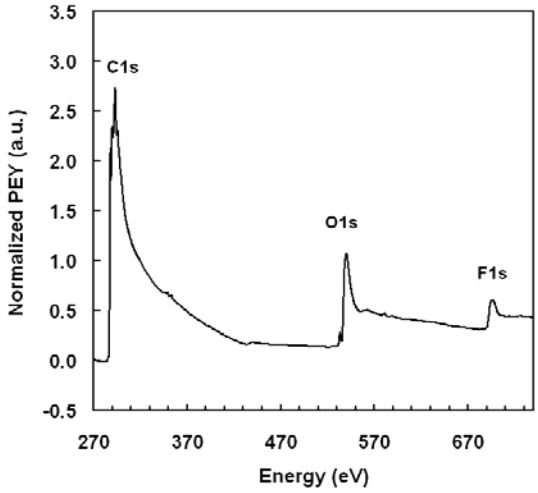

Figure 38: NEXAFS spectrum of K3 PS-*b*-P(E/B)-*b*-PI-Amp-40 surface.

Upon further examination of the C 1s spectra for a series of K3 PS-*b*-P(E/B)-*b*-PI polymers containing amphiphilic side chains formed at three different temperatures (Figure 39), several things were apparent. The higher σ^*_{C-F} intensity and the lower π^*_{Φ} intensity for a reaction temperature of 40 °C indicates that a higher reaction temperature results in higher side chain attachment, which is also consistent with the results of ^{1}H

NMR and IR spectroscopy. The higher surface concentration of the amphiphilic side chains is also evident in the F 1s NEXAFS spectra shown in Figure 40. When examing O 1s and F 1s spectra, the polymers synthesized at room temperature (25° C) and 40° C showed higher intensities in both oxygen and fluorine edges than the polymer synthesized at 0° C. This indicated a correlation between surface concentration of amphiphilic side chains and reaction temperature. The F edge intensity is a true indication of side chain incorporation because the O edge signal has contributions from the unreacted ether groups and the alcohol groups formed upon ring-opening of the epoxy groups in the precursor polymer.

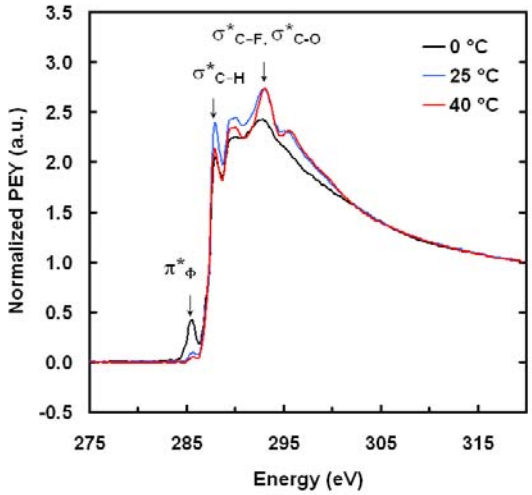

Figure 39. C 1s NEXAFS spectra of K3 PS-*b*-P(E/B)-*b*-PI block copolymers with the amphiphilic PEGylated fluoroalkyl (Zonyl FSO 100) side chains obtained from reactions performed at three different temperatures.

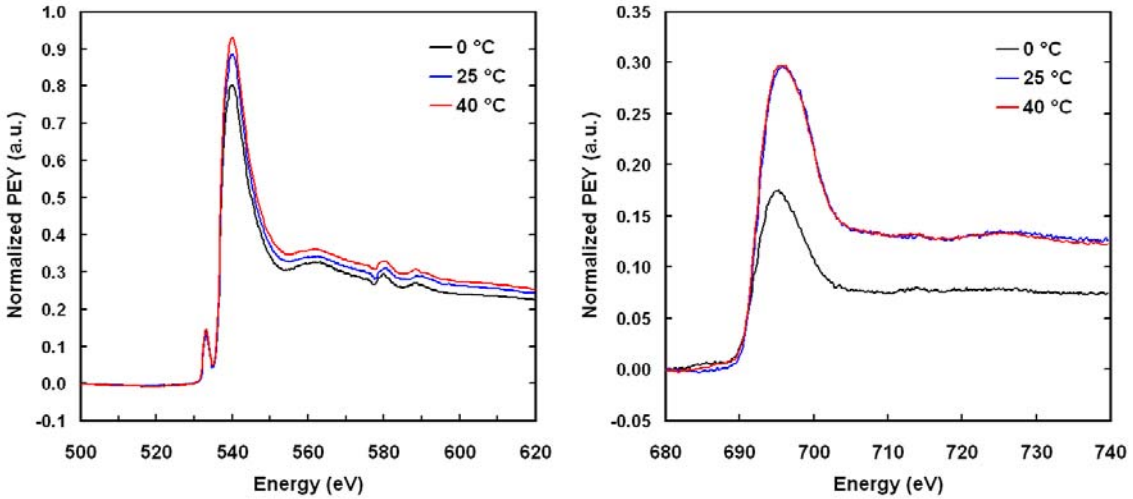

Figure 40. O 1s (left) and F 1s (right) NEXAFS spectra of K3 PS-*b*-P(E/B)-*b*-PI block copolymers with the amphiphilic PEGylated fluoroalkyl (Zonyl FSO 100) side chains obtained from reactions performed at three different temperatures

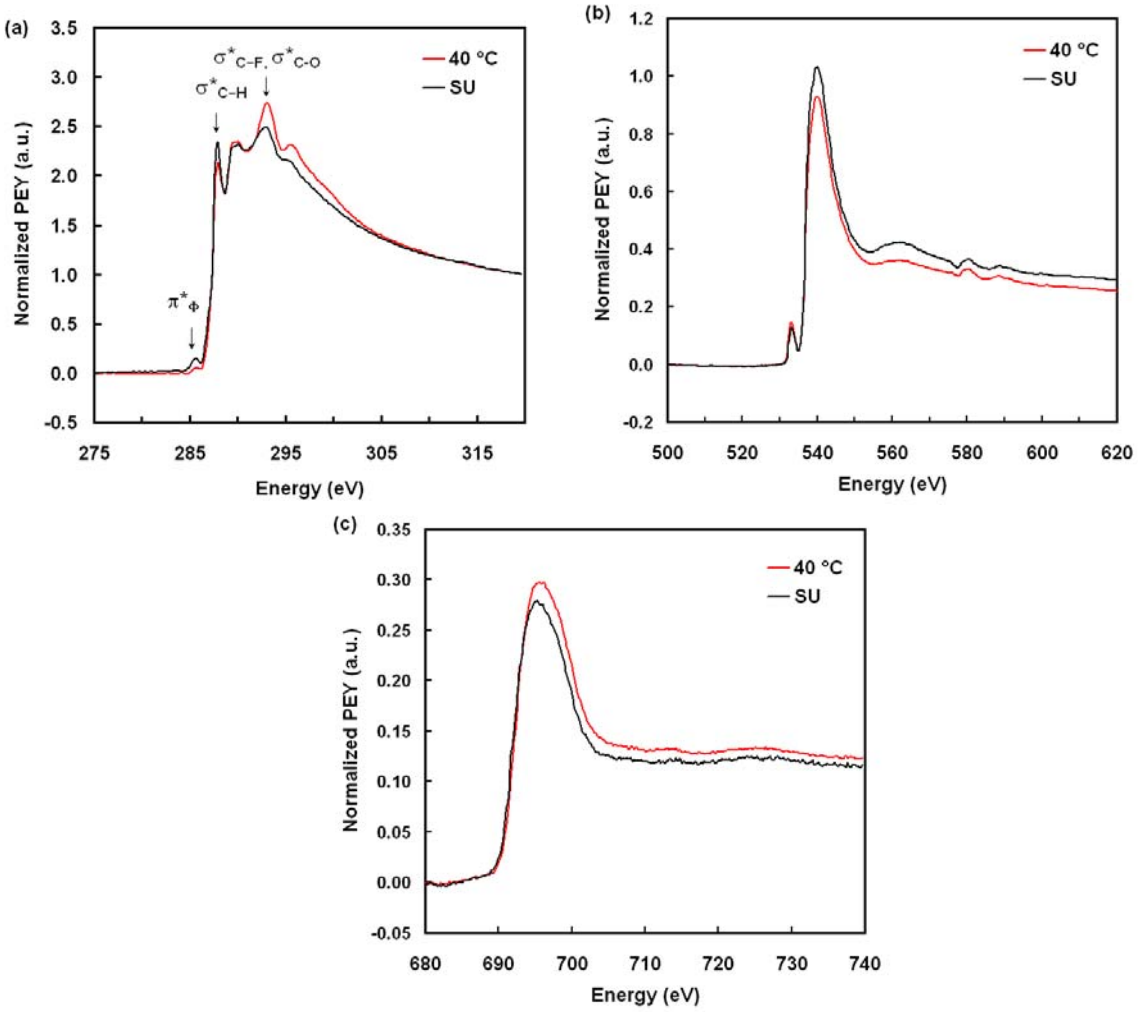

Figure 41. C 1s (top left), O 1s (top right) and F 1s (bottom) spectra comparison of polymer samples obtained in a small scale reaction at 40 °C and a scaled-up reaction at 55 °C (SU).

When a high attachment small scale reaction at 40 °C of amphiphilic side chains on K3 PS-*b*-P(E/B)-*b*-PI was compared to a scaled up reaction at 55 °C, slightly lower intensity was seen in the NEXAFS spectra due to the lower incorporation of side chains in the scaled up sample. Differences were negligible however (Figure 41).

Additionally, NEXAFS spectra were collected for C 1s, N 1s, and F 1s edges for the quaternized PS-*b*-P(E/B)-*b*-PI-F8H4I SABC and its respective aminated precursor. C 1s spectroscopy (Figure 42) clearly demonstrates the attachment of F8H4I through quaternization. The N 1s spectra depicted in Figure 43A demonstrates the presence of nitrogen at the surface of aminated PS-*b*-P(E/B)-*b*-PI. Meanwhile, the F 1s spectra in Figure 43B demonstrates the presence of fluorine at the surface of the quaternized PS-*b*-P(E/B)-*b*-PI-F8H4I polymer. As expected, polymer A did not show any signal in the F 1s region of the NEXAFS spectrum. Polymer B showed only a weak nitrogen edge, which is

attributed to the low atomic content of nitrogen at the surface of this polymer due to high levels of fluorination.

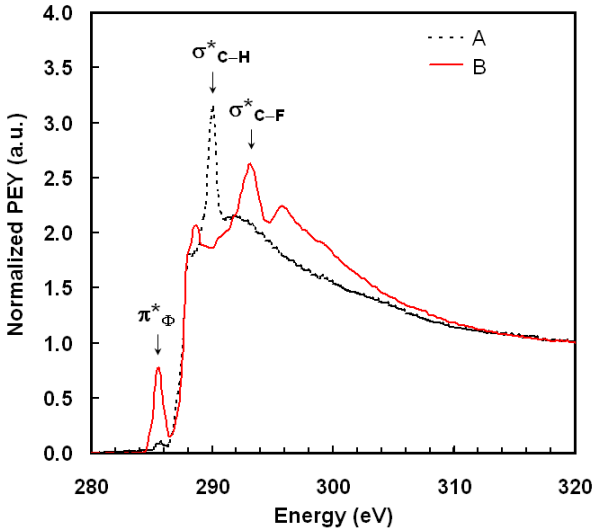

Figure 42. (A) PS-*b*-P(E/B)-*b*-PI precursor after epoxidation of the PI block and amination using dimethylaminopropyl amine; (B) the aminated PS-*b*-P(E/B)-*b*-PI polymer A following quaternization using 4-perfluorooctyl-1-iodobutane.

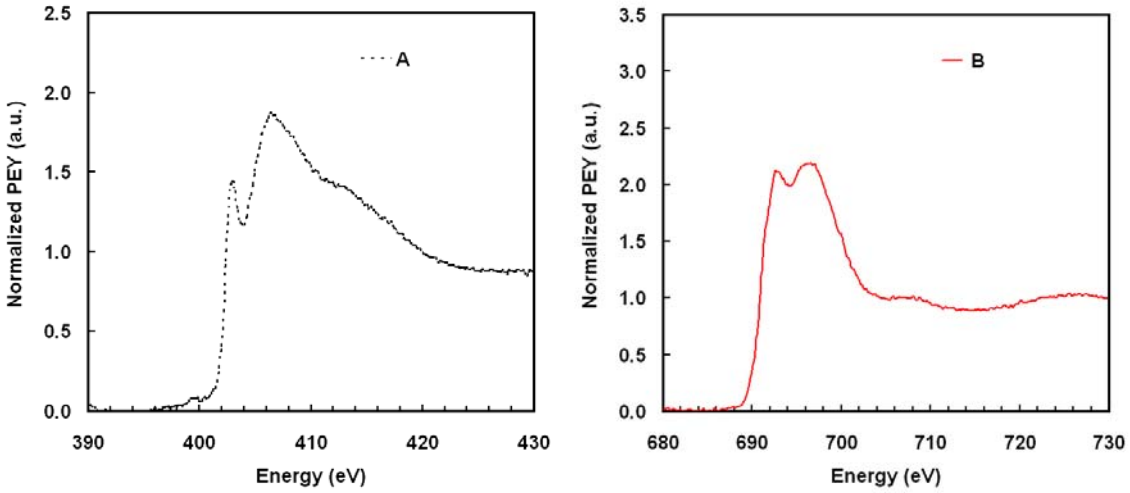

Figure 43. N 1s NEXAFS spectrum of the aminated PS-*b*-P(E/B)-*b*-PI polymer A (left) and F 1s NEXAFS spectrum of the quaternized PS-*b*-P(E/B)-*b*-PI polymer B (right).

Additionally, AFM experiments on K3 PS-*b*-P(E/B)-*b*-PI-Amp produced in a scaled-up reaction yielded what appears to be either perpendicular cylinders or a spherical surface morphology (Figures 44 and 45). This is especially evident in the phase image (Figure 45).

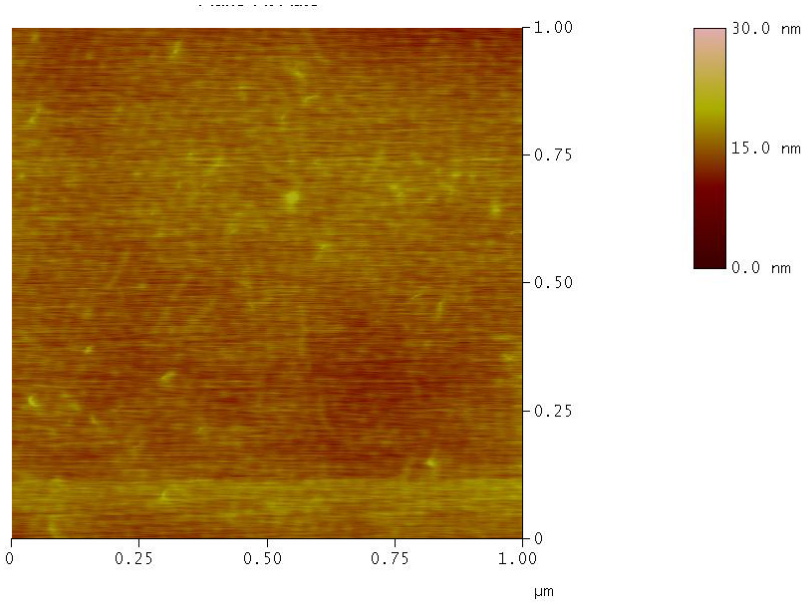

Figure 44: SFM height image of K3 PS-*b*-P(E/B)-*b*-PI-Amp recorded in tapping mode.

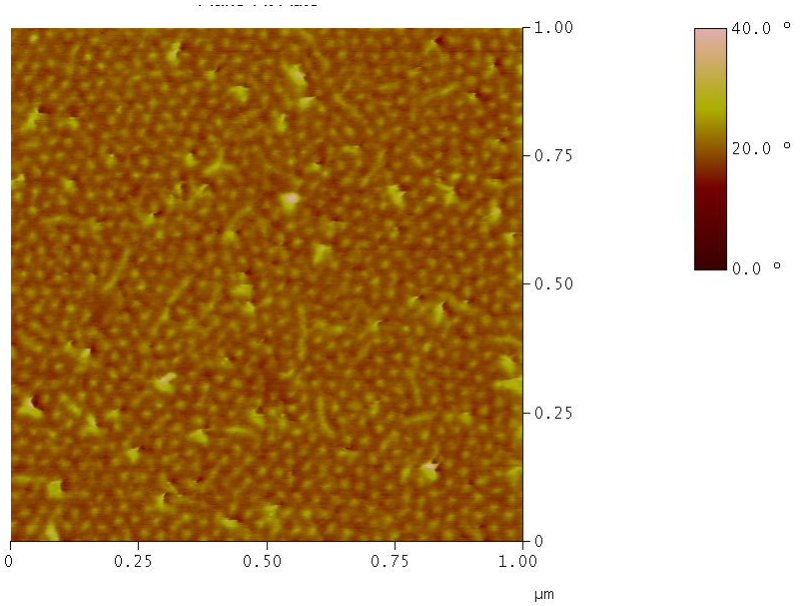

Figure 45: SFM phase image of K3 PS-*b*-P(E/B)-*b*-PI-Amp recorded in tapping mode.

NEXAFS spectroscopy experiments were conducted on ether-linked SABCs derived from PS_{8K}-*b*-$P(E/B)_{25K}$-b-PI_{10K}**.** All spectra were obtained at 50° X-ray incidence and -150 V entrance grid bias of an "in-plane" electron detector. Figure 46 shows the C 1s partial electron yield NEXAFS spectra of the PS_{8K}-*b*-$P(E/B)_{25K}$-*b*-PI_{10K}-Amp (top) and PS_{8K}-*b*-$P(E/B)_{25K}$-*b*-PI_{10K}-PEG550 (bottom) SABC surfaces spin coated on silicon. The amphiphilic SABC exhibits the characteristic C 1s $\rightarrow \sigma^*_{C\text{-}F}$ peak, arising from the C atoms of the perfluorinated carbons of the side chains. The sharp peak near 288 eV is a result of C 1s $\rightarrow \sigma^*_{C\text{-}H}$ transitions. Ketone formation on the back-bone is a possible side

reaction of the etherification reaction. If this reaction had occurred to a significant extent, a C 1s → $\pi^*_{C=O}$ peak is also expected in the vicinity of 288 eV.

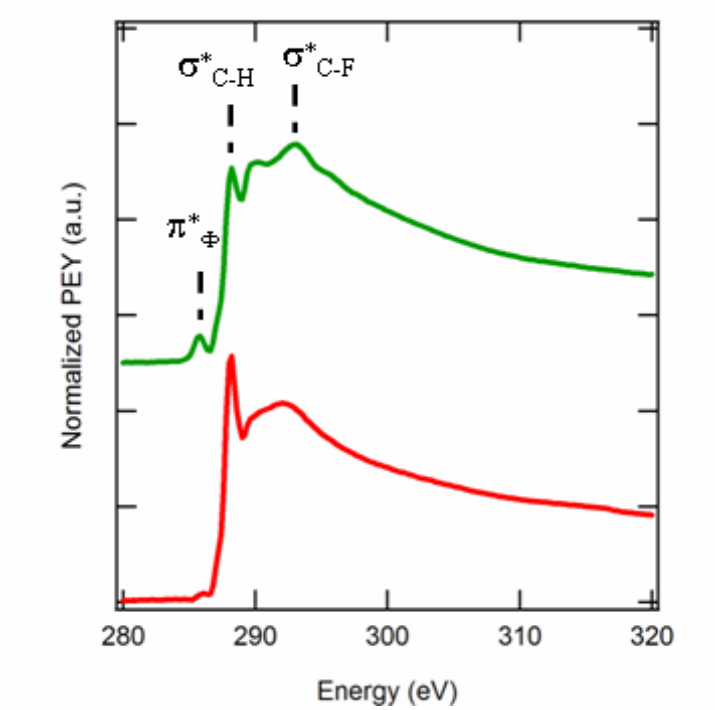

Figure 46. C 1s NEXAFS spectra of PS_{8K}-*b*-$P(E/B)_{25K}$-*b*-PI_{10K}-Amp (top, green) and PS8K-*b*-$P(E/B)_{25K}$-*b*-PI_{10K}-PEG550 (bottom, red) SABCs.

XPS data has also been taken on several different PS_{8K}-*b*-$P(E/B)_{25K}$-b-PI_{10K} derived ether-linked SABC polymer samples. Both spray coated and spun coat samples were analyzed. Figure 47 depicts XPS spectra taken of spray coated PS_{8K}-*b*-$P(E/B)_{25K}$-*b*-PI_{10K}-Amp SABC on glass slides. In this analysis, we spray coated the final SABC layer of the multilayer coating system from both TFT and chloroform to look for differences in sample preparation technique. Surprisingly, spray coating from chloroform appears to aid in segregation of the amphiphilic ethoxylated fluoroalkyl surface active side groups to the surface of the sample. This is supported by the stronger intensity of the CF_2 and CF_3 peaks and the weaker intensity of the C-C peak (which is indicative of the polymer back bone). These results suggested that solvent used for spray coating played an important role in surface functionality. So for all the synthesized SABCs we have analyzed the polymer surface by NEXAFS with different solvents as and when it is possible.

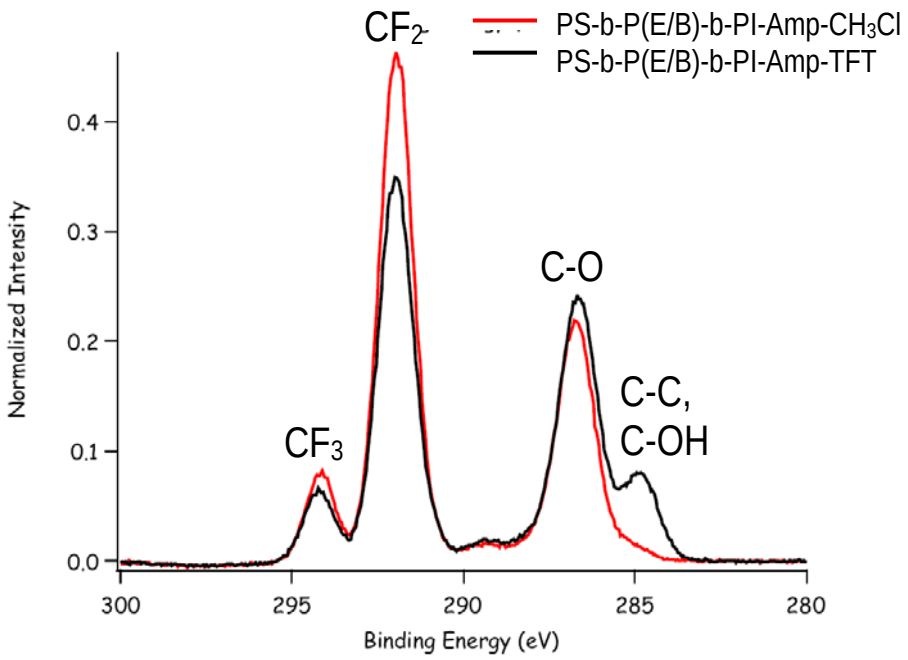

Figure 47. XPS analysis of the PS_{8K}-*b*-$P(E/B)_{25K}$-*b*-PI_{20K}-Amp sample suggested strong segregation of amphiphilic side chains to surface for spray coated samples.

5.2.3 Surface Characterization of SF Quaternized PS-*b*-P(E/B)-*b*-PI

Figure 48A shows high-resolution carbon 1s XPS spectra of aminated PS_{8K}-*b*-$P(E/B)_{25K}$-*b*-PI_{20K}, semifluorinated quaternized PS_{8K}-*b*-$P(E/B)_{25K}$-*b*-PI_{20K}, SQTC-F8H6Br-H6Br, and semifluorinated quaternized PS_{8K}-*b*-$P(E/B)_{25K}$-*b*-PI_{20K} with additional quaternization using H6Br, SQTC-F8H6Br-H6Br. SQTC-F8H6Br, and SQTC-F8H6Br-H6Br. The spectra are normalized so that the total area under the carbon peaks was equal to unity. The aminated PS_{8K}-*b*-$P(E/B)_{25K}$-*b*-PI_{20K} showed strong intensity peaks of C=C and C-C near 285 eV with no evidence of -CF_2- and -CF_3 peaks as expected. The surface of SQTC-F8H6Br quaternized with perfluorooctyl hexylbromide, $F(CF_2)_8(CH_2)_6Br$, showed distinct -CF_2- and -CF_3 peaks near 292 and 294 eV, respectively. The lowered intensity of the peaks associated with C=C and C-C combined with the appearance of -CF_2- and -CF_3 peaks is evidence of the attachment of fluorinated side chains through the quaternization with F8H6Br. The further reaction by addition of H6Br resulted in not only a slight decrease in the C=C and C-C peak intensities but also an increase in -CF_2- and -CF_3 peak intensities. This suggests that there was still unreacted F8H6Br present in the reaction mixture which was attached during this additional reaction time. Figure 49B shows the N 1s XPS spectra of the polymer before and after the quaternization reaction with F8H6Br, followed by quaternization with H6Br. The quaternization reaction resulted in the shift of nitrogen peak near 398 eV, which corresponds to unquaternized nitrogen, to a higher binding energy near 400.5 eV, corresponding to quaternized nitrogen. The percentage of quaternized nitrogen atoms present in SQTC-F8H6Br and SQTC-F8H6Br-H6Br calculated by comparing the areas under the two peaks are 45 and 70 %, respectively.

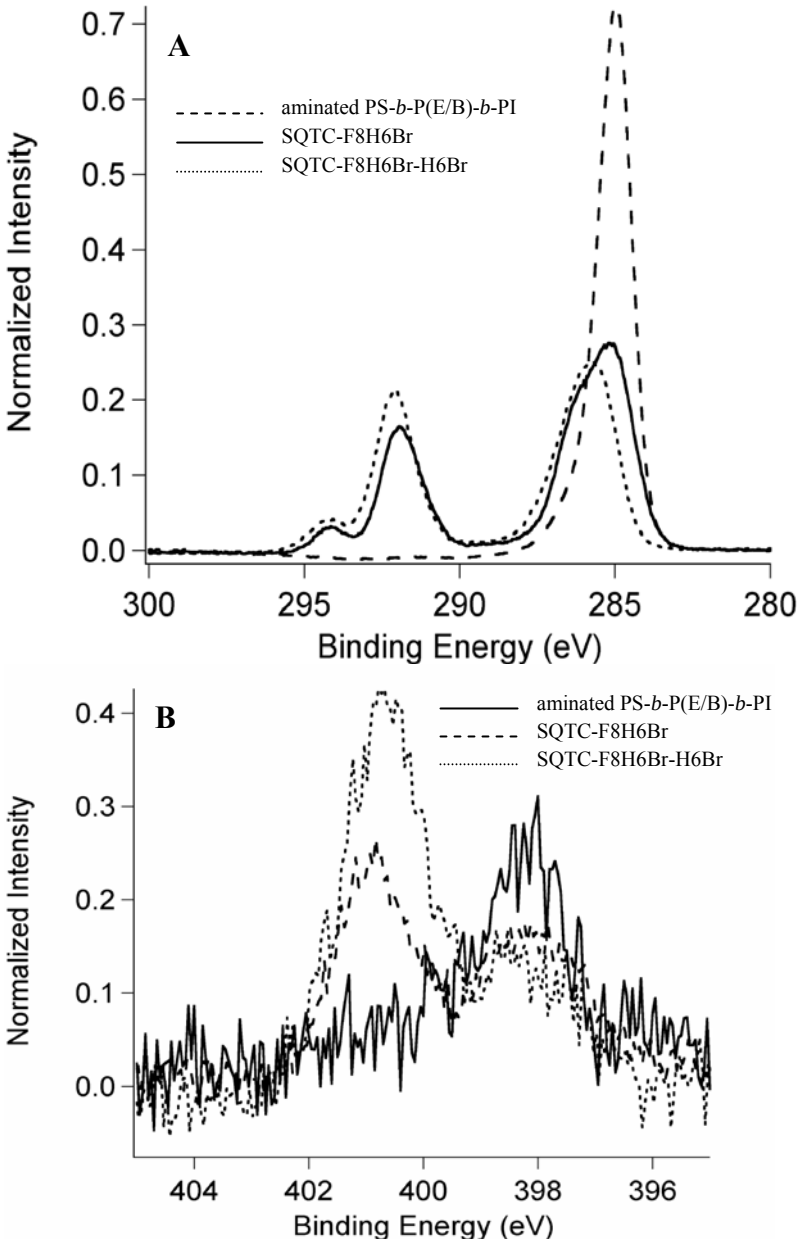

Figure 48. XPS (A) C 1s and (B) N 1s spectra of the surfaces of aminated PS_{8K}-*b*-$P(E/B)_{25K}$-*b*-PI_{20K}, semifluorinated quaternized PS_{8K}-*b*-$P(E/B)_{25K}$-*b*-PI_{20K}, SQTC-F8H6Br-H6Br and semifluorinated quaternized PS_{8K}-*b*-$P(E/B)_{25K}$-*b*-PI_{20K}, SQTC-F8H6Br-H6Br.

Figure 49 shows the normalized C 1s NEXAFS spectra of spin-coated surfaces of aminated PS_{8K}-*b*-$P(E/B)_{25K}$-*b*-PI_{20K}, semifluorinated quaternized PS_{8K}-*b*-$P(E/B)_{25K}$-*b*-PI_{20K}, SQTC-F8H6Br, and semifluorinated quaternized PS_{8K}-*b*-$P(E/B)_{25K}$-*b*-PI_{20K} reacted further with H6Br, SQTC-F8H6Br-H6Br. The characteristic C 1s $\rightarrow \pi^*_{C=C}$ signals derived from the polystyrene block were observed near 285 eV for all three spectra. The

characteristic C 1s $\rightarrow\sigma^*_{C\text{-}F}$ signal near 293 eV can be seen in the NEXAFS spectra of SQTC-F8H6Br and SQTC-F8H6Br-H6Br which showed the presence of the semifluorinated alkyl groups on the surfaces. No evidence of C 1s $\rightarrow\sigma^*_{C\text{-}F}$ signal was observed with aminated PS_{8K}-*b*-$P(E/B)_{25K}$-*b*-PI_{20K} as expected. The intensity of the $\sigma^*_{C\text{-}F}$ resonance of the SQTC-F8H6Br-H6Br increased compared with the one of SQTC-F8H6Br due to the unreacted F8H6Br during the first quaternization which is in good agreement with our XPS analysis.

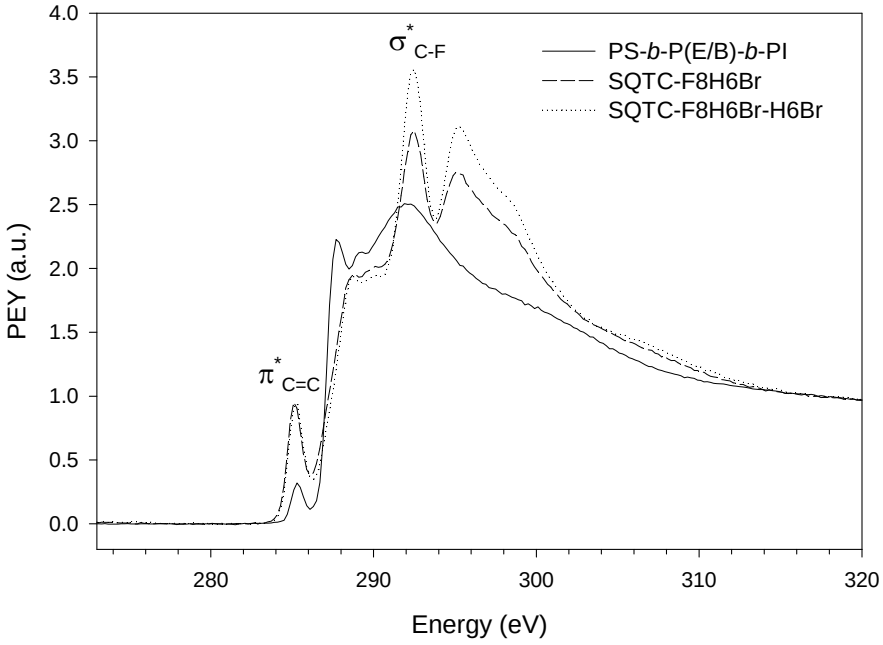

Figure 49. Normalized C 1s NEXAFS spectra of the surfaces of aminated PS_{8K}-*b*-$P(E/B)_{25K}$-*b*-PI_{20K}, SQTC-F8H6Br, and SQTC-F8H6Br-H6Br.

5.2.4 Surface Characterization Mixed Amphiphilic SABCs Synthesized from Kraton K4 Precursor

XPS analysis of mixed amphiphilic PS_{8K}-*b*-$P(E/B)_{25K}$-*b*-PI_{20K} SABCs taken at both 0° and 75° emission angle yielded the expected results (Figure 50). The peaks associated with $-CF_3$ and $-CF_2-$ were visible at ca. 294 eV and ca. 292 eV respectively. In general, peak intensity for fluorine increased with additional F10H10 content and decreasing PEG550 content. In addition, presence of the C-O-C peak at ca. 286.5 eV became very apparent with an emission angle of 0° (which profiles deeper into the surface) for the 60:40 and 40:60 PEG550:F10H10 feed ratio samples. The greater intensity of the C-C peak demonstrated for the 80:20 and 60:40 PEG550:F10H10 samples (especially at an emission angle of 75°) suggest the presence of the polystyrene block of the SABC at the immediate surface with the PEG550 groups most likely found underneath this block (which is supported by the 0° emission angle data).

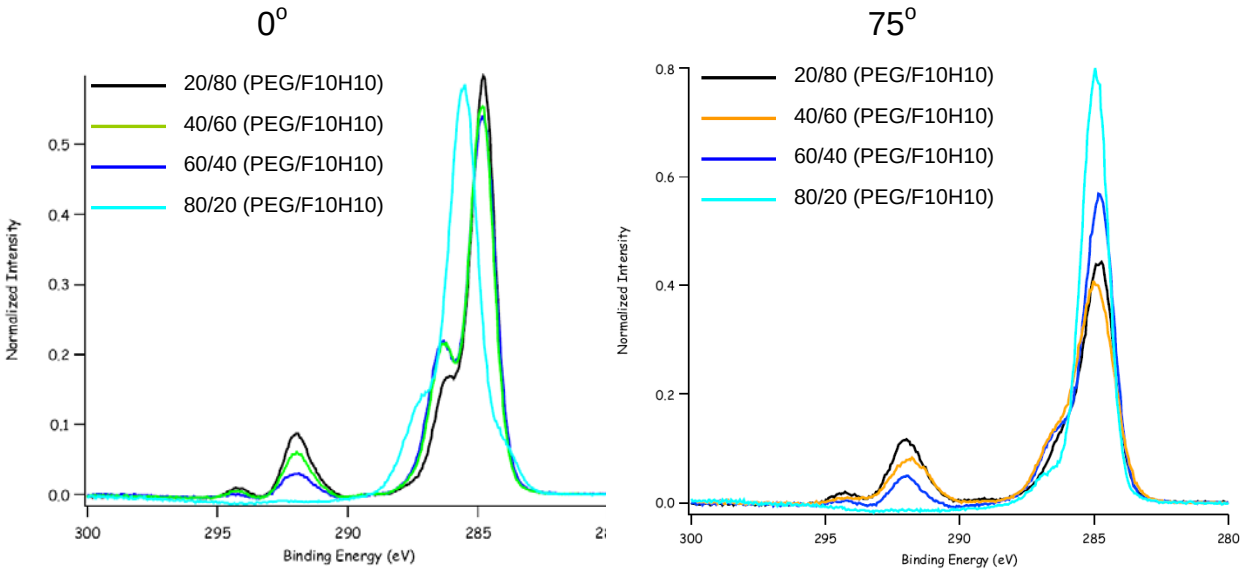

Figure 50. XPS analysis of mixed amphiphilic PS_{8K}-*b*-$P(E/B)_{25K}$-*b*-PI_{20K} SABCs taken at both 0° and 75° emission angle. Samples are labeled by relative feed ratio of PEG550:F10H10 used in etherification reactions. Characteristic peaks demonstrated are -CF_3 at ca. 294 eV, -CF_2- at ca. 292 eV, C-O-C at ca. 286.5 eV and C-C at ca. 284.5 eV.

Dynamic water contact angle analysis of spun coat amphiphilic ethoxylated fluoroalkyl SABC samples on Si wafers indicated the presence of low surface energy, hydrophobic fluorinated moieties at the surface with $\theta_{w,\ advancing} = 107 \pm 2°$. High contact angle hysteresis was observed with $\theta_{w,\ receding} = 26 \pm 2°$. This suggests a dynamic surface capable of facile reordering of the side chains to readily orient the hydrophilic PEGylated groups at the surface. This is similar to what was observed for the ethoxylated fluoroalkyl polystyrene-*block*-poly(acrylic acid) derived SABC reported previously, but with significantly higher contact angle hysteresis (81° versus 60°) observed for the PS-*b*-P(E/B)-*b*-PI triblock derived SABC.

5.2.5 Surface Characterization Mixed Amphiphilic SABCs Synthesized from Kraton K3 Precursor

Figure 51 depicts a typical high resolution C 1s XPS spectra of amphiphilic SABC derived from the PS_{8K}-*b*-$P(E/B)_{25K}$-*b*-PI_{10K} precursor with ethoxylated fluoroalkyl side chains when spun directly on Si. The strong intensity peak near 284.5 eV associated with C-C and C=C bonds is most likely indicative of the presence of the polymer back-bone. The peak associated with C-O-C groups present at near 286.5 eV meanwhile is indicative of the PEGylated groups of the amphiphilic side chain. Finally, the peaks at 292 eV and 294 eV are indicative of CF_2 and CF_3 groups respectively, further suggesting successful segregation of the ethoxylated fluoroalkyl side chains to the surface of the polymer coating. One can also note that the peaks associated with the side chain (CF_3, CF_2, and C-O-C) show higher intensities at a 75° incidence angle than at a 0° incidence angle. This suggests the preferential segregation of the side chains to the surface as desired.

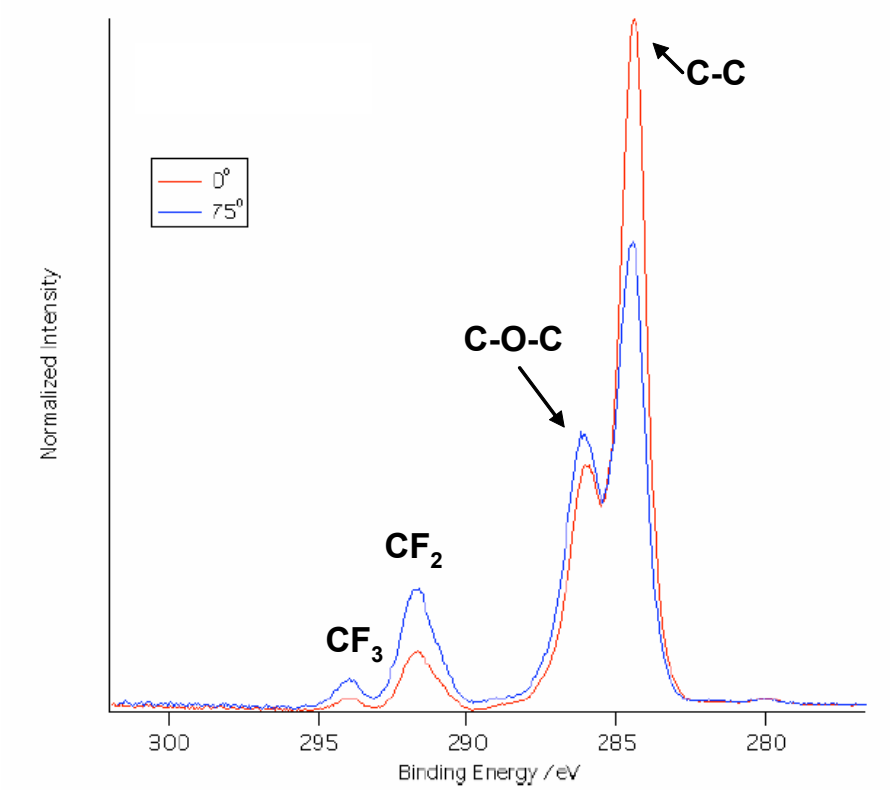

Figure 51. XPS C 1s spectra of the surface of the amphiphilic SABC with ethoxylated fluoroalkyl side chains derived from the PS_{8K}-*b*-$P(E/B)_{25K}$-*b*-PI_{10K} precursor polymer spun coat on Si taken at both 0° and 75° incidence angles.

Further characterization by XPS to determine if these model surfaces formed by spin coating were similar to those formed in the fabrication of samples for biofouling assays was performed. Figure 52 depicts a typical high resolution C 1s XPS spectra of amphiphilic SABC derived from the PS_{8K}-*b*-$P(E/B)_{25K}$-*b*-PI_{10K} precursor with ethoxylated fluoroalkyl side chains when sprayed on top of the MD6945 SEBS thermoplastic elastomer for biofouling assays. While the same set of chemical signatures is present for the spray coated samples as for the spun coat samples, peak intensities associated with the ethoxylated fluoroalkyl side chains greatly increased across the board. Particularly striking was that at the 75° incidence angle, the contribution from the polymer back-bone was so minimal that the C-C peak simply appeared as a shoulder on the much stronger C-O-C peak. This suggests that successful segregation of surface active groups may be highly dependent on the process conditions used. Hence spray coating was used as the standard method for the surface preparation for biofouling assays.

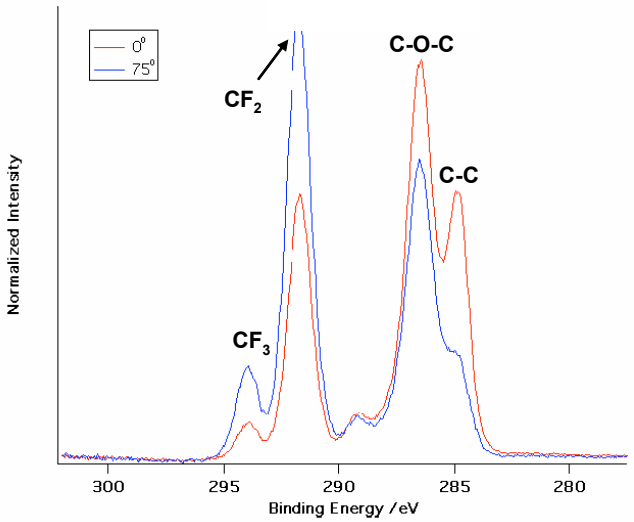

Figure 52. XPS C 1s spectra of the surface of the amphiphilic SABC with ethoxylated fluoroalkyl side chains derived from the PS_{8K}-*b*-$P(E/B)_{25K}$-*b*-PI_{10K} precursor polymer spray coated on MD6945 SEBS thermoplastic elastomer taken at both 0° and 75° incidence angles.

5.2.6 Surface Characterization of "Mixed" Amphiphilic Derived From Attachment of PEG 550/F10H10OH on to K3 Kraton Polymer

The advancing and receding contact angles of these polymers were done using water droplet on surface. The results are shown in table 7

Table 7. Advancing and receding dynamic water contact angle measurements for both sets of SABCs produced through the incorporation of different amounts of the F10H10 and PEG550 side chains.

PS_{8K}-*b*-$P(E/B)_{25K}$-*b*-PI_{10K} Precursor		
Sample	Θw,a	Θw,r
PS_{8K}-b-$P(E/B)_{25K}$-b-PI_{10K}-0F-33P	104 ± 3	21 ± 4
PS_{8K}-b-$P(E/B)_{25K}$-b-PI_{10K}-22F-27P	125 ± 3	25 ± 3
PS_{8K}-b-$P(E/B)_{25K}$-b-PI_{10K}-19F-28P	128 ± 3	26 ± 4
PS_{8K}-b-$P(E/B)_{25K}$-b-PI_{10K}-24F-24P	128 ± 3	27 ± 4
PS_{8K}-b-$P(E/B)_{25K}$-b-PI_{10K}-28F-19P	127 ± 3	28 ± 3
PS_{8K}-b-$P(E/B)_{25K}$-b-PI_{10K}-41F-13P	127 ± 2	31 ± 2
PS_{8K}-b-$P(E/B)_{25K}$-b-PI_{10K}-50F-0P	126 ± 2	42 ± 4

The samples derived from the PS_{8K}-*b*-$P(E/B)_{25K}$-*b*-PI_{10K} precursor polymer did not show a clear trend with respect to advancing water contact angle, with all the coatings except for PS_{8K}-b-$P(E/B)_{25K}$-b-PI_{10K}-0F-33P showing an advancing water contact angle on the order of ca. ~ 125°. Receding angles did show a slight trend however, varying from 21° for PS_{8K}-b-$P(E/B)_{25K}$-b-PI_{10K}-0F-33P to 42° for PS_{8K}-b-$P(E/B)_{25K}$-b-PI_{10K}-50F-

0P. High water contact angle hysteresis was demonstrated for both sets of SABCs, suggesting a dynamic surface capable of significant reorganization was realized in all cases. Contact angle hysteresis was generally a bit more pronounced for polymers derived from the PS_{8K}-b-$P(E/B)_{25K}$-b-PI_{10K} precursor however. These observed differences in wettability behavior between each set of SABCs can most likely be attributed to the combination of higher attachment and significantly higher side chain grafting density realized for the PS_{8K}-b-$P(E/B)_{25K}$-b-PI_{10K} derived samples.

Figure 53 shows high-resolution C 1s XPS spectra of amphiphilic SABCs derived from the PS_{8K}-*b*-$P(E/B)_{25K}$-*b*-PI_{10K} precursor with different attachment percents of PEG550 and F10H10. The percent attachment of F10H10 (F) and PEG550 (P) relative to epoxidized isoprene in the precursor is given in the legend. The spectra are normalized so that the total area under the carbon peaks is equal to unity. All polymers showed strong intensity peaks from C=C and C-C near 285 eV, most likely indicative of the block copolymer backbone. There was clear evidence for all but the PS_{8K}-*b*-$P(E/B)_{25K}$-*b*-PI_{10K}-0F-33P sample of peaks associated with $-CF_2-$ and $-CF_3$ near 292 and 294 eV, respectively. As expected, the intensities of both $-CF_2-$ and $-CF_3$ decreased with increasing attachment of PEG550 and decreasing attachment of F10H10 in the mixture. A pronounced shoulder at ca. ~ 287 eV associated with C-O was present in many of the samples, which can be attributed to both the ether-linked groups of the PEG550 moiety and also the alcohol functionality resulting on the polyisoprene block after ring opening of the oxirane group.

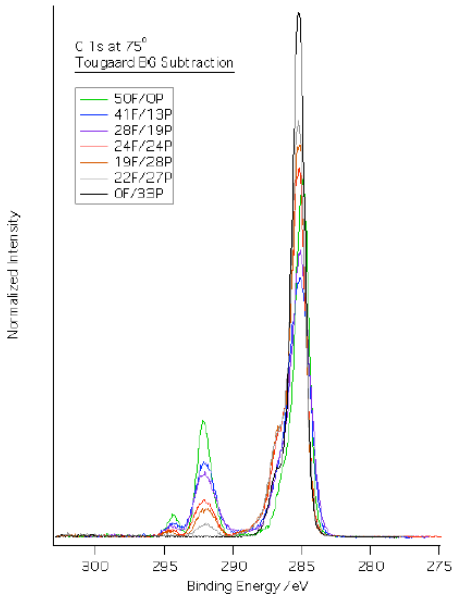

Figure 53. XPS C 1s spectra of the surfaces of amphiphilic SABCs containing mixed hydrophobic F10H10 and hydrophilic PEG550 side chains derived from the PS_{8K}-*b*-$P(E/B)_{25K}$-*b*-PI_{10K} precursor polymer taken at a 75° incident angle processed using Tougaard background subtraction. Sample labels give amounts of PEG550 (P) and F10H10 (F) side chains incorporated relative to epoxy functionality in the precursor polymer.

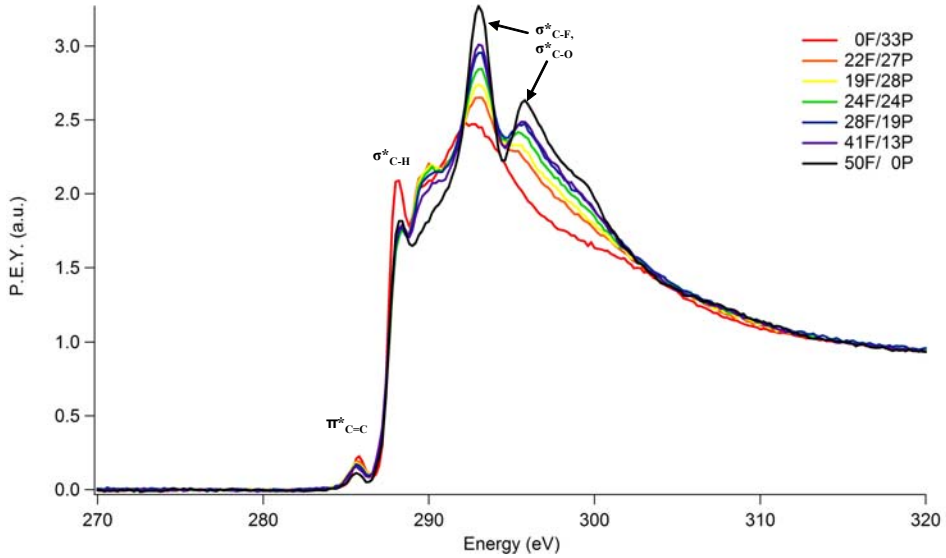

Figure 54. NEXAFS spectra of spin-coated surfaces of PS_{8K}-b-$P(E/B)_{25K}$-b-PI_{10K} derived SABCs on a silicon wafer after annealing at 120 °C for 12 hr at an angle of 50˚ between the surface and the soft X-ray beam with major resonance transition peaks labeled.

Figure 54 depicts the normalized C 1s NEXAFS spectra of spin-coated surfaces of amphiphilic SABCs derived from the PS_{8K}-*b*-$P(E/B)_{25K}$-*b*-PI_{10K} precursor with different amounts of PEG550 and F10H10 side chains attached taken at an angle of 50˚ between the surface and the soft X-ray beam. The characteristic C 1s → $\pi^*_{C=C}$ signals derived from the polystyrene block were observed near 285.5 eV for all seven of the spectra, but the intensity of this peak was very low because the SABC surfaces were dominated by the PEG550 and F10H10 side chains. Other peak assignments can be based on calibrated NEXAFS spectra of poly(ethylene oxide) and poly(methyl methacrylate). The sharp resonance peak near 288 eV can be attributed to the C 1s →σ^*_{C-H} signal. This peak was particularly prevalent for the PS_{8K}-b-$P(E/B)_{25K}$-b-PI_{10K}-0F-33P sample, likely due to the absence of fluorinated moieties, indicating a surface dominated by the low surface energy poly(ethylene-*ran*-butylene) block, with possible contributions from the PEGylated moieties. The characteristic signals near 293 eV and 295.8 eV can be easily seen for the other six samples, and they are indicative of both the C 1s →σ^*_{C-F} and C 1s →σ^*_{C-O} resonances, demonstrating the presence of the semifluorinated groups on the surfaces with possible contributions from the PEG containing side chains. The intensity profiles of C 1s →σ^*_{C-F} signal were quite similar to the ones in XPS spectra which decreased with increasing incorporation of PEG550 and decreasing incorporation of F10H10OH in the mixture.

5.2.7 Surface Characterization of SABCs derived from Non-fluorinated, Non-Ionic Compounds (Brij)

Dynamic water contact angle analysis of spun coat SABC samples on Si wafers indicated the presence of low surface energy, hydrophobic moieties at the surface for all Brij side chain polymers with $\theta_{w,\ advancing}$ ranging from 84.1° to 109.6°. High contact angle hysteresis was seen for all polymers, with $\theta_{w,\ receding}$ measured between 16.9° and 28.7°, suggesting the facile reordering of the side chains to orient the hydrophilic PEGylated groups at the surface (Table 8). It was notable that both advancing and receding water contact angle measurements for all samples were not statistically different, demonstrating that all Brij non-ionic surfactant derived samples had very similar wettability characteristics.

Table 8. Water contact angles and film thickness of the triblock copolymer surface with grafted amphiphilic side chains.

Compounds	Advancing contact angle (deg)	Receding contact angles (deg)	Film thickness (nm)
Silicon wafer	21.6±1.6	8.9±0.5	-
SEBS	119.8±3.2	59.8±3.9	258.2±0.4
PEG.BE	103.6±3.1	28.7±0.7	167.7±0.2
Brij 30	107.9±1.2	24.9±0.6	181.3±0.5
Brij 72	109.6±1.6	26.6±1.8	152.2±0.4
Brij 76	98.5±2.6	18.1±3.2	191.2±0.6
Brij 78	84.1±2.3	16.9±2.7	164.6±0.5
Brij 97	105.3±1.8	22.4±1.7	143.6±0.4

Figure 55 shows high-resolution C 1s XPS spectra of the amphiphilic SABC derived from the PS_{8K}-*b*-$P(E/B)_{25K}$-*b*-PI_{10K} precursor with attached Brij non-ionic surfactant side chains taken at two different incident angles (0° and 75°). The spectra are normalized so that the total area under the carbon peaks is equal to unity. All samples showed a strong intensity peak from C=C and C-C near 285 eV, most likely indicative of a combination of the polymer backbone and the low surface energy aliphatic section of the Brij derived side chain. Additionally, a pronounced shoulder at ca. ~ 287 eV

associated with C-O, suggesting the presence of the PEGylated moieties of the Brij side-chain near the surface. Analysis of the XPS survey scans show the surfaces dominated by the peaks associated with C 1s and O 1s, located at ca. ~ 285 eV and ca. ~ 535 eV respectively.

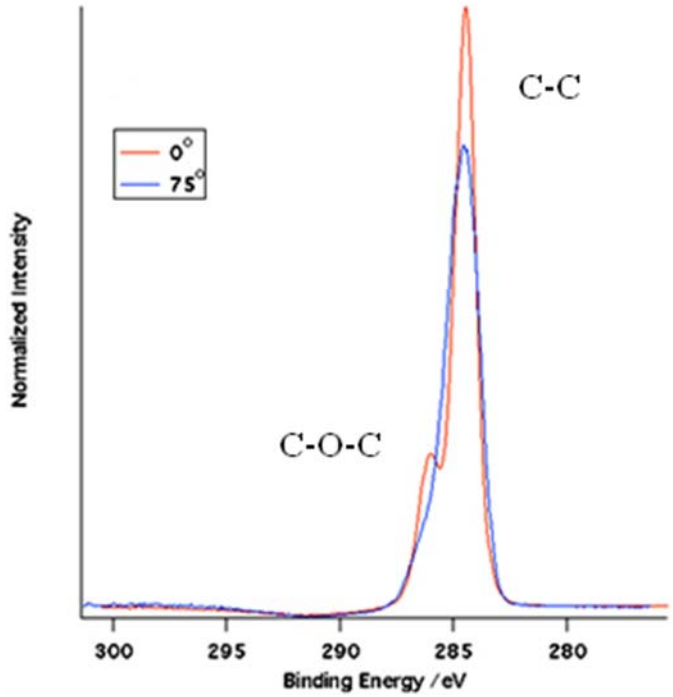

Figure 55. XPS C 1s spectra of the surface of the amphiphilic SABC with Brij non-ionic surfactant side chains derived from the PS_{8K}-*b*-$P(E/B)_{25K}$-*b*-PI_{10K} precursor polymer spun coat on Si taken at both 0° and 75° incidence angles.

Figure 56 depicts the normalized C 1s NEXAFS spectra of spray-coated surfaces of Brij amphiphilic SABCs derived from the PS_{8K}-*b*-$P(E/B)_{25K}$-*b*-PI_{10K} precursor at an angle of 20~125˚ between the surface and the soft X-ray beam. The characteristic C 1s → $\pi^*_{C=C}$ signals derived from the polystyrene block were observed near 285.5 eV, but the intensity of this peak was very low because the SABC surfaces were dominated by the Brij side chains. The sharp resonance peak near 288 eV can be attributed to the C 1s →σ^*_{C-H} signal. The characteristic signal near 293 eV is indicative of C 1s →σ^*_{C-O} resonances, demonstrating the presence of the PEG containing side chains.

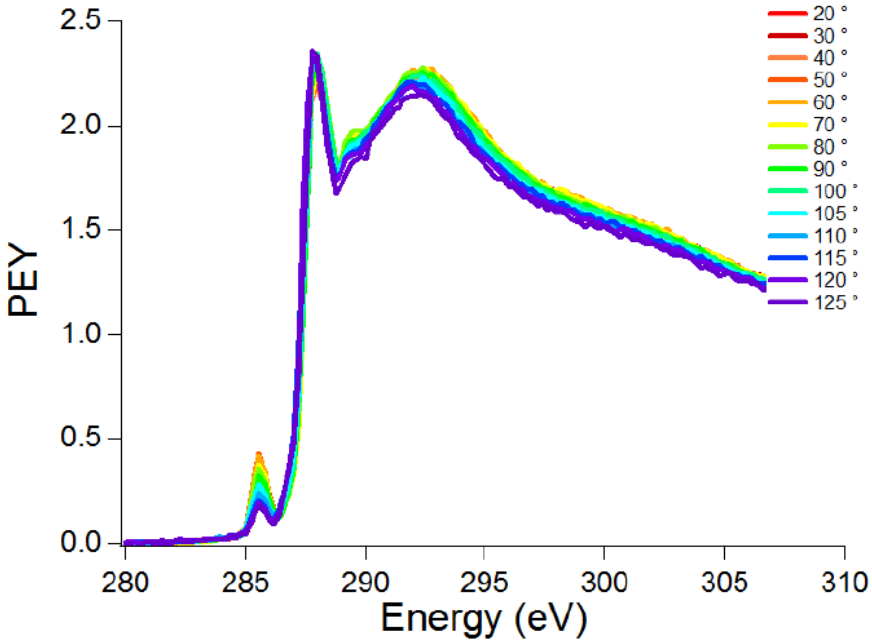

Figure 56. NEXAFS spectra of spray-coated surfaces of PS_{8K}-b-$P(E/B)_{25K}$-b-PI_{10K} derived Brij side chain on SEBS coated glass between the surface and the soft X-ray beam with major resonance transition peaks labeled.

5.2.8 Surface Characterization of SABCs derived from Non-Fluorinated and Non-Ionic Pluronic Compounds

Dynamic water contact angle analysis of spun coat SABC samples on Si wafers indicated the presence of low surface energy, hydrophobic moieties at the surface for all Pluronic side chain polymers with $\theta_{w,\ advancing}$ ranging from 99.0° to 106.2°. High contact angle hysteresis was seen for all three samples, with $\theta_{w,\ receding}$ measured between 22.1° and 31.9°, suggesting the facile reordering of the side chains to orient the hydrophilic PEGylated groups at the surface (Table 9). It was notable that both advancing and receding water contact angle measurements for all samples were not statistically different, demonstrating that all Pluronic non-ionic surfactant derived samples had very similar wettability characteristics.

Table 9. Water contact angles and film thickness of the triblock copolymer surface with grafted amphiphilic side chains.

Compounds	Advancing contact angle (deg)	Receding contact angles (deg)	Film thickness (nm)
Silicon wafer	21.6±1.6	8.9±0.5	-
SEBS	119.8±3.2	59.8±3.9	258.2±0.4
K3-Plu L31	103.6±1.9	29.8±3.2	75.78±0.18
K3-Plu L35	99.0±2.5	22.1±3.7	72.61±0.14
K3-Plu 10R5	106.2±2.8	27.3±1.3	79.54±0.20

Figure 57 shows high-resolution C 1s XPS spectra of the amphiphilic SABC derived from the PS_{8K}-*b*-$P(E/B)_{25K}$-*b*-PI_{10K} precursor with attached Pluronic non-ionic surfactant side chains taken at two different incident angles (0° and 75°). The spectra are normalized so that the total area under the carbon peaks is equal to unity. All samples showed a strong intensity peak from C=C and C-C near 285 eV, most likely indicative of a combination of the polymer backbone and the low surface energy aliphatic section of the Pluronic derived side chain. Additionally, a pronounced shoulder at ca. ~ 287 eV associated with C-O, suggesting the presence of the PEGylated and PPGylated moieties of the Pluronic side-chain near the surface. Analysis of the XPS survey scans show the surfaces dominated by the peaks associated with C 1s and O 1s, located at ca. ~ 285 eV and ca. ~ 535 eV respectively.

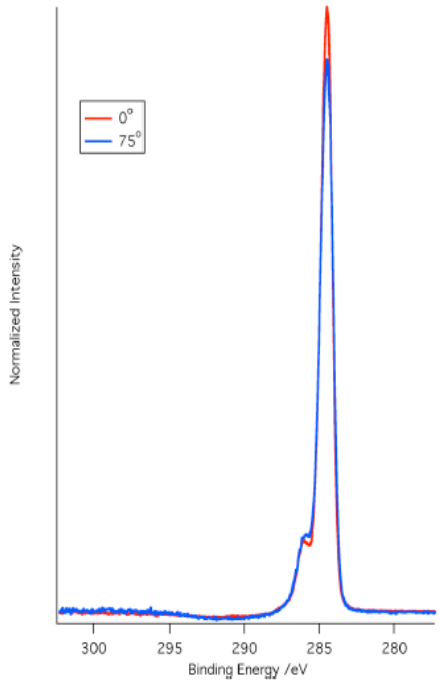

Figure 57. XPS C 1s spectra of the surface of the amphiphilic SABC with ethoxylated fluoroalkyl side chains derived from the PS_{8K}-*b*-$P(E/B)_{25K}$-*b*-PI_{10K} precursor polymer spun coat on Si taken at both 0° and 75° incidence angles.

Figure 58 depicts the normalized C 1s NEXAFS spectra of spray-coated surfaces of Pluronic amphiphilic SABCs derived from the PS_{8K}-*b*-$P(E/B)_{25K}$-*b*-PI_{10K} precursor at an angle of 20~125˚ between the surface and the soft X-ray beam. The characteristic C 1s $\rightarrow \pi^*_{C=C}$ signals derived from the polystyrene block were observed near 285.5 eV, but the intensity of this peak was very low because the SABC surfaces were dominated by the non-protected Pluronic side chains (K3 Plu 10R5). The characteristic C 1s $\rightarrow \pi^*_{C=C}$ signals derived from the polystyrene block were observed near 285.5 eV, but the intensity of this peak was very string because the SABC surfaces were dominated by flurobenzenesulfonyl protected Pluronic side chains (K3 Plu Plu L35). The sharp resonance peak near 288 eV can be attributed to the C 1s $\rightarrow\sigma^*_{C-H}$ signal. The characteristic signal near 293 eV is indicative of C 1s $\rightarrow\sigma^*_{C-O}$ resonances, demonstrating the presence of the PEG and PPG containing side chains.

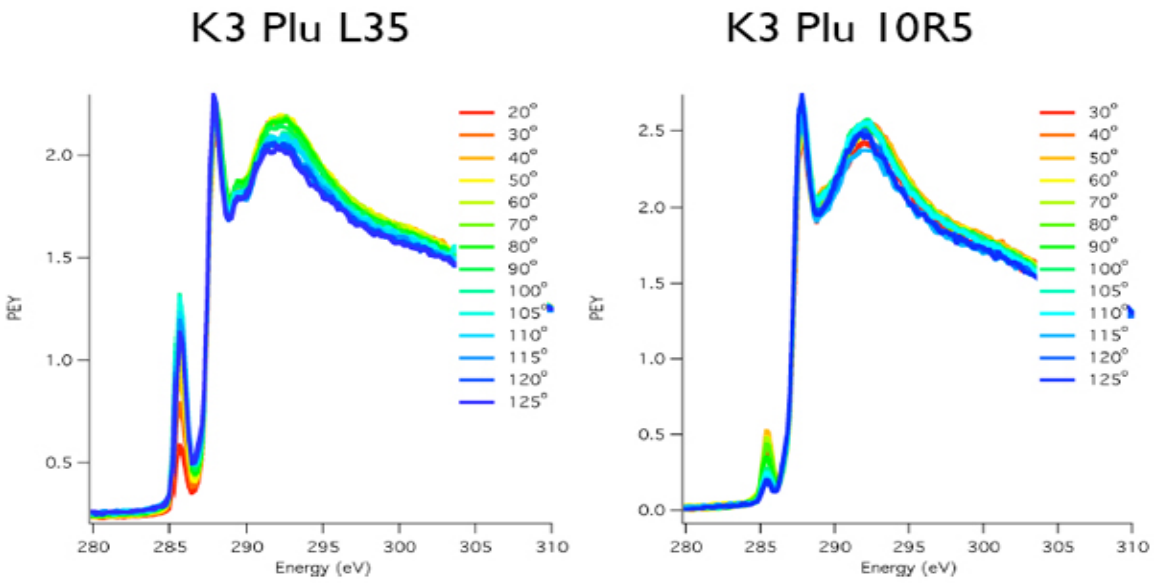

Figure 58. NEXAFS spectra of spray-coated surfaces of PS_{8K}-b-$P(E/B)_{25K}$-b-PI_{10K} derived Pluronic side chain on SEBS coated glass between the surface and the soft X-ray beam with major resonance transition peaks labeled

5.2.9 Surface Characterization of SABCs Synthesized by Anchoring Hydrocarbon and PEG to Kraton K3 Polymer

The samples derived from the PS_{8K}-*b*-$P(E/B)_{25K}$-*b*-PI_{10K} precursor polymer did not show a clear a trend with respect to advancing and receding water contact angle. Dynamic water contact angle analysis of spun coat SABC samples on Si wafers indicated the presence of low surface energy, hydrophobic moieties at the surface for all mixed side chain polymers with $\theta_{w,\ advancing}$ ranging from 98.1° to 107.3°. High contact angle hysteresis was seen for all polymers, with $\theta_{w,\ receding}$ measured between 31.5° and 51.0°, suggesting the facile reordering of the side chains to orient the hydrophilic PEGylated groups at the surface (Table 10). High water contact angle hysteresis was demonstrated for both sets of SABCs, suggesting a dynamic surface capable of significant reorganization was realized in all cases. These observed differences in wettability behavior between each set of SABCs can most likely be attributed to the combination of higher attachment and significantly higher side chain grafting density realized for the PS_{8K}-b-$P(E/B)_{25K}$-b-PI_{10K} derived samples.

Table 10. Advancing and receding dynamic water contact angle measurements for both sets of SABCs produced through the incorporation of different amounts of the 1-Octadecanol and PEG550 side chains.

Feed % 1-Octadecanol	Feed % PEG550	Advancing contact angle (deg)	Receding contact angles (deg)
Silicon wafer		21.6	8.9
SEBS		119.8	59.8
0	100	98.1	38.6
25	75	105.8	32.9
50	50	105.6	31.5
75	25	107.1	35.2
100	0	107.3	51.0

Figure 59 shows high-resolution C 1s XPS spectra of amphiphilic SABCs derived from the PS_{8K}-*b*-$P(E/B)_{25K}$-*b*-PI_{10K} precursor with 0% feeding PEG550 and 100% feeding 1-Octadecanol. All polymers showed strong intensity peaks from C=C and C-C near 285 eV, most likely indicative of the block copolymer backbone. A pronounced shoulder at ca. ~ 287 eV associated with C-O was not showed in this data, which can be attributed to both the ether-linked groups of the PEG550 and 1-Octadecanol.

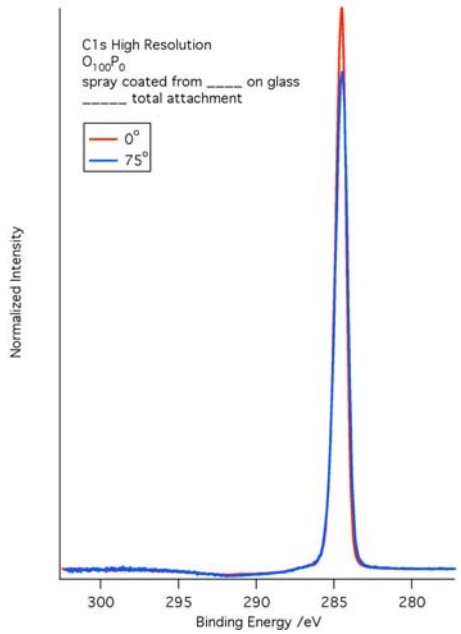

Figure 59. XPS C 1s spectra of the surfaces of amphiphilic SABCs containing mixed hydrophobic 1-Octadecanol and hydrophilic PEG550 side chains derived from the PS_{8K}-*b*-$P(E/B)_{25K}$-*b*-PI_{10K} precursor polymer taken at a 0° and 75° incident angle.

Figure 60 depicts the normalized C 1s NEXAFS spectra of spray-coated surfaces of mixed amphiphilic SABCs derived from the PS_{8K}-*b*-$P(E/B)_{25K}$-*b*-PI_{10K} precursor at an angle of 20~125˚ between the surface and the soft X-ray beam. The characteristic C 1s → $\pi^*_{C=C}$ signals derived from the polystyrene block were observed near 285.5 eV, but the intensity of this peak was very low because the SABC surfaces were dominated by the PEG550 and 1-octadecanol side chains. The sharp resonance peak near 288 eV can be attributed to the C 1s →σ^*_{C-H} signal. The characteristic signal near 293 eV is indicative of C 1s →σ^*_{C-O} resonances, demonstrating the presence of the PEG and 1-octadecanol containing side chains.

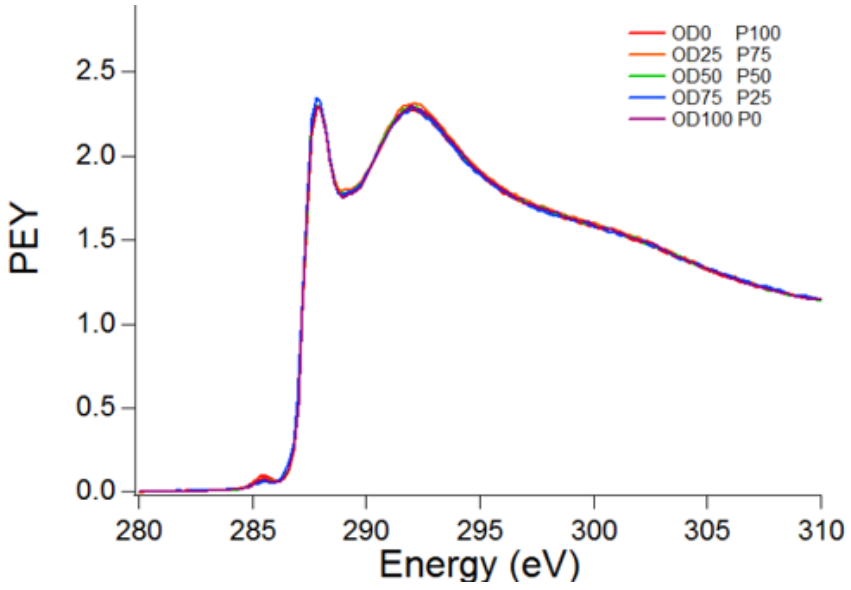

Figure 60. NEXAFS spectra of spray-coated surfaces of PS_{8K}-b-$P(E/B)_{25K}$-b-PI_{10K} derived the mixed PEG 550 and 1-Octadecanol side chain on SEBS coated glass between the surface and the soft X-ray beam with major resonance transition peaks labeled

5.3 Biofouling tests of synthesized SABCs

5.3.1 Biofouling Tests with SBS-Br-F8H2 SABC

5.3.1.1 Results of SABC Leachate Toxicity Test

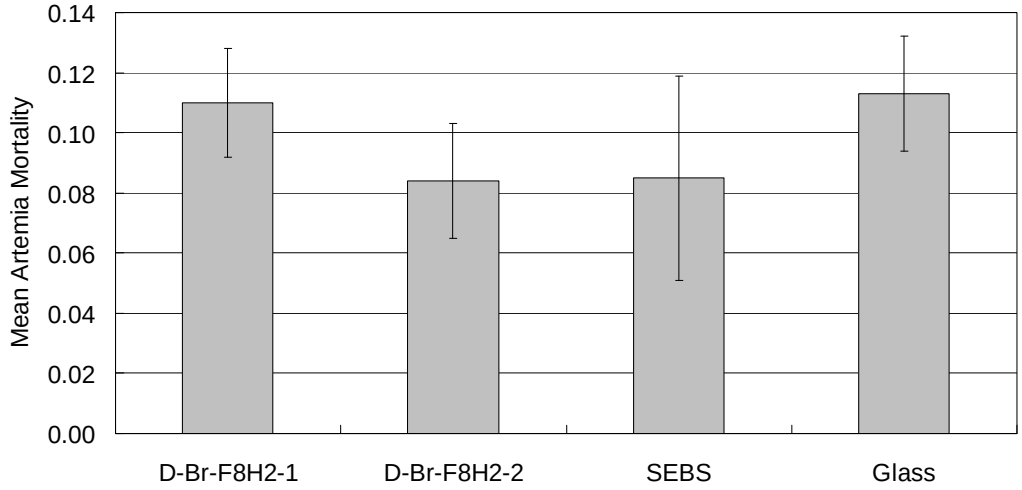

Figure 61: Brine shrimp nauplii mortality in leachates produced from two SBS-Br-F8H2 samples, a SEBS coating, and a glass control slide.

No evidence of toxic leaching was observed when comparing brine shrimp nauplii mortality rates between the two SABC coatings and the glass control slide as the results are shown in Figure 61.

5.3.1.2 Results of *Ulva* Spore Settlement, Growth and Release Testing

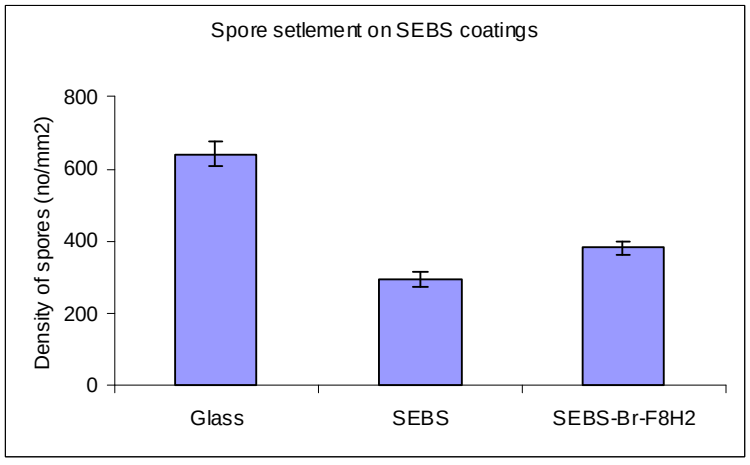

Figure 62: *Ulva* spore settlement on a SEBS-Br-F8H2 multilayer coating, plain SEBS, and a glass control slide.

From testing at the University of Birmingham, several things were learned about the performance of Br-F8H2 SABC. First of all, the spore settlement density on both plain SEBS and Br-F8H2-SEBS was approximately half that of the settlement on glass (Figure 62). Additionally, sporeling growth on the SABC surfaces was lower than that on glass, SEBS or PDMS standards (Figure 63).

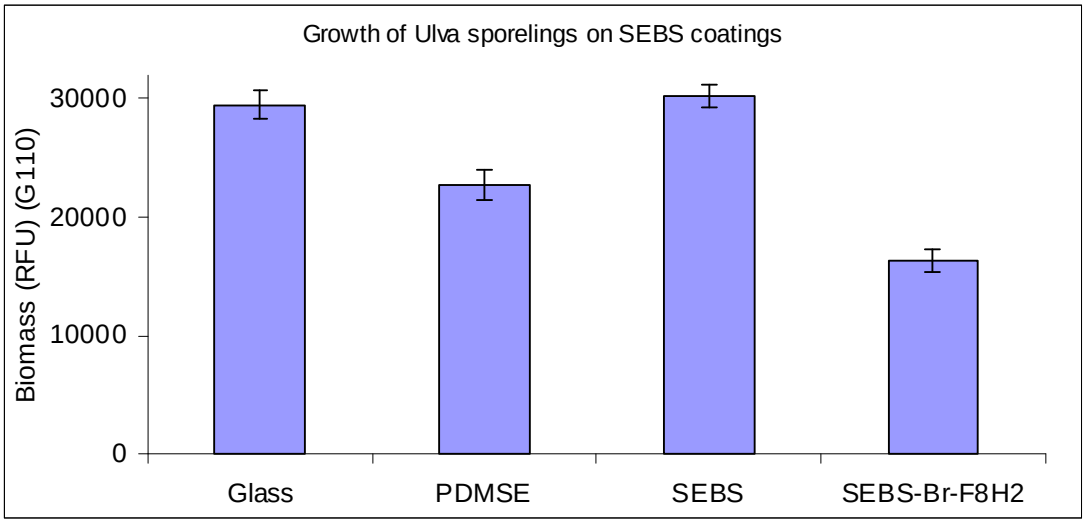

Figure 63: Sporeling growth testing of the SEBS-Br-F8H2 multilayer coating versus plain SEBS, PDMS, and a glass control slide.

5.3.1.3 Results of Barnacle Settlement, Growth and Release Testing

The settlement assay indicated that there was a significant difference between the settlement rate of barnacle cypris larvae on the experimental coatings and the settlement rates on the control surfaces (ANOVA, F=3.882, p=0.0191). Fisher's PLSD post-hoc tests indicated that all three test-surfaces had significantly lower settlement than the polystyrene controls. The experimental coatings were not, however, statistically different from the glass controls, or each other (Figure 64). Force gauge testing performed with mature barnacles on the Br-F8H2 coating showed that the basal plates of the barnacles fractured.

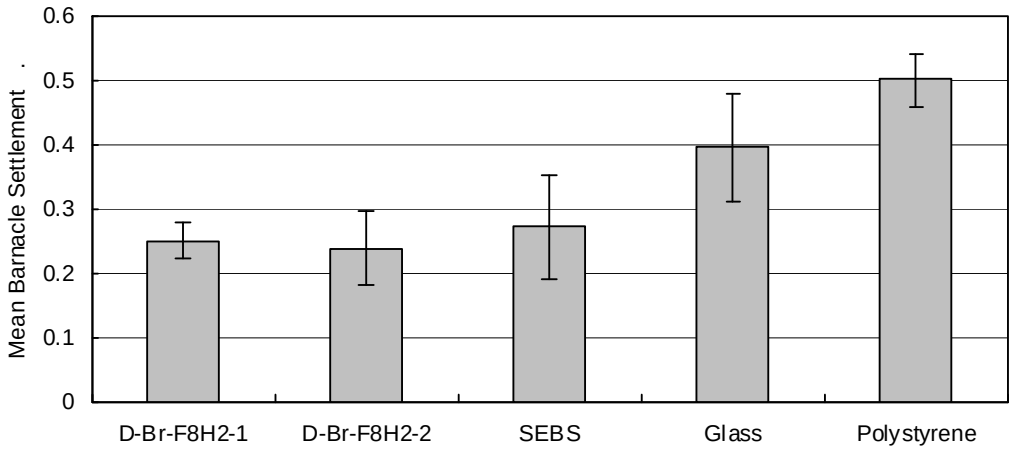

Figure 64: Barnacle cypris larvae settlement comparison data.

5.3.2 Biofouling Tests with PS-b-PAA SABCs

5.3.2.1 Results of PS_{38K}-*b*-PAA_{3K} SABC Leachate Toxicity Testing

The results of the leachate test indicated (shown in figure 65) no significant difference between mortality of brine shrimp subjected to the leachate of experimental coatings derived from the PS_{38K}-b-PAA_{3K} precursor and mortality from glass controls (ANOVA, F=0.560, p=0.6515).

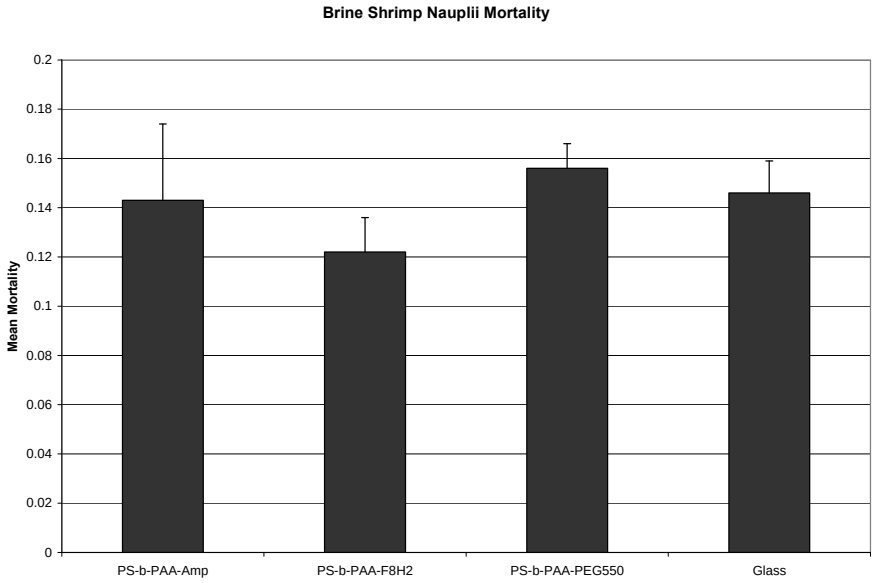

Figure 65: Brine shrimp nauplii mortality rates in leachates produced from three PS_{38K}-b-PAA_{3K} derived samples and a glass control slide.

5.3.2.2 Results of PS_{38K}-*b*-PAA_{3K} SABC Barnacle Settlement and Growth Testing

There was a significant difference observed between cypris larvae settlement on experimental coatings of PS_{38K}-*b*-PAA_{3K}-F8H2, PS_{38K}-*b*-PAA_{3K}-Amp, and PS_{38K}-*b*-PAA_{3K}-PEG550 and settlement controls of glass and Silastic T2 PDMS (ANOVA, $F=84.454$, $p<0.0001$) (figure 66). Silastic T2 was selected as a standard since its fouling-release efficacy against barnacles has previously been established. Subsequent tests indicate that all three experimental coatings had significantly lower settlement than glass and PDMS controls.

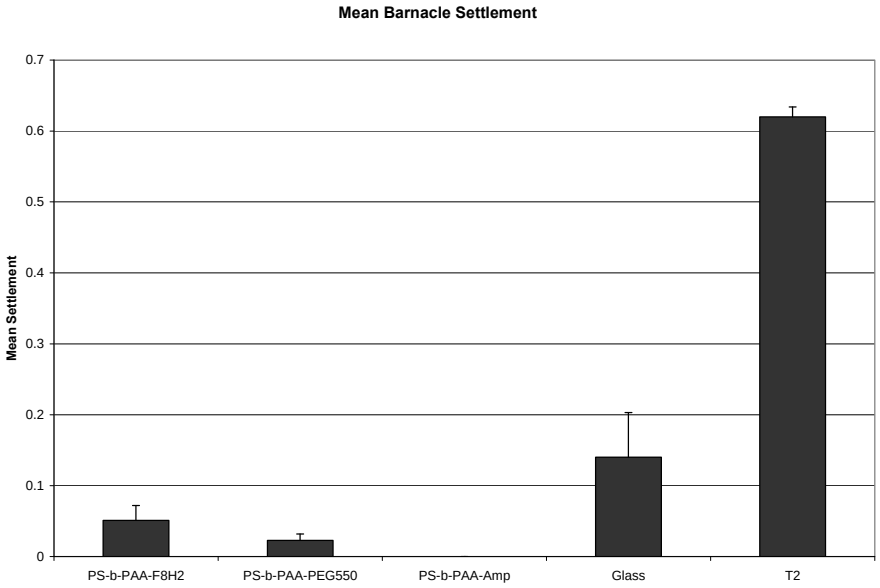

Figure 66: Barnacle cypris larvae settlement data demonstrating the very low settlement of barnacles on our PS_{38K}-*b*-PAA_{3K} derived coatings relative to controls.

5.3.2.3 Biofouling Assay – Barnacle Release Testing on PS_{38K}-*b*-PAA_{3K} SABCs

Removal force testing on PS_{38K}-*b*-PAA_{3K}-Amp was unable to be performed due to no initial settlement of barnacles. Furthermore, removal force testing on PS_{38K}-*b*-PAA_{3K}-PEG550 was also not able to be accurately performed due to very low initial settlement of barnacle larvae. This is an indication that these coatings were functioning well as anti-fouling surfaces. Although there was a very low number of barnacles on the PS_{38K}-*b*-PAA_{3K}-F8H2 coating (about 5 barnacles per coating), removal force testing performed on the surfaces showed breakage of all of the barnacles' basal plates. All barnacles left a complete basal plate on the surface of each coating. This indicates that the force measured was not the strength of adhesion of the barnacle to the surface, but rather the cohesive strength of the barnacle itself. Consequently, the barnacles were adhering to the PS_{38K}-*b*-PAA_{3K}-F8H2 surfaces with greater strength than could be measured by our test. Silicon controls showed clean removal of the barnacle basal plates and performed as expected as fouling release surfaces. This shows that amphiphilic and PEG groups anchored PS-*b*-PAA showed very good antifouling properties against barnacles.

These tests with CalPoly were repeated for reproducibility with an additional set of cyprid larvae (Figure 67). Resettlement produced more typical results for the glass control. We also saw the settlement relative to controls increase dramatically on both the PS-*b*-PAA-PEG550 and PS-*b*-PAA-F8H2 SABCs. Most notable however was the lack of settlement yet again on PS-*b*-PAA-Amp.

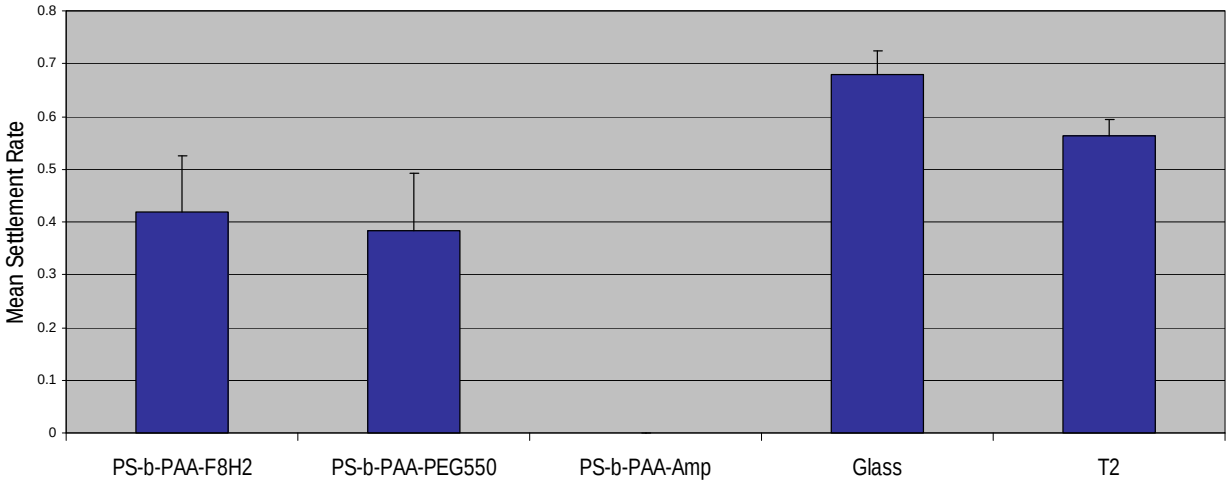

Figure 67. Barnacle cyprid larvae resettlement data used to check reproducibility of results.

5.3.2.4 Results of Immersion Panel Testing of PS-*b*-PAA-Amp at Calpoly

A great deal of data was generated during the six month sea-water immersion large-scale panel testing of PS-*b*-PAA-Amp SABC. Thus, only a summary of our results will be provided for this report. During the first two to three months of testing (which was started during the colder water temperatures), we observed slower fouling of our PS-*b*-PAA-Amp multilayer coating panel versus SEBS and PVC controls. Data here is extremely difficult to quantify, but what appeared to happen was that the development of the fouling community was slowed down on our coated test panels. It took longer for the predominant fouling present to transition from bioslimes to soft fouling (algae) to the appearance of hard fouling (bryozoans, barnacles).

At roughly four months into the testing, we asked CalPoly to water jet a small section of each panel to record the critical removal stress for the biofouling material present. Our results are summarized in Table 11. In general, PS-*b*-PAA-Amp appears to have had a critical removal stress for 50% of fouling between 40 and 80 psi while the SEBS control had a critical removal stress for 50% of fouling between 80 and 120 psi. PDMS meanwhile experiences nearly 100% removal of fouling by 80 psi. Thus, while PS-*b*-PAA-Amp appears to be functioning as a fouling release coating, it did not match the performance of the PDMS derived Intersleek control in this trial.

Near the end of the testing period once ample barnacle settlement had occurred, force gauge release testing was done on individual barnacles in a manner analogous to that used during lab scale assays on glass slides. Here, we found that barnacles were not readily released and instead were leaving some or all of their basal plate on the coating surface. Thus, despite clear evidence that our coating was functioning as a fouling release material for soft fouling during water jet testing, it did not perform well as a fouling release coating for barnacles.

Table 11. Biofouling coverage data post water jetting at different pressures for large scale test panels of PS-*b*-PAA-Amp and a SEBS control.

Panel	Replicate Patch	Coverage 0 psi	Coverage 40 psi	Coverage 80 psi	Coverage 120 psi	Coverage 180 psi	Coverage 240 psi
Amp	1	100	90	15	5	5	0
	2	100	90	10	10	5	0
	3	100	90	30	5	5	0
SEBS	1	100	100	50	10	5	0
	2	100	100	80	10	5	0
	3	100	100	100	90	0	0

5.3.2.5 Results of Immersion Panel Testing of PS-*b*-PAA-Amp at FIT

The panel immersion testing of PS-*b*-PAA-Amp can also be briefly summarized. All surfaces fouled after one month. Fouling primarily consisted of the barnacle *Amphibalans eburneus*. Other foulers included slime, sponge, encrusting bryozoan and the soft tubes formed by gammarid amphipods. There was a difference in the fouling between north and south directions. The panels facing north had heavier slime and more tubes. The panels facing south had sponge and encrusting bryozoan.

After two months, all surfaces were heavily fouled as shown by the photographs in figures 68 and 69. Fouling primarily consisted of the barnacle *Amphibalanus eburneus*. Other foulers included slime, sponge, encrusting bryozoan and the soft tubes formed by gammarid amphipods. Barnacle adhesion measurements revealed that these surfaces do not readily release them. Shear forces applied to the base of the barnacles caused the shells to break, leaving their bases attached to the coating.

Panels were not water jetted during their testing at FIT, so we did not get an accurate portrayal of their performance relative to release of soft fouling during the field immersion testing. It was important to conduct this study at FIT in addition to CalPoly since the fouling environment at FIT is much more aggressive than that at Calpoly. Additionally, testing our coatings at more than one site will give us a more universal idea of how they perform in different environments. Based on these final field trials, we have decided to no longer pursue the diblock PS-*b*-PAA-Amp coating system for additional

testing since despite its positive lab assays, the field testing results were mixed and it does not appear to be performing as well as PDMS based controls.

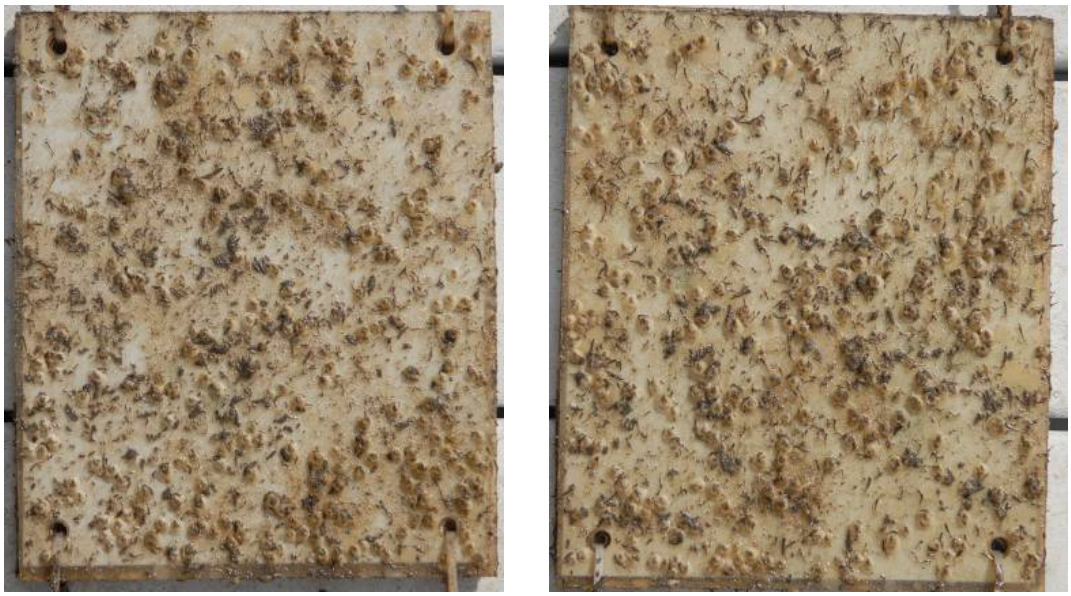

Figure 68. North facing test panels after one month of exposure at FIT. Left, SEBS control, right PS-*b*-PAA-Amp.

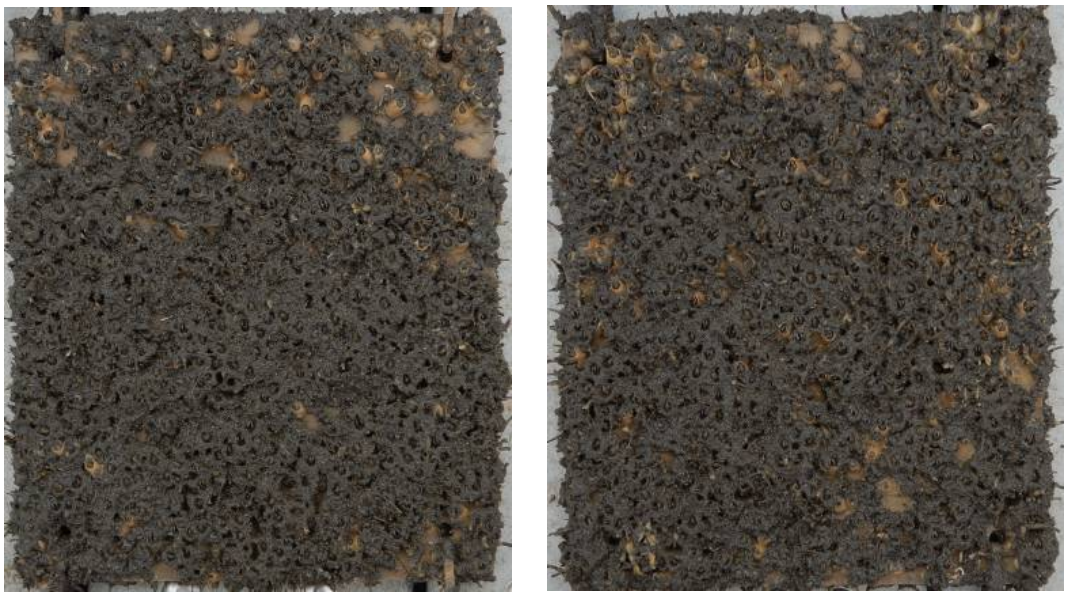

Figure 69. North facing test panels after two months of exposure at FIT. Left, SEBS control, right PS-*b*-PAA-Amp.

5.3.3 Biofouling tests with semifluorinated quaternized PS-*b*-P(E/B)-*b*-PI SABCs

5.3.3.1 Settlement and Release of *Ulva* on SF Quaternized PS-*b*-P(E/B)-*b*-PI

The settlement densities of *Ulva* spores and the removal of *Ulva* sporelings on semifluorinated quaternized PS_{8K}-*b*-$P(E/B)_{25K}$-*b*-PI_{20K}, SQTC-F8H6Br-H6Br and SEBS and PDMSe control surfaces are shown in Figure 70. Spore settlement density was much higher on the quaternized surface than on the PDMSe and SEBS standards. The removal of sporelings from the SQTC-F8H6Br-H6Br surface proved to be much more difficult than removal from the PDMSe surface. The highest observed removal of sporelings on the SQTC-F8H6Br-H6Br surface was only about 40 %, even at 250 kPa. This demonstrates the strong attachment strength of sporelings to the semifluorinated quaternized PS_{8K}-*b*-$P(E/B)_{25K}$-*b*-PI_{20K}, SQTC-F8H6Br-H6Br surface. In general, low-energy surfaces are used as fouling release coatings because the fouling organisms adhere to the surfaces weakly and are released under certain levels of hydrodynamic shear. Fluorinated polymers generally possess low surface energy and are hydrophobic, which suggests their possibility of being practical antifouling/fouling-release coatings for marine surfaces. Unfortunately, the semifluorinated quaternized PS_{8K}-*b*-$P(E/B)_{25K}$-*b*-PI_{20K}, SQTC-F8H6Br-H6Br surface showed the highest settlement of *Ulva* spores and the lowest removal of *Ulva* sporelings regardless of the relatively high content of fluorine in this material (ca. 33% based on elemental analysis). This suggests that the large amount of N^+ ions from the quaternization reactions led more spores to adhere to the surfaces due to the electrostatic attraction between positively charged surfaces and negatively charged spores. These electrostatic effects appear to greatly dominate over any desirable traits provided by the addition of the surface active side group, and thus we have moved on from pursuing this approach for fouling control, despite these materials showed impressive antimicrobial character.

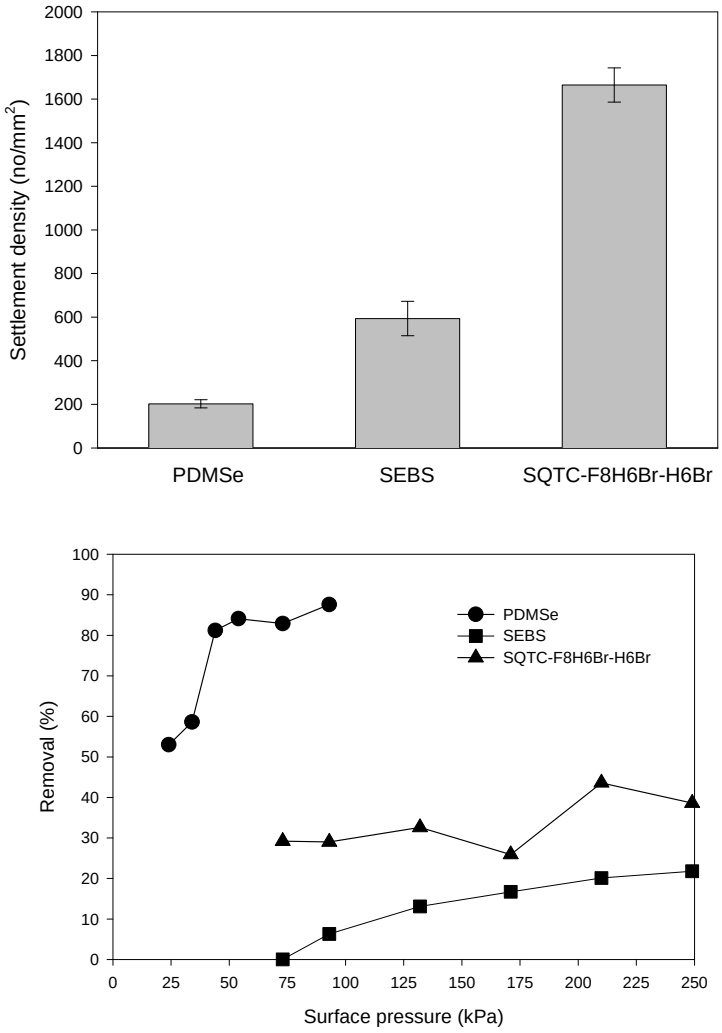

Figure 70. The settlement and removal of *Ulva* spores on semifluorinated quaternized PS-*b*-P(E/B)-*b*-PI SQTC-F8H6Br-H6Br surfaces versus PDMSe and SEBS controls.

5.3.3.2 Antibacterial Behavior of Semifluorinated Quaternized PS-*b*-P(E/B)-*b*-PI

The antibacterial activity of semifluorinated quaternized PS_{8K}-*b*-$P(E/B)_{25K}$-*b*-PI_{20K}, SQTC-F8H6Br-H6Br was determined by comparing the number of bacterial colonies of *S. aureus* and *C. marina* grown on coated test surfaces relative to plain glass slides. As shown in Figure 71, the mean value of bacterial colonies of *S. aureus* grown on plain glass slides after overnight incubation was ca. 125 colonies/cm^2 indicating little if any antibacterial activity. Meanwhile, less than 4 bacterial colonies if any were grown on coated surfaces with SQTC-F8H6Br-H6Br, which reflected high antibacterial activity. We were unable to perform colony count assays on *C. marina* due to the lack of adherence of the bacterial cells to the surfaces leading to the inconsistent growth. However, further study by Live/Dead *Bac*Light Bacterial Viability Assay gave us more

information to understand the antibacterial behavior of SQTC-F8H6Br-H6Br surface on both *S. aureus* and *C. marina*.

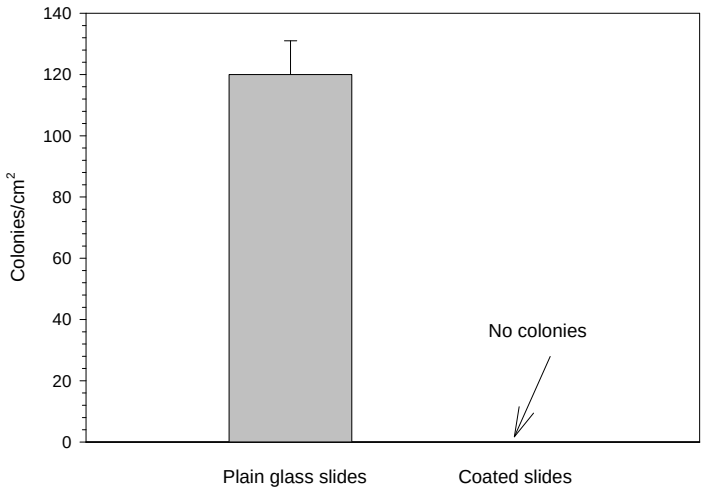

Figure 71. Antibacterial activities of SQTC-F8H6Br-H6Br against *S. aureus*.

Figure 72 shows the fluorescence microscopy images of the Live/Dead Assay at 45 min. Figure 73 depicts the percentage of damaged cells determined by comparison of the live/intact cells (green) and dead/damaged cells (red). At first, the images on *S. aureus* showed no discernable difference between control and coated surfaces (Figures 72A and 72B). However, analysis of the images for total fluorescence by software (Slidebook software, Intelligent Imaging Inc.) showed more cells (ca. 2 fold) on the coated surfaces were damaged with no significant changes in an hour which seemed to be bacteriostatic. The images of *C. marina* showed more cells on the SQTC-F8H6Br-H6Br coated surface were damaged compared with cells on the glass control (Figures 72C and 72D). Additionally, the percentage of damaged cells seemed to increase constantly while the damaged cells on the controls had no significant changes but rather small fluctuations (figure 73). Thus, the antibacterial activity of SQTC-F8H6Br-H6Br surfaces seems to be bacteriostatic through the inhibition of cell divisions for *S. aureus* and bactericidal through the loss of membrane integrity for *C. marina*.

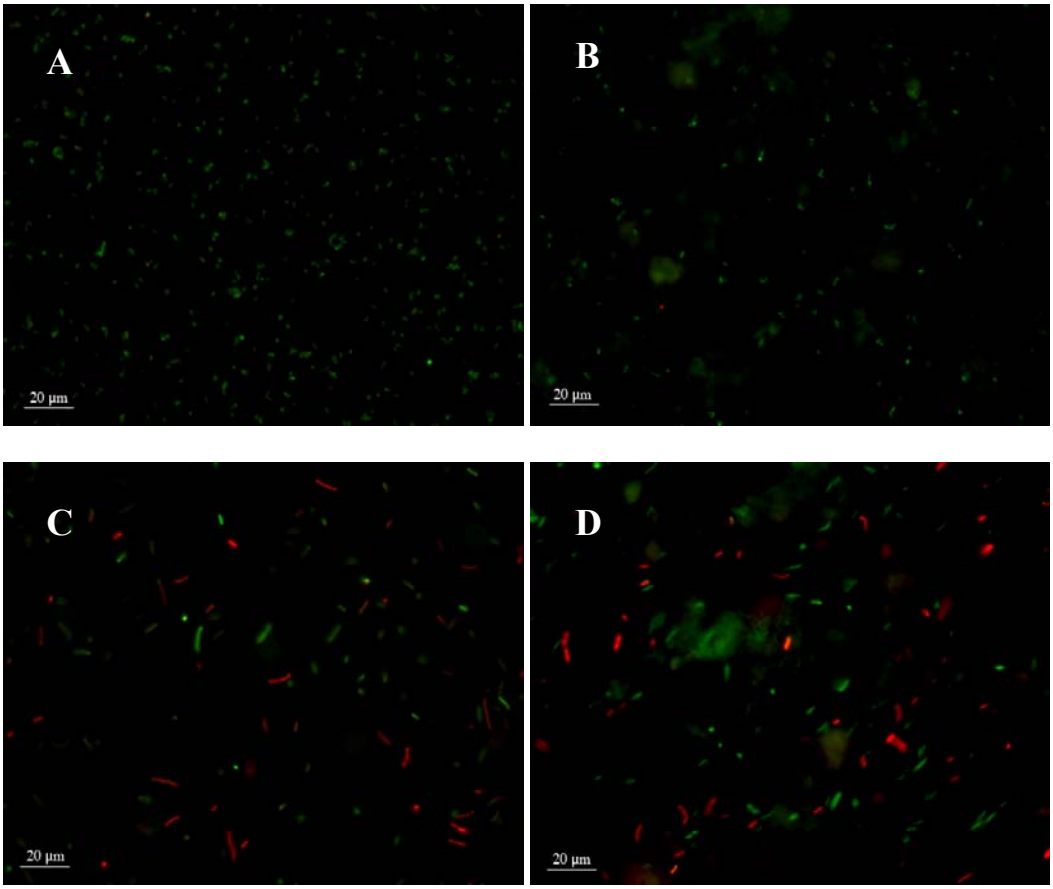

Figure 72. Images of *S. aureus* on (A) glass control; (B) SQTC-F8H6Br-H6Br coated surfaces and images of *C. marina* on (C) glass control; (D) SQTC-F8H6Br-H6Br coated surfaces by Live/Dead *Bac*Light Bacterial Viability Assay. Cells with intact cell membranes are stained green, and those with damaged ones are stained red.

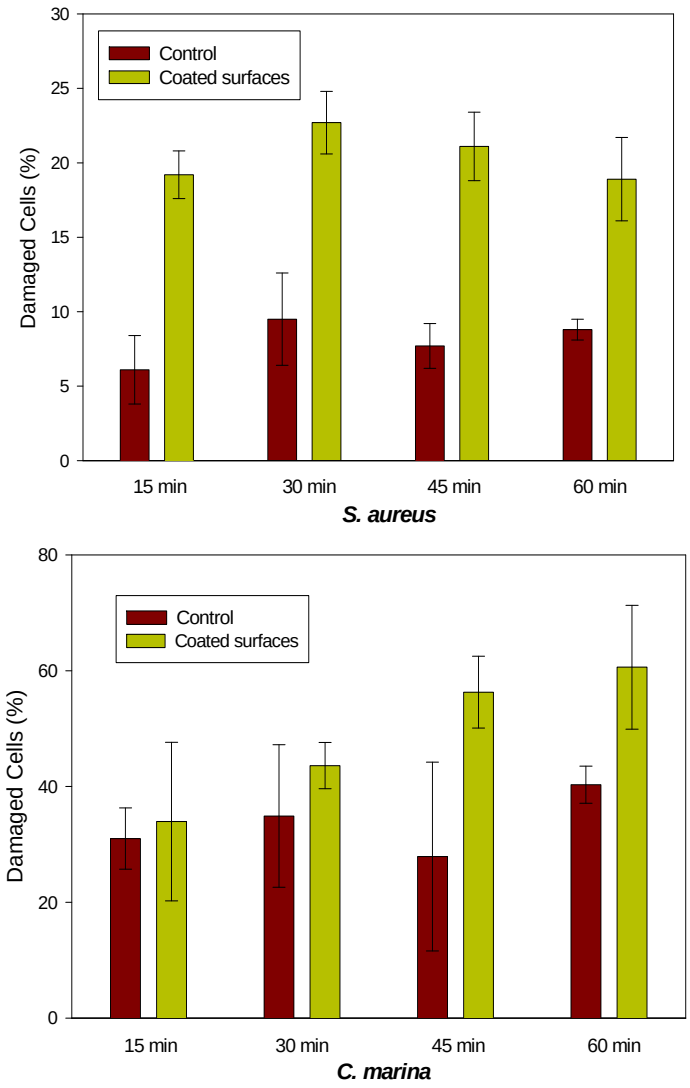

Figure 73. Antibacterial behavior of semifluorinated quaternized PS_{8K}-*b*-$P(E/B)_{25K}$-*b*-PI_{20K}, SQTC-F8H6Br-H6Br against *S. aureus* and *C. marina* by Live/Dead *Bac*Light Bacterial Viability Assay.

5.3.4 Biofouling Tests with PS-b-P(E/B)-b-PI Derived SABCs

5.3.4.1 Leachate Toxicity Test on PS-*b*-P(E/B)-*b*-PI SABCs

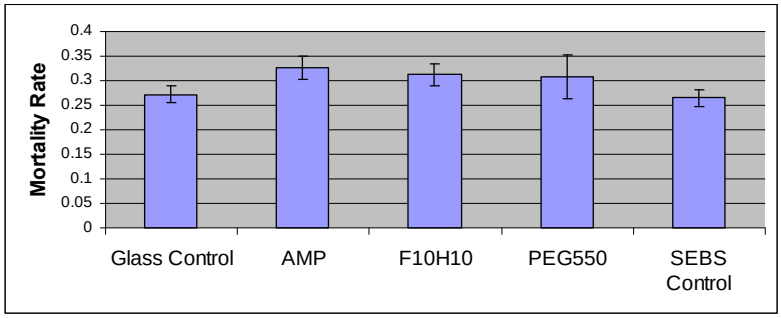

Figure 74. Brine shrimp nauplii mortality rates in leachates produced from three PS_{8K}-*b*-$P(E/B)_{25K}$-PI_{10K} derived samples and a glass control slide.

The results of the leachate test as shown in figure 74 indicated no statistically significant difference between mortality of brine shrimp subjected to the leachate of experimental coatings derived from the triblock PS_{8K}-*b*-$P(E/B)_{25K}$-*b*-PI_{10K} precursor and mortality from glass controls. Amphiphilic ethoxylated fluoroalkyl, PEG550, and F10H10 semifluorinated side chains were tested.

5.3.4.2 Settlement and Release of *Ulva* on PS-*b*-P(E/B)-*b*-PI Derived SABCs

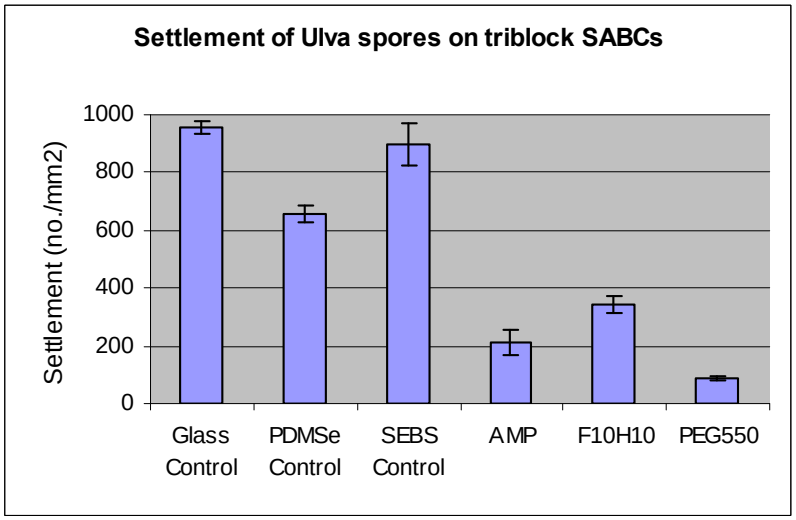

Figure 75. Settlement of *Ulva* spores on triblock PS_{8K}-*b*-$P(E/B)_{25K}$-*b*-PI_{10K} derived SABCs.

Ulva settlement for SABCs derived from the epoxidized PS_{8K}-*b*-$P(E/B)_{25K}$-*b*-PI_{10K} precursor polymer is depicted in figure 75. Ether-linked SABCs of ethoxylated

fluoroalkyl PS_{8K}-*b*-$P(E/B)_{25K}$-*b*-PI_{10K}-Amp, PEGylated PS_{8K}-*b*-$P(E/B)_{25K}$-*b*-PI_{10K}-PEG550 and fluorinated PS_{8K}-*b*-$P(E/B)_{25K}$-*b*-PI_{10K}-F10H10 were examined along with glass, SEBS, and PMDSe silicone controls. Noticeably lower settlement of *Ulva* spores was experienced on all three experimental coatings, with PS_{8K}-*b*-$P(E/B)_{25K}$-*b*-PI_{10K}-PEG550 and PS_{8K}-*b*-$P(E/B)_{25K}$-*b*-PI_{10K}-Amp performing the best. Sporeling growth was normal on all coatings with no signs of toxicity and biomass directly related to settlement.

Critical water jet forces for sporeling removal meanwhile are depicted in Figure 76. Of particular note here is the fact that the PS_{8K}-*b*-$P(E/B)_{25K}$-*b*-PI_{10K}-Amp sample is functioning better than the PDMSe control as a foul release material. Furthermore, PS_{8K}-*b*-$P(E/B)_{25K}$-*b*-PI_{10K}-PEG550 is functioning on the order of the PDMSe control. Surprisingly, the PS_{8K}-*b*-$P(E/B)_{25K}$-*b*-PI_{10K}-F10H10 sample functioned very poorly at releasing sporelings; only on the order of the SEBS control. We speculate that this may be caused by an insufficient packing density of the F10H10 side chains on the polymer backbone to sufficiently prevent the F10H10 surface active side groups from reconstructing and "being buried" once the SABC is exposed to an aqueous environment. Our contact angle data showing a large hysteresis for this sample suggests that this may be the case. Nevertheless, the performance of the PEGylated, and especially the amphiphilic sample in this assay were superb.

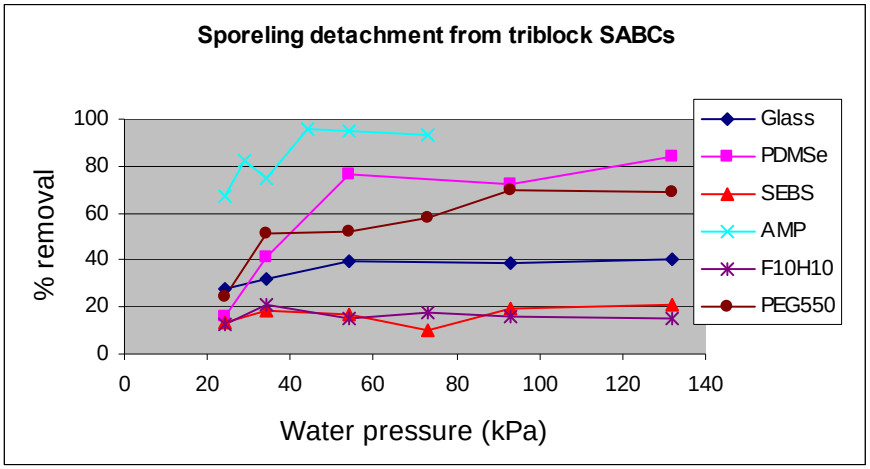

Figure 76. Critical detachment force curves for *Ulva* sporelings on PS_{8K}-*b*-$P(E/B)_{25K}$-*b*-PI_{10K} derived SABCs when exposed to a water jet.

5.3.4.3 Settlement and Release of *Navicula* on PS-*b*-P(E/B)-*b*-PI Derived SABCs

Navicula settlement for SABCs derived from the epoxidized PS_{8K}-*b*-$P(E/B)_{25K}$-*b*-PI_{10K} precursor polymer is depicted in Figure 77. Ether-linked SABCs of ethoxylated fluoroalkyl PS_{8K}-*b*-$P(E/B)_{25K}$-*b*-PI_{10K}-Amp, PEGylated PS_{8K}-*b*-$P(E/B)_{25K}$-*b*-PI_{10K}-PEG550 and fluorinated PS_{8K}-*b*-$P(E/B)_{25K}$-*b*-PI_{10K}-F10H10 were examined along with glass, SEBS, and PMDSe silicone controls. Noticeably lower settlement of *Navicula* diatoms was experienced on the PS_{8K}-*b*-$P(E/B)_{25K}$-*b*-PI_{10K}-PEG550 and PS_{8K}-*b*-

$P(E/B)_{25K}$-*b*-PI_{10K}-Amp coatings, but results were not as drastic as those experienced for the *Ulva* spores.

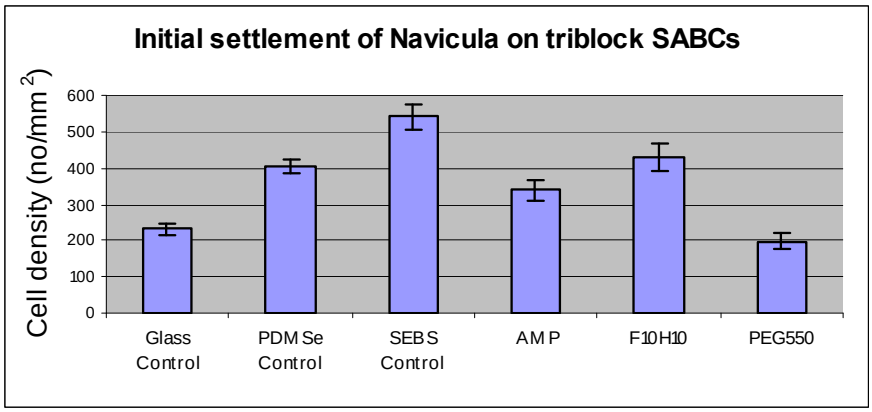

Figure 77. Settlement of *Navicula* diatoms on PS_{8K}-*b*-$P(E/B)_{25K}$-*b*-PI_{10K} derived SABCs.

Figure 78 meanwhile depicts the removal data for *Navicula* diatoms from the three triblock PS_{8K}-*b*-$P(E/B)_{25K}$-*b*-PI_{10K} derived SABCs. The most important observation here is that the ethoxylated fluoroalkyl containing PS_{8K}-*b*-$P(E/B)_{25K}$-*b*-PI_{10K}-Amp SABC is again performing extremely well as a fouling release material. Generally, *Ulva* released well from hydrophobic surfaces while *Navicula* released well from hydrophilic surfaces. This suggests that our triblock PS_{8K}-*b*-$P(E/B)_{25K}$-*b*-PI_{10K}-Amp has more universal antifouling properties and is in line with what we previously saw for PS-*b*-PAA-Amp. Of particular interest here is that the PEG550 functionalized SABC had unexpectedly low release properties for *Navicula* diatoms (despite showing good settlement results).

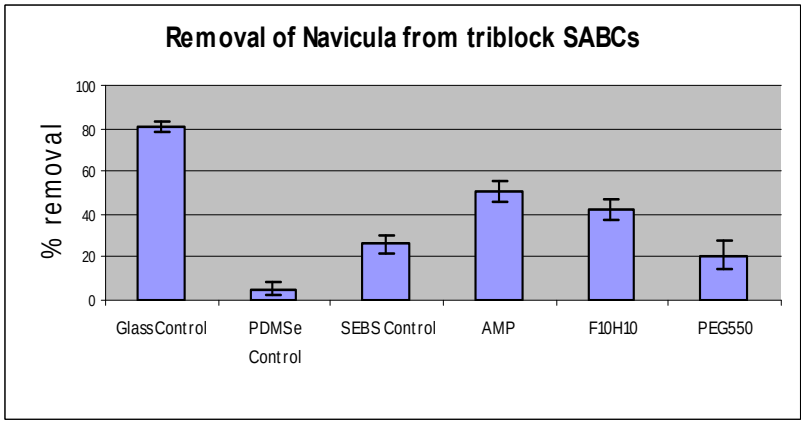

Figure 78. Removal of *Navicula* diatoms from PS_{8K}-*b*-$P(E/B)_{25K}$-*b*-PI_{10K} derived SABCs.

5.3.4.4 Results of PS-*b*-P(E/B)-*b*-PI Triblock SABC Barnacle Settlement and Growth Testing

As depicted in figure 79, barnacles cyprid larvae settlement was conducted on the three PS_{8K}-*b*-$P(E/B)_{25K}$-*b*-PI_{10K} derived SABCs. PS_{8K}-*b*-$P(E/B)_{25K}$-*b*-PI_{10K}-Amp was the best performing coating in terms of settlement rate, performing significantly better than all three controls. Settlement on the glass control was lower than expected. PS_{8K}-*b*-$P(E/B)_{25K}$-*b*-PI_{10K}-PEG550 also showed decent settlement results while PS_{8K}-*b*-$P(E/B)_{25K}$-*b*-PI_{10K}-F10H10 does not appear to have deterred settlement. Grow out and release testing were inconclusive since the few barnacles that settled on the PS_{8K}-*b*-$P(E/B)_{25K}$-*b*-PI_{10K}-Amp and PS_{8K}-*b*-$P(E/B)_{25K}$-*b*-PI_{10K}-PEG550 coatings died before reaching full maturity. PS_{8K}-*b*-$P(E/B)_{25K}$-*b*-PI_{10K}-F10H10 did not function as a fouling release coating for barnacles; the basal plates broke.

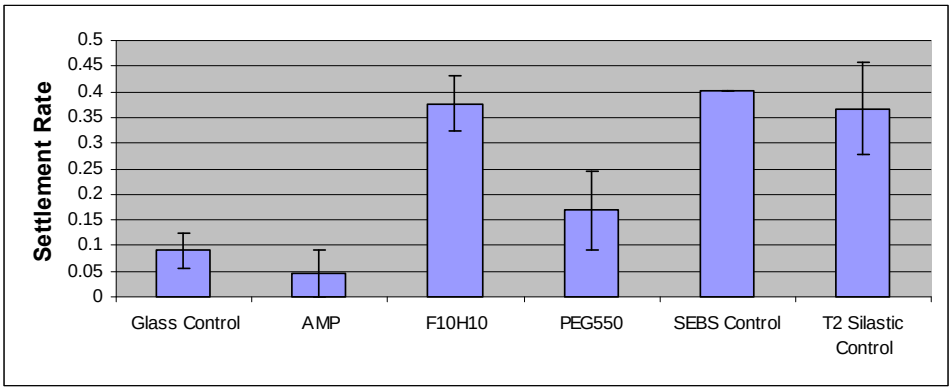

Figure 79. Barnacle cyprid larvae settlement on PS_{8K}-*b*-$P(E/B)_{25K}$-*b*-PI_{10K} derived SABCs.

5.3.5 PS-*b*-P(E/B)-*b*-PI Functionalized with "Mixed" Hydrophobic and Hydrophilic Side Chains

5.3.5.1 Protein Adsorption Results on "Mixed" Amphiphilic PS-*b*-P(E/B)-*b*-PI SABCs

Figure 80 depicts fluorescence microscopy images of adsorbed BSA protein on surfaces of the four mixed amphiphilic SABCs derived from PS_{8K}-*b*-$P(E/B)_{25K}$-*b*-PI_{20K} along with results form a SEBS control. From visual inspection, one can discern the decreasing fluorescence with increasing PEG550 content. When BSA protein adsorption was quantified relative to the SEBS control using image analysis software, the data in figure 81 was obtained. Here, our analysis clearly shows the trend between BSA adsorption and the content of PEG550 alcohol in the feed (and subsequently, attached).

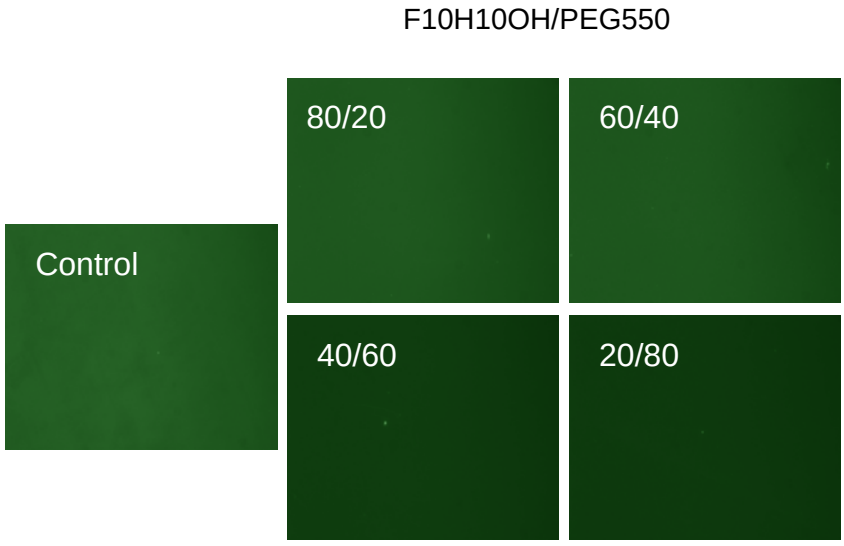

Figure 80. Fluoresence microscopy images of BSA protein adsorption on mixed amphiphilic surfaces derived from PS_{8K}-*b*-$P(E/B)_{25K}$-*b*-PI_{20K} SABC precursor.

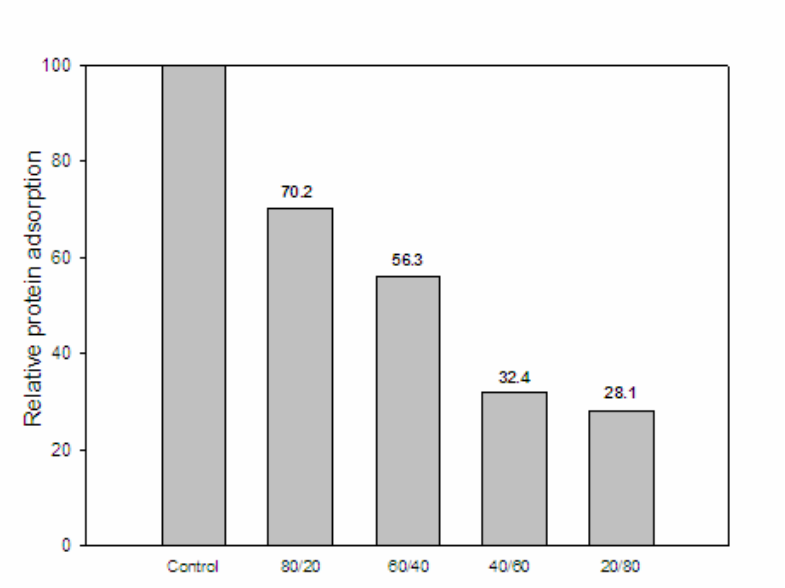

Figure 81. Quantified fluorescence microscopy data for mixed amphiphilic surfaces derived from PS_{8K}-*b*-$P(E/B)_{25K}$-*b*-PI_{20K} SABC precursor.

5.3.5.2 Settlement and Release of *Ulva* on "Mixed" Amphiphilic PS-*b*-P(E/B)-*b*-PI SABCs

Ulva spore settlement density on the various mixed amphiphilic SABCs derived from PS_{8K}-*b*-$P(E/B)_{25K}$-*b*-PI_{20K} is depicted in figure 82. There is a downward trend in settlement relative to the amount of PEG550 alcohol incorporated in the SABC, but this trend is inconclusive with 60% PEG550 alcohol in the feed showing more settlement than for 40% PEG550 alcohol in the feed despite the very low relative settlement for the sample with 80% PEG550 alcohol in the feed. Figure 83 meanwhile depicts growth of *Ulva* sporelings on the mixed amphiphiplic SABCs derived from PS_{8K}-*b*-$P(E/B)_{25K}$-*b*-PI_{20K}. No clear relationship between the ratio of PEG550 and F10H10 side groups incorporated in the SABC and sporeling growth can be determined here, but it is interesting to note that the two samples derived from the 80% feed ratios showed lower growth. Finally, figure 84 and table 12 depict the critical removal force for *Ulva* sporelings on the various mixed amphiphilic SABCs derived from PS_{8K}-*b*-$P(E/B)_{25K}$-*b*-PI_{20K}. Here, the removal results for both the 60:40 and 40:60 PEG550:F10H10 samples were extremely impressive (>95% at low water jet pressure), with both samples performing at and or better than the PDMSe control. Additionally, relatively high removal of *Ulva* sporelings was also possible on the 20:80 and 80:20 PEG550:F10H10 samples at slightly higher applied water jet force.

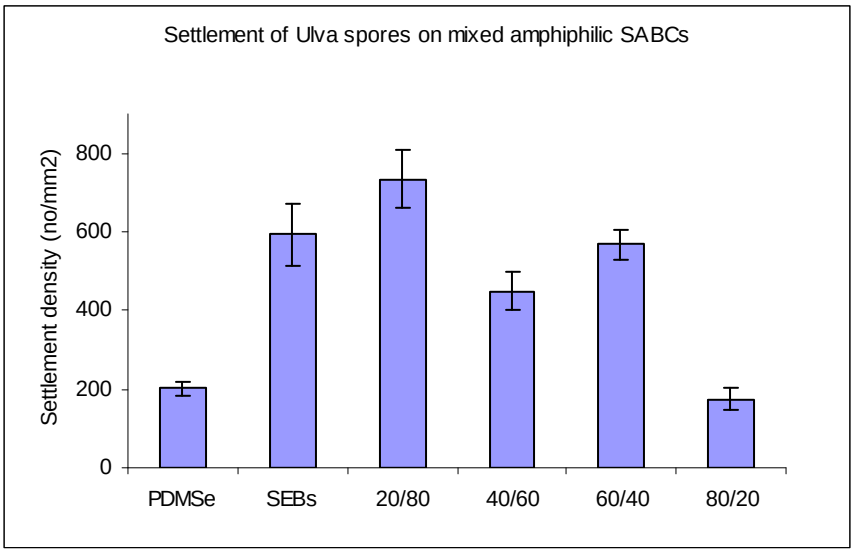

Figure 82. Settlement of *Ulva* spores on mixed amphiphilic PS_{8K}-*b*-$P(E/B)_{25K}$-*b*-PI_{20K} derived SABCs. Ratios listed are PEG550:F10H10 in the reaction feed.

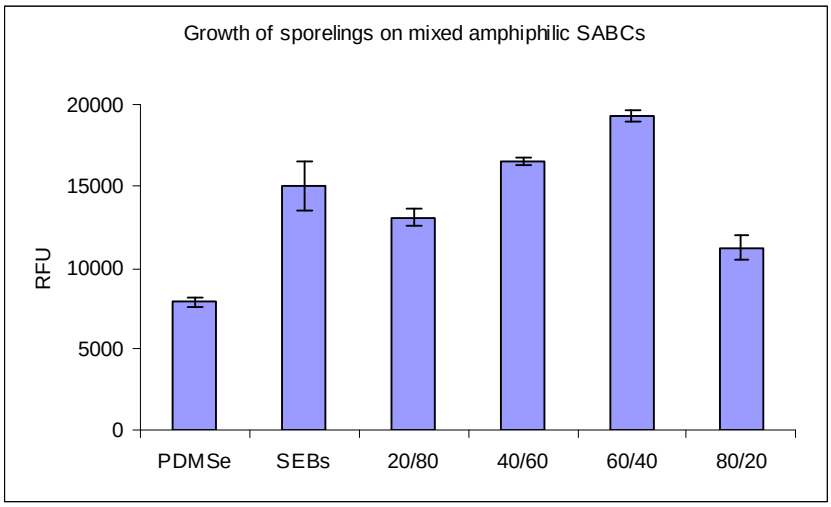

Figure 83. Growth of *Ulva* sporelings on mixed amphiphilic PS_{8K}-*b*-$P(E/B)_{25K}$-*b*-PI_{20K} derived SABCs. Ratios listed are PEG550:F10H10 in the reaction feed.

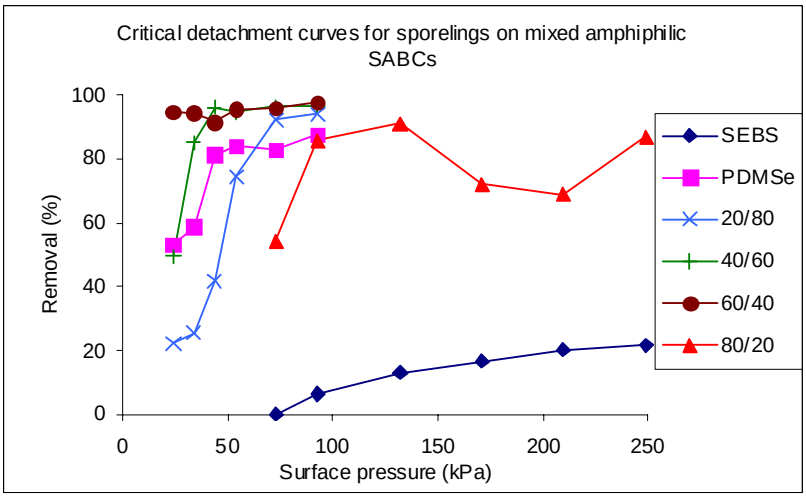

Figure 84. Critical detachment force curves for *Ulva* sporelings on mixed amphiphilic PS_{8K}-*b*-$P(E/B)_{25K}$-*b*-PI_{20K} derived SABCs when exposed to a water jet. Ratios listed are PEG550:F10H10 in the reaction feed.

Table 12. Summary of results for critical detachment force for *Ulva* sporelings on mixed amphiphilic PS_{8K}-*b*-$P(E/B)_{25K}$-*b*-PI_{20K} derived SABCs when exposed to a water jet.

Label (PEG/fluorinated side chain ratio)	Estimated surface pressure (kPa) for 50% removal
60/40	<25
40/60	25
PDMSe	25
20/80	45
80/20	70
SEBS	>250

5.3.5.3 Settlement of *Ulva* Spores and Release of *Ulva* Sporelings From SABCs Based on PS_{8K}-b-$P(E/B)_{25K}$-b-PI_{10K}

Figure 85A shows the settlement density of *Ulva* spores on glass, PDMS, G1652 SEBS and amphiphilic SABCs derived from the PS_{8K}-b-$P(E/B)_{25K}$-b-PI_{10K} precursor and the ethoxylated fluoroalkyl nonionic surfactant. For the experimental surfaces, the lowest spore settlement was recorded for the amphiphilic SABC. *Ulva* spores are known to preferentially settle on hydrophobic, low energy surfaces. This was true for the PDMS control surface, which showed the greatest settlement of *Ulva* spores. The lower observed settlement on the amphiphilic SABC however suggests that the materials' apparent ability to readily reorganize in a polar environment likely deters settlement of spores. Also of note is the stark contrast between the high observed settlement on the G1652 SEBS base layer and the low observed settlement for the amphiphilic SABC, clearly highlighting the ability of the thin layer of SABC to drastically modify the surface properties and settlement behavior of the multilayer coating system. Figure 85B meanwhile depicts *Ulva* sporeling growth on the experimental surfaces. *Ulva* growth generally scaled with settlement, with the least biomass recorded on the amphiphilic SABC.

Finally, the percentage removal of *Ulva* sporelings from the experimental surfaces at a range of applied water jet pressures is given in figure 86. The amphiphilic SABC demonstrated extremely robust fouling release behavior with regards to *Ulva* sporelings, releasing ca. ~ 67% of *Ulva* biomass at an applied water jet pressure of 24 kPa, and over 95% biomass at an applied pressure of just 44 kPa. This contrasted to the PDMS control which only released 16% *Ulva* biomass at an applied water jet pressure of 24 kPa, and even at an applied water jet pressure of 132 kPa only released 84% of biomass. The

combination of favorable settlement results with exceptional release results for *Ulva* in this initial assay led us to question what effect substituting the new, softer Kraton MD6945 thermoplastic elastomer in place of Kraton G1652 would have on the fouling release characteristics of the coating. While multiple studies have been published previously equating lower modulus with enhanced fouling release of calciferous "hard" macrofouling organisms such as barnacles, minimal data has been reported on "soft" fouling organisms such as *Ulva* and *Navicula*. Chaudhury *et al*. examined a range of PDMS coatings with different degrees of polymerization and determined that there was a sharp drop off in fouling release performance at modulus values above 2 MPa (13). This suggested that further reduction of the bulk modulus of the coating could prove advantageous to its fouling release performance.

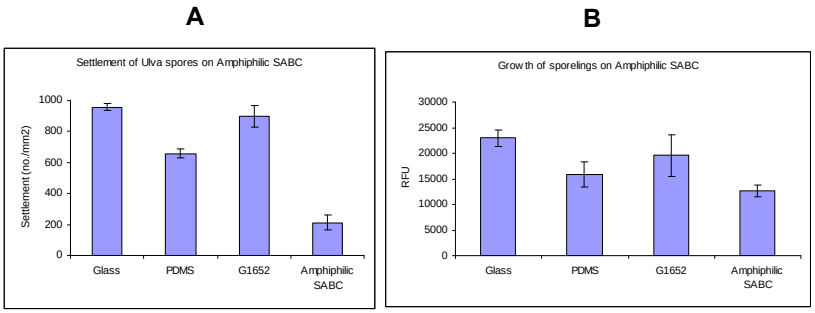

Figure 85. Results of *Ulva* biofouling assays on glass, G1652 SEBS, PDMS and the PS_{8K}-*b*-$P(E/B)_{25K}$-*b*-PI_{10K} derived amphiphilic SABC with ethoxylated fluoroalkyl side chains. A) The settlement of *Ulva* spores. Each point is the mean from 90 counts on 3 replicate slides. Bars show 95% confidence limits. B) The growth of *Ulva* sporelings. Each point is the mean biomass from 6 replicate slides measured using a fluorescence plate reader. Bars show standard error of the mean.

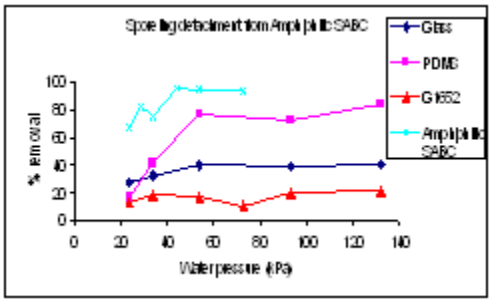

Figure 86. The removal of *Ulva* sporelings. Slides were exposed to a water jet over a range of pressures. One slide was used for each reported pressure.

To pursue this goal and also to check the repeatability of the initial *Ulva* testing, samples for biofouling assay of the amphiphilic SABC containing ethoxylated fluoroalkyl side chains were again prepared. In this experiment however, both the high modulus G1652 SEBS and the low modulus MD6945 SEBS were tested independently for their effect on settlement and release characteristics of *Ulva* spores and *Ulva* sporelings

respectively when used as the base layer for the multilayer coating system. Figure 87A depicts the result of the *Ulva* spore settlement assay. Despite similar settlement performance for multilayer coatings of the amphiphilic SABC incorporating both G1652 and MD6945, the base layer controls on their own surprisingly showed very different settlement behavior with the low modulus MD6945 SEBS thermoplastic elastomer showing the lowest overall biomass of any of the five surfaces evaluated. The hydrophobic, low surface energy PDMS elastomer showed high settlement as expected. The growth of *Ulva* sporelings in the assay, given in Figure 87B, generally correlated to the amount of biomass settled, indicating no unexpected toxicity for any of the coatings as in the initial test. Meanwhile, Figure 87C depicts the percentage removal of *Ulva* sporelings from the experimental surfaces at a range of different applied water jet pressures in this additional iteration of testing. Again, the amphiphilic SABC demonstrated exceptional fouling resistance with both the high modulus G1652 and the low modulus MD6945 base layers, but with the low modulus MD6945 base layer was particularly notable for imparting extremely robust release properties to the coating even at the lowest tested applied water jet pressures. Even at an applied water jet pressure of 19 kPa, the amphiphilic SABC coating on a base layer of the low modulus MD6945 demonstrated ca. ~ 87% removal of *Ulva* sporeling biomass. This contrasted to ca. ~ 17% removal for the amphiphilic SABC on a base layer of the high modulus G1652 at an applied pressure of 19 kPa, and ca. ~ 21% removal for the PDMS control at an applied pressure of 23 kPa. This trend continued with greater than 99% of *Ulva* sporeling biomass removed from the amphiphilic SABC with the MD6945 base layer at an applied water jet pressure of 26 kPa. This contrasted the maximum observed biomass removal for PDMS (ca. ~ 89% at 63 kPa) and the amphiphilic SABC on the G1652 base layer (ca. ~ 94% at 46 kPa). This suggests clearly that the order of magnitude drop in modulus between the high modulus G1652 and the low modulus MD6945 resulted in a drastic increase in fouling release efficacy. Results are summarized in Table 13 which gives the critical applied water jet pressure to remove 50% of the *Ulva* sporeling biomass for each experimental surface. These results generally agree with the determination in Chaudhury et al. that the ease of *Ulva* sporeling removal greatly increases for substrates with a modulus below 2.7 MPa (13). Care must be taken however since clearly the surface chemistry presented to fouling organisms by our amphiphilic SABC is significantly different than that of PDMS. Nevertheless, these findings taken in conjunction with those previously reported clearly support a hypothesis that the release of soft fouling organisms can greatly be facilitated through the use of very low modulus materials with an elastic modulus value on the order of 3 MPa or less.

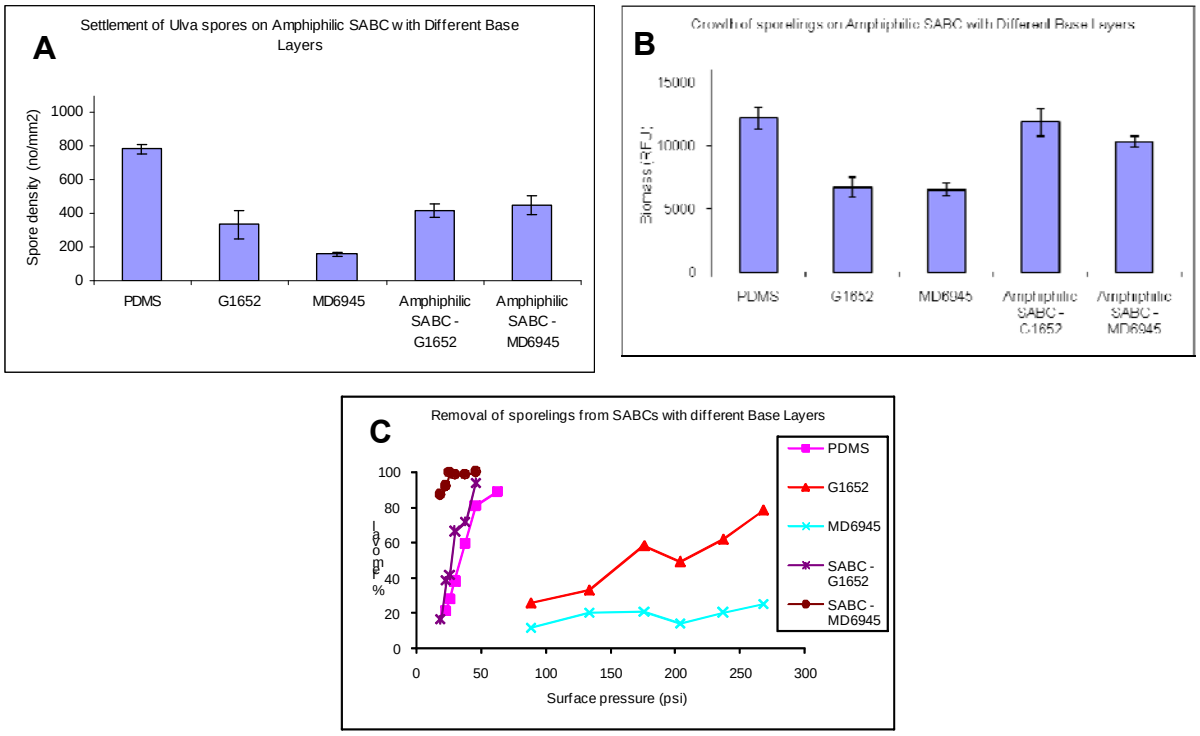

Figure 87. Results of *Ulva* biofouling assays on G1652 SEBS, MD6945 SEBS, PDMS and the PS_{8K}-*b*-$P(E/B)_{25K}$-*b*-PI_{10K} derived amphiphilic SABC with ethoxylated fluoroalkyl side chains on both thermoplastic elastomer base layers. A) The settlement of *Ulva* spores. Each point is the mean from 90 counts on 3 replicate slides. Bars show 95% confidence limits. B) The growth of *Ulva* sporelings. Each point is the mean biomass from 6 replicate slides measured using a fluorescence plate reader. Bars show standard error of the mean. C) The removal of *Ulva* sporelings. Slides were exposed to a water jet over a range of pressures. One slide was used for each reported pressure.

Table 13. Estimated critical applied water jet surface pressure for 50% removal of *Ulva* sporeling biofilm derived from the curve in Figure 87C.

Sample	Est. Surface Pressure for 50% Removal (kPa)
PDMS	34
G1652	152
MD6945	>270
Amphiphilic SABC – G1652	26
Amphiphilic SABC - MD6945	<10

5.3.5.4 Settlement and Removal of *Navicula* Diatoms on SABCs Prepared From PS_{8K}-*b*-$P(E/B)_{25K}$-*b*-PI_{10K}

Navicula diatom settlement is depicted in Figure 88A on the amphiphilic SABC with ethoxylated fluoroalkyl side chains in conjunction with glass, G1652 SEBS and PDMS controls. Since diatoms reach a fouling surface by sinking through the water column under the influence of gravity (they do not sample the surface like *Ulva*), measured attachment is more a function of differences in adhesion strength following gentle washing. Settlement of *Navicula* diatoms on the amphiphilic SABC was found to be noticeably lower than that on both the hydrophobic PDMS elastomer control, and the G1652 SEBS base layer control. As expected, glass showed lower settlement due to its hydrophilic nature. Removal results for *Navicula* diatoms, given in Figure 88B, inversely correlate to settlement as expected, with the highest removal being seen on the samples with the lowest settlement (where weak adhesion was implied). The most important thing to note here is that while the PDMS elastomer only showed ca. ~ 5% removal of the *Navicula* diatoms, the amphiphilic SABC demonstrated ca. ~ 51% removal. This clearly demonstrates the ability of the amphiphilic SABC to also function as an effective antifouling and fouling-release coating for *Navicula* diatoms, despite their generally contrary settlement and release behavior relative to the green alga *Ulva*. This highlights this approaches potential versus traditional PDMS derived fouling-release elastomers.

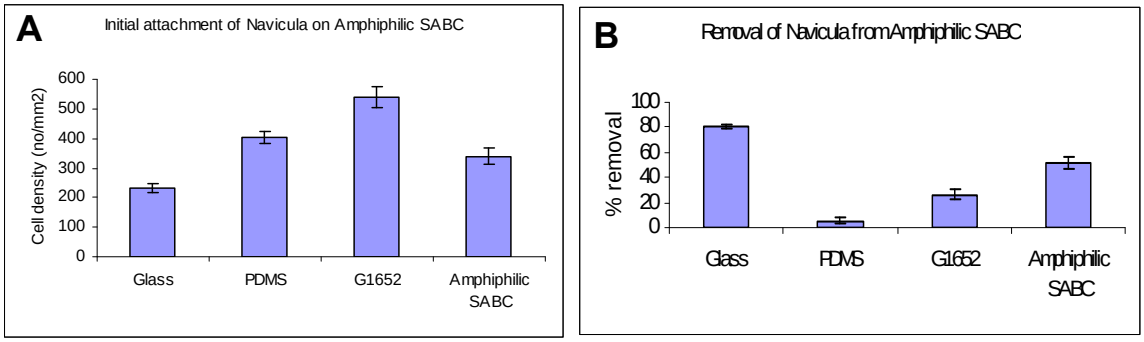

Figure 88. A) Initial attachment after gentle washing of *Navicula* diatoms to PS_{8K}-*b*-$P(E/B)_{25K}$-*b*-PI_{10K} derived amphiphilic SABC with ethoxylated fluoroalkyl side chains. B) Detachment of *Navicula* diatoms from same SABC as a result of exposure to a shear stress of 23 Pa. Each point is the mean from 90 counts on 3 replicate slides. Bars show 95% confidence limits.

5.3.5.5 Leachate Toxicity and Barnacle Settlement

The results of the leachate test indicated no significant difference between mortality of brine shrimp subjected to the leachate of experimental coatings and mortality of those from glass controls (ANOVA, $F = 0.615$, $p = 0.6587$). Barnacle cyprid larvae testing indicated that both experimental coatings had significantly lower settlement than glass and PDMS (T2) and SEBS controls. For this assay however, we noticed a lower than

expected settlement of barnacle cyprid larvae on the glass control. There was a significant difference in the settlement of barnacle cyprid larvae between coatings (ANOVA, $F = 43.210$, $p < .0001$, see figure 89). Post-hoc testing showed that SABC-MD (ethoxylated fluoroalkyl SABC on low modulus SEBS MD6945) and SABC-G (ethoxylated fluoroalkyl SABC on high modulus SEBS G1652) had significantly lower settlement than all other test coatings and controls. Settlement on glass was significantly higher than SABC-MD and SABC-G but was significantly lower than the other controls. In the case of SABC-MD, SABC-G and glass, the drops spread out due to the hydrophilic nature of the surfaces. However, in most cases there was still enough liquid for the cyprids to swim around and settlement did occur in low numbers on SABC-MD and SABC-G and was near 40% on glass. These data show that SABC-MD and SABC-G were functioning well as anti-fouling coatings by inhibiting settlement of barnacle cyprid larvae.

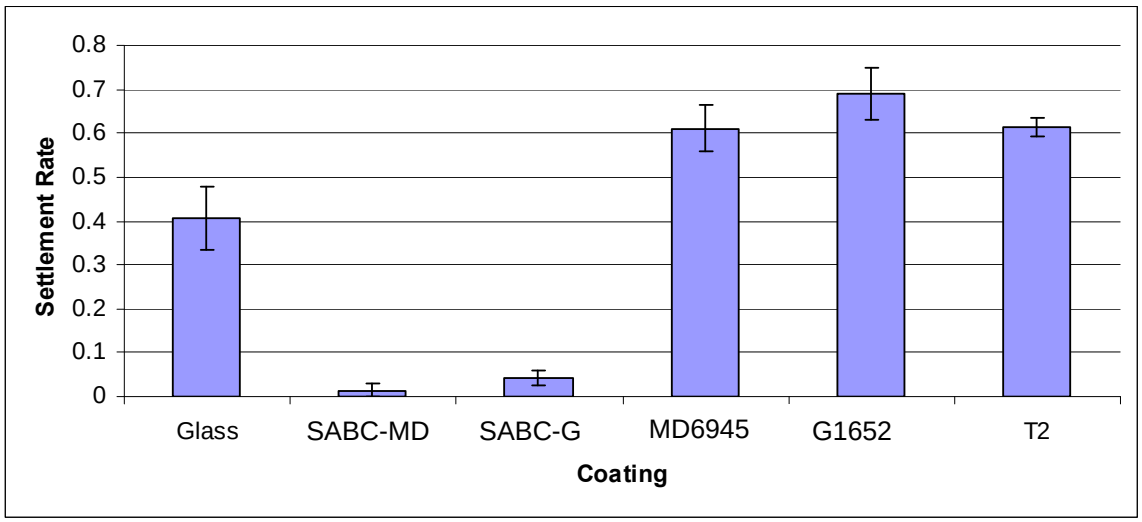

Figure 89. Settlement rate of barnacle cypris larvae analyzed by coating. Error bars represent the standard error of the mean.

5.3.5.6 Barnacle Growth and Release

Removal force testing performed on all the surfaces showed breakage of all individuals. All barnacles broke and left a complete basal plate on the surface of each coating. This indicates that the force measured was not the strength of adhesion of the barnacle to the surface, but the cohesive strength of the barnacle itself. Consequently, the barnacles were adhering to the experimental surfaces with greater strength than could be measured by our test. Previous experiments have shown that basal plate breakage is an indication of coating performance with regards to barnacle fouling release. Better performing coatings such as Gelest and Sylgard have lower percentages of basal plate remaining with an increase in basal plate area. The coatings tested showed results similar to those of glass from previous studies with 100% breakage at all sizes. This indicated that the coatings were not performing well as foul-release coatings with regards to these organisms.

This was true of all coatings that could be tested. Both the SABC coatings showed significantly lower settlement than the G1652 and MD6945 base layer controls, as well as the T2 PDMS and glass controls. During the grow out period, several of these barnacles died or were removed because they were too close to or over the edge of the slide (where we are unable to test their cohesive attachment force by pushing them). Therefore, at the time of removal testing there were relatively low numbers of barnacles to push from SABC-G and none remaining on SABC-MD. However, even though the numbers were lower, all barnacles removed showed the same result as the rest with 100% basal plate remaining on the surface of the coating. This would suggest that the SABC-G coating (with a bulk modulus of 18 MPa) was not functioning as a fouling release coating with regards to barnacles. Additional experiments are needed however to probe if the SABC-MD coating, with its significantly lower modulus, has better fouling release properties (as we expect it will).

5.3.5.7 Immersion Panel testing of PS-*b*-P(E/B)-*b*-PI Derived Coatings at FIT

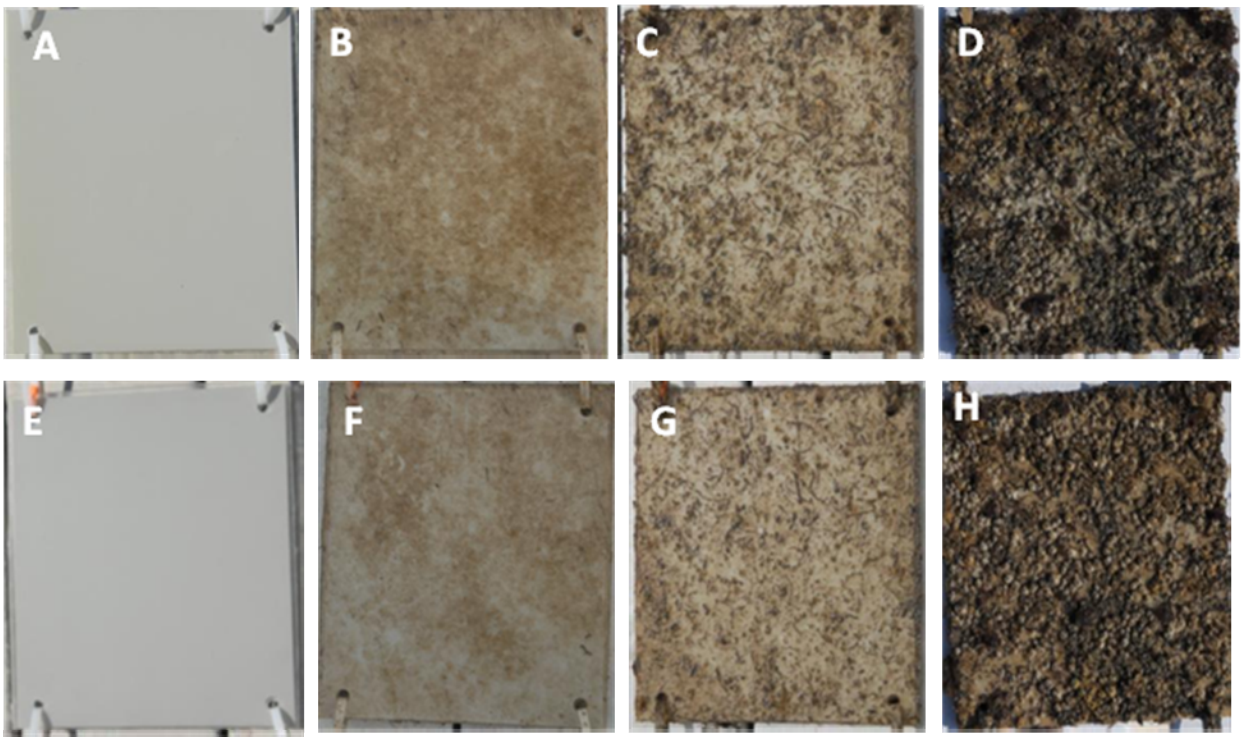

Figure 90. Pictures depicting the development of marine fouling on SEBS control (top) and SABC replicate 3 panels at FIT's sea-water immersion site. For the SEBS control, A = 0 weeks (initial), B = 2 weeks, C = 4 weeks, and D = 6 weeks. For the SABC replicate 3, E = 0 weeks (initial), F = 2 weeks, G = 4 weeks and H = 6 weeks.

After 6 weeks of immersion, fouling consisted of slime, arborescent and encrusting bryozoans, hydroids, sponges, tubeworms, softworms, and barnacles. Generally, fouling appeared similar on the control and three replicates. Water jet testing was performed on all four panels. None completely cleaned at maximum pressure (240 psi), however, the

best release was seen on the SABC replicate 3. Barnacle adhesion strength measurements were not possible due to shell breakage and base plates remaining adhered to the coating, suggesting that the coatings were not functioning as effective fouling release materials with regards to barnacles. Pictures depicting the development of the fouling community on both the control and SABC replicate 3 are given in figure 90. In general, development of the fouling community appears to have taken place a bit faster on the control than the SABC coating, but overall results were quite similar.

5.3.5.8 Settlement and Removal of *Ulva* Spores and Removal of *Ulva* Sporelings

The set of SABCs derived from the PS_{8K}-*b*-$P(E/B)_{25K}$-*b*-PI_{10K} polymer were evaluated for *Ulva* spore settlement, and *Ulva* sporeling growth and release to see if information regarding the fouling-release performance of these materials could be ascertained. Since this sample set was produced at a later date than that derived from the PS_{8K}-*b*-$P(E/B)_{25K}$-*b*-PI_{20K} polymer (previously evaluated last year), we hoped that the inclusion of purely PEGylated and purely fluorinated SABCs in conjunction with the more symmetric attachment distribution of side chains would aid in optimization of this approach.

Figure 91A shows the settlement density of *Ulva* spores on PDMS, MD6945 SEBS and SABCs derived from the PS_{8K}-b-$P(E/B)_{25K}$-b-PI_{10K} precursor. Trends were generally as expected and correlated very closely with the PS_{8K}-b-$P(E/B)_{25K}$-b-PI_{20K} derived samples reported on previously, with those samples containing the largest proportion of the PEG550 side chain showing the lowest settlement. As expected in this case, the hydrophobic PDMS control showed a high amount of settlement. The removal of *Ulva* spores for the PS_{8K}-b-$P(E/B)_{25K}$-b-PI_{10K} derived samples (Figure 91B) showed an interesting trend similar to that for *Ulva* sporeling release from the PS_{8K}-b-$P(E/B)_{25K}$-b-PI_{20K} derived samples with some optimal mixture of hydrophilic PEG550 and hydrophobic F10H10 side chains appearing to give exceptional release. In this case, the polymer with 19% attachment of F10H10 side chains and 28% attachment of PEG550 side chains show ca. ~ 51% removal of *Ulva* spores, better than the ca. ~ 42% removal demonstrated by the PDMS control. A very similar polymer in this test with regards to bulk and surface characterization (derived from 22% attachment of F10H10 side chains and 27% attachment of PEG550 side chains) only demonstrated ca. ~ 27% removal of *Ulva* spores however. This suggests that the optimal "mixture" of side chains for *Ulva* spore release may still benefit from further optimization. Again, the growth of *Ulva* sporelings (Figure 92A) was generally consistent with the settlement density of spores, suggesting no inherent coating toxicity. Figure 92B depicts the results of sporeling removal tests using a range of water jet pressures. Whilst the lower boundary for relative incorporation of PEG550 to F10H10 side chains was not as well pronounced as was seen for the PS_{8K}-b-$P(E/B)_{25K}$-b-PI_{20K} derived coatings, both of the samples incorporating slightly more PEGylated than fluorinated side chains, along with the purely PEGylated sample, showed extremely promising fouling-release characteristics. When taken with the previous experiment, in conjunction with the spore release data, the sample incorporating 19% F10H10 and 28% PEG550 side chains appears to be particularly promising with regards to *Ulva* spore settlement and release, and growth and release of sporelings.

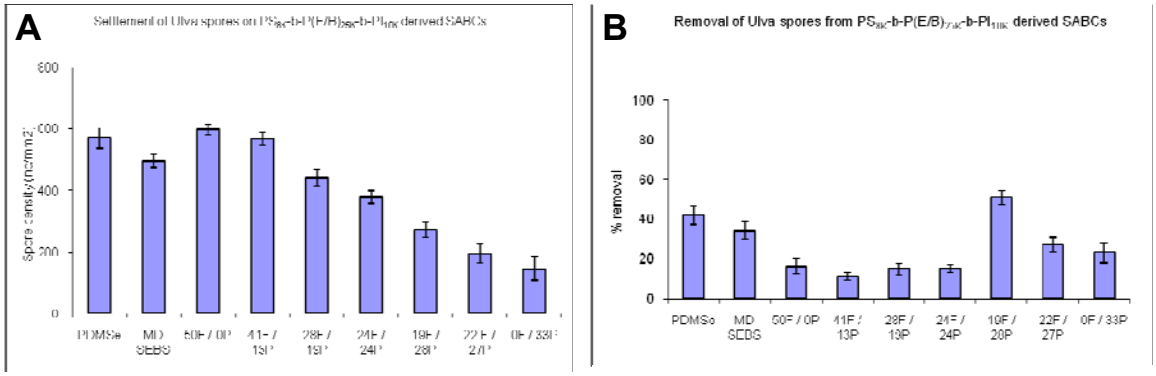

Figure 91. A) The settlement densities of *Ulva* spores on PS_{8K}-*b*-$P(E/B)_{25K}$-*b*-PI_{10K} derived SABCs. B) The removal of *Ulva* spores from PS_{8K}-*b*-$P(E/B)_{25K}$-*b*-PI_{10K} derived SABCs coatings. Each point is the mean from 90 counts on 3 replicate slides. Bars show 95% confidence limits.

Table 14 summarizes the estimated critical pressure to release 50% of the attached *Ulva* sporelings for both sets of coatings. The combination of the PS_{8K}-b-$P(E/B)_{25K}$-b-PI_{10K} derived SABCs with the MD6945 thermoplastic elastomer base layer led to a wide range of coatings that performed similarly, or better than, the PDMS control. This further suggests that a wide range of sample chemistries can be explored with regards to antifouling and fouling-release performance relative to other marine organisms while retaining robust performance against the green alga *Ulva*.

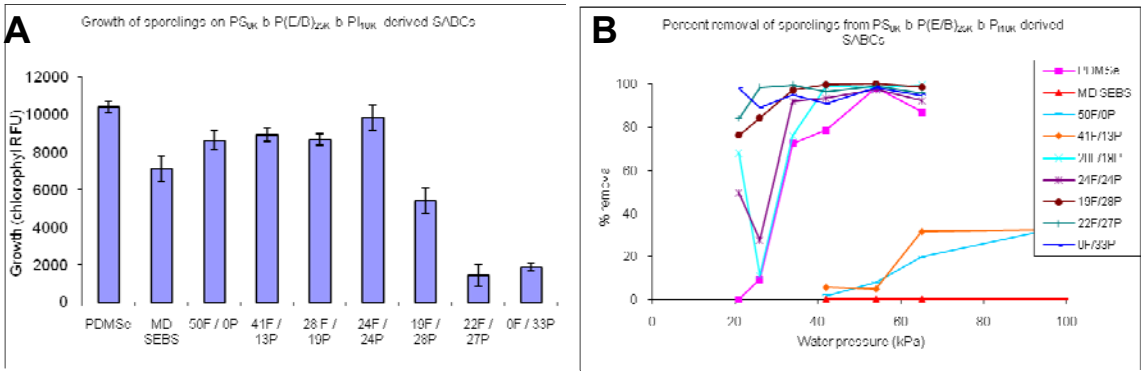

Figure 92. A) The growth of *Ulva* sporelings on PS_{8K}-*b*-$P(E/B)_{25K}$-*b*-PI_{10K} derived SABCs after 7 days. Each point is the mean biomass from 6 replicate slides measured using a fluorescence plate reader (RFU; relative fluorescence unit). Bars show standard error of the mean. B) Detachment of *Ulva* sporelings from PS_{8K}-*b*-$P(E/B)_{25K}$-*b*-PI_{10K} derived SABCs. Coated slides were exposed to the water jet over a range of water pressures. One slide was used at each pressure.

Table 14. Critical surface pressures for 50% removal of *Ulva* sporeling biofilm derived from *Ulva* sporeling removal curves in figure 92B.

PS_{8K}-b-P(E/B)$_{25K}$-b-PI_{10K} Precursor	
Sample	Est. Surface Pressure for 50% Removal (kPa)
PS_{8K}-b-P(E/B)$_{25K}$-b-PI_{10K}-0F-33P	<21
PS_{8K}-b-P(E/B)$_{25K}$-b-PI_{10K}-22F-27P	<21
PS_{8K}-b-P(E/B)$_{25K}$-b-PI_{10K}-19F-28P	<21
PS_{8K}-b-P(E/B)$_{25K}$-b-PI_{10K}-24F-24P	29
PS_{8K}-b-P(E/B)$_{25K}$-b-PI_{10K}-28F-19P	31
PS_{8K}-b-P(E/B)$_{25K}$-b-PI_{10K}-41F-13P	165
PS_{8K}-b-P(E/B)$_{25K}$-b-PI_{10K}-50F-0P	250
PDMSe	31
MD 6945 SEBS	>288

5.3.5.9 Settlement and Removal of *Navicula* Diatoms

Diatom cells are not motile in the water column, hence in a laboratory assay, cells reach a surface by falling through the water by gravity. Thus, at the end of the incubation period, in principle the same number of cells will be present on every surface. Therefore, any differences in the number of cells attached after the slides have been manipulated after the settlement period, including the gentle washing step, represents differences in the ability of cells to adhere initially to the substratum. The gentle washing process (which was carried out by submerging the samples in seawater) caused water to flow over the surfaces of the coatings and removed unattached and/or weakly attached cells. A strong trend between the density of attached cells and the fluorinated/PEGylated content of the coatings can be seen (Figure 93). The density of attached cells decreased as the PEG550 content increased. This concurs with previous studies which have consistently shown that diatoms adhere more strongly to hydrophobic surfaces. Samples with F10H10 content of 28% or less had cell densities lower than those seen on the glass standards. Exposure to a shear stress of 20 Pa in a water channel caused loss of *Navicula* cells from the surfaces (Figure 93). The number of cells remaining on the surfaces of the coatings followed the same trend as that seen after gentle washing i.e. decreasing strength of attachment with increasing PEG550 content.

Data expressed as percentage removal of *Navicula* following exposure to the 20 Pa shear stress are shown in Figure 94. The data indicate that for most surfaces, including the PDMSe standards, a further 40-50 % of the cells detached, but there was no trend with PEG550 content. Removal from the 22% F10H10 / 27% PEG550 and 0% F10H10 / 33% PEG550 coatings was highest (60-70%), and similar to that from the glass standards.

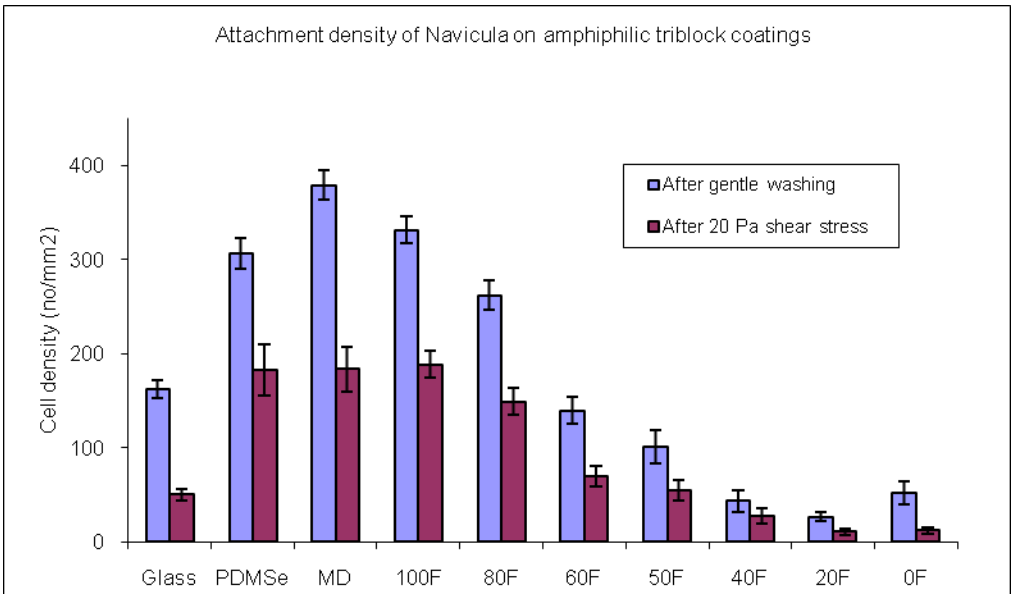

Figure 93. The attachment densities of *Navicula* cells on fluorinated and PEGylated amphiphilic triblock copolymer coatings after gentle washing and after exposure to a shear stress of 20 Pa in the water channel. Each point is the mean from 90 counts on 3 replicate slides. Bars show 95% confidence limits.

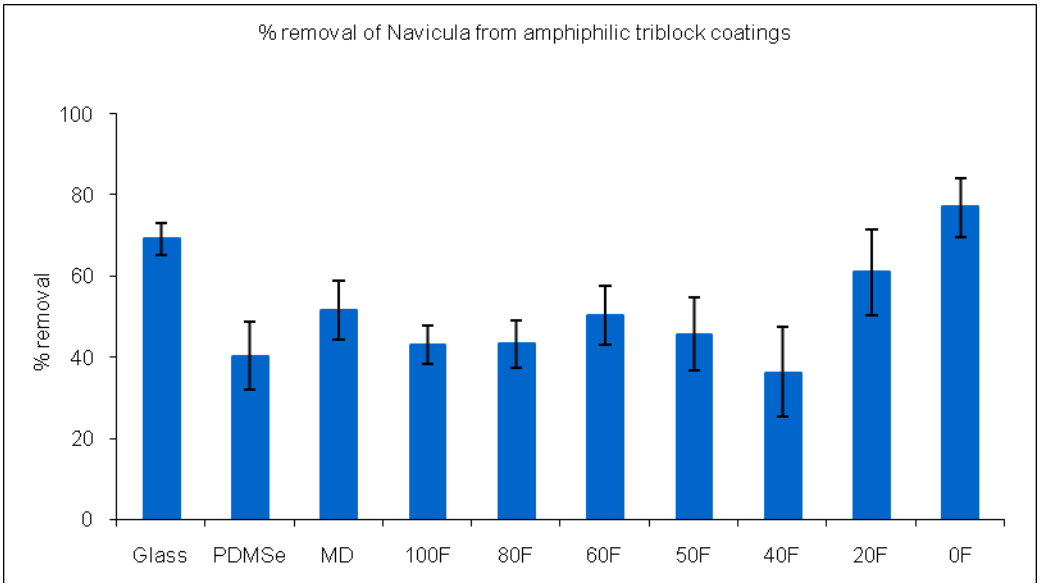

Figure 94. The percentage removal of *Navicula* cells from fluorinated and PEGylated triblock amphiphilic copolymer coatings caused by exposure to a shear stress of 20 Pa in the water channel. Each point is the mean from 90 counts on 3 replicate slides. Bars show 95% confidence limits derived from arc-sine transformed data.

5.3.6 Settlement and Removal of *Ulva* Spores and Removal of *Ulva* Sporelings From Brij Attached PS-b-P(E/B)-b-PI SABCs

Figure 95 shows the settlement density of *Ulva* spores on glass, PDMS, MD6945 SEBS and Brij amphiphilic SABCs derived from the PS_{8K}-b-$P(E/B)_{25K}$-b-PI_{10K} precursor. For the experimental surfaces, the lowest spore settlement was recorded for the amphiphilic SABC. *Ulva* spores are known to preferentially settle on hydrophobic, low energy surfaces. This was true for the PDMS control surface, which showed the greatest settlement of *Ulva* spores. The lower observed settlement on the amphiphilic SABC however suggests that the materials' apparent ability to readily reorganize in a polar environment likely deters settlement of spores. Spore settlement densities were lower on all the SABC surfaces than on the glass and PDMSe standards or SEBS control. On all the samples apart from the K3-Brij 30, spore density was approx. 30 % of that on the standards / control. On K3-Brij 30, the settlement density was approx. 60 % of that on the standards / control.

The percentage removal of *Ulva* sporelings from the experimental surfaces at a range of applied water jet pressures is given in figure 96. Sporeling strength of attachment on the K3-Brij 72 was low and similar to that on the PDMSe standard. Attachment strength was also weak on the K3-Brij76 and K3-Brij 78 coatings (nearly as low as on PDMSe). The K3-Brij 72 amphiphilic SABC demonstrated robust fouling release behavior with regards to *Ulva* sporelings, releasing 50% of *Ulva* biomass at an applied water jet pressure of 38 kPa. This similar to the PDMS control which released 50% *Ulva* biomass at an applied water jet pressure of 32 kPa (Table 15).

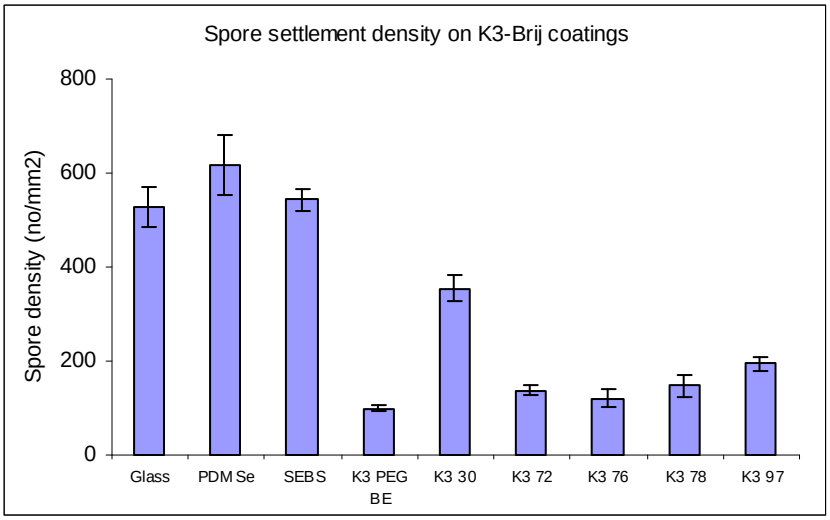

Figure 95. The settlement densities of *Ulva* spores on K3-Brij copolymer coatings. Each point is the mean from 90 counts on 3 replicate slides. Bars show 95% confidence limits.

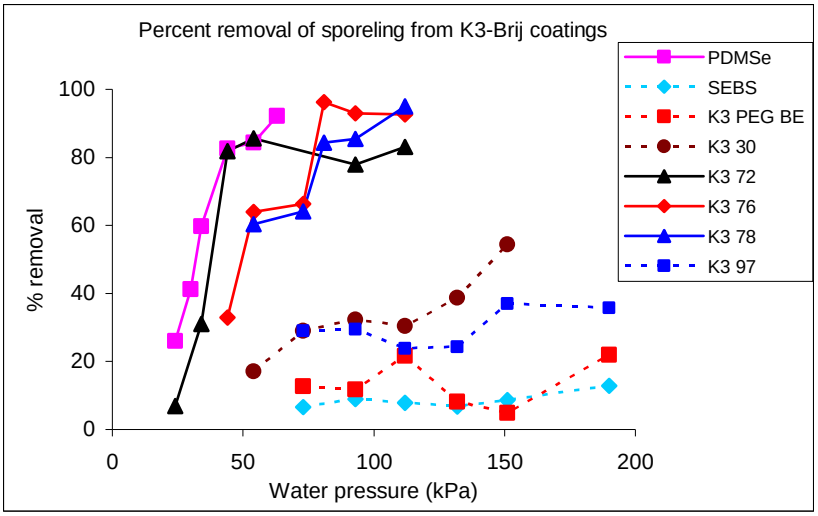

Figure 96. Detachment of *Ulva* sporelings from K3-Brij copolymer coatings. Coated slides were exposed to the water jet over a range of water pressures. One slide was used at each pressure.

Table 15. Surface pressures for 50% removal of poreling biofilm derived from curves in figure 96.

Compounds	Estimated surface pressure (kPa) for 50% removal
PDMSe	32
K3-Brij 72	38
K3-Brij 76	50
K3-Brij 78	50 (interpolated)
Glass	112
K3-Brij 30	146
K3-PEG.BE	>190
K3-Brij 97	>190
SEBS	>190

5.3.7 Settlement and Removal of *Ulva* Spores and Removal of *Ulva* Sporelings From Pluronic Attached PS-b-P(E/B)-b-PI SABCs

Figure 97 shows the settlement density of *Ulva* spores on glass, PDMS, and Pluronic amphiphilic SABCs derived from the PS_{8K}-b-$P(E/B)_{25K}$-b-PI_{10K} precursor.
For the experimental surfaces, the slightly lower spore settlement was recorded for the amphiphilic SABC compare to the PDMS. Spore settlement densities were higher on the K3-PluL35 than on the K3PluL31 and K3-Plu10R5 polymers. The lowest density of spores was on the K3-Plu10R5 which was approximately half that on the K3-PluL35. Sporeling growth broadly followed the trend seen with spore settlement (Figure 97). Growth on the K3-Plu10R5 was lower than might be expected from the spore settlement data, and observations under the microscope showed that although plant numbers were low there were no signs of toxicity (Figure 98). Sporeling strength of attachment on the K3-pluronic polymer was high (Figure 99). None had a fouling-release performance that matched that of the PDMSe standard. The typical grown Ulva sporelings on glass slides

are shown in figure 100. There was no removal from the SEBS base control over the range of water pressures tested. Removal was highest from the K3-PluL35. This supports the spore attachment strength data shown in Figure 99. However, it should be pointed out that the release of sporelings from K3-PluL35 was no greater than from glass. The antifouling and fouling-release performance of the K3-Pluronic polymers was poor compared with that shown for other K3-nonionic surfactant formulations in previous studies.

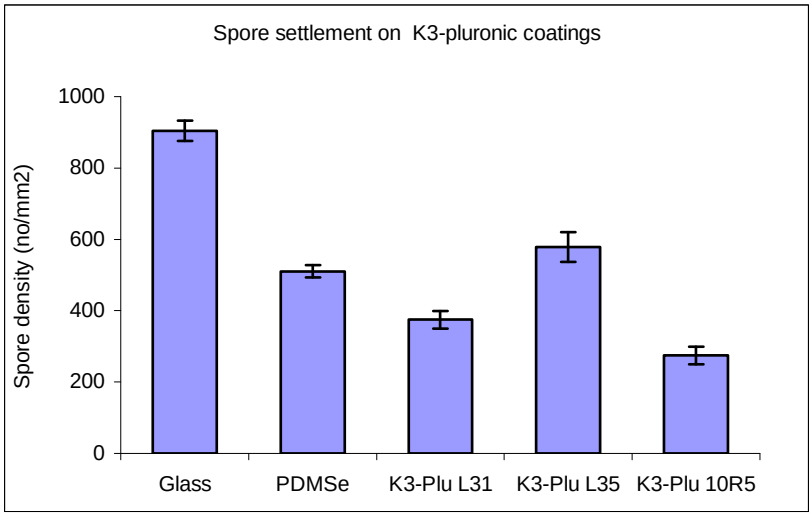

Figure 97. The settlement densities of *Ulva* spores on K3-pluronic copolymer coatings. Each point is the mean from 90 counts on 3 replicate slides. Bars show 95% confidence limits.

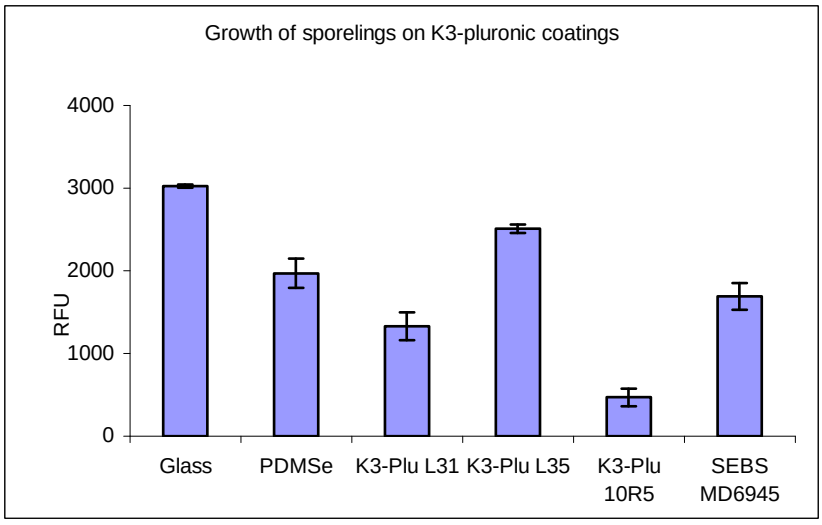

Figure 98. The growth of *Ulva* sporelings on K3-Pluronic copolymer coatings after 7 days. Each point is the mean biomass from 6 replicate slides measured using a fluorescence plate reader (RFU; relative fluorescence unit). Bars show standard error of the mean.

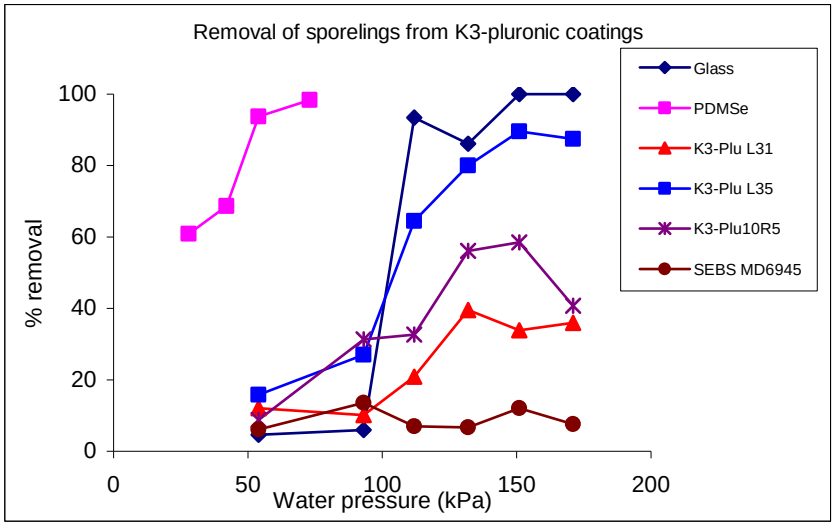

Figure 99. Detachment of *Ulva* sporelings from K3-pluronic copolymer coatings. Coated slides were exposed to the water jet over a range of water pressures. One slide was used at each pressure.

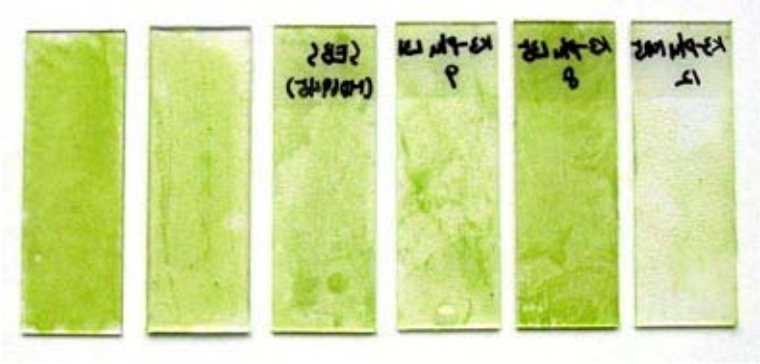

Figure 100. Typical growth of *Ulva* sporelings on K3- pluronic copolymers coatings after 7 days. From left; Glass PDMSe, SEBS, K3-pluL31, K3-pluL35, K3-plu10R5.

5.3.8 Settlement and Removal of *Ulva* Spores and Removal of *Ulva* Sporelings From Hydrocarbon/PEG "Mixed" Amaphiphilic Attached to K3

Spore settlement densities on the amphiphilic coatings decreased with octadecanol content (Figure 101). Settlement densities on all the amphiphilic coatings were lower than on PDMSe and MD.

Biomass production on the amphiphilic coatings followed that of spore settlement described in Figure 102. On some coatings biomass was greater than on the PDMSe and MD standards (contrary to spore settlement density). The higher 1-octadecanol contained amphiphilic coatings is shown the lower growth. Sporelings grew normally on all coatings with no indications of toxicity (Figure 103).

Sporeling strength of attachment on the amphiphilic coatings was relatively weak, but stronger than on the PDMSe standards. (ie at any given water pressure slightly less

detached than from PDMSe standard). The weakest attachment was on the coating with no octadecanol (O0) and was similar to that on the PDMSe. However, there was no obvious trend in attachment strength on the other amphiphilic coatings. The glass slides with grown biofilm before exposing to water jet is shown in figure 104.

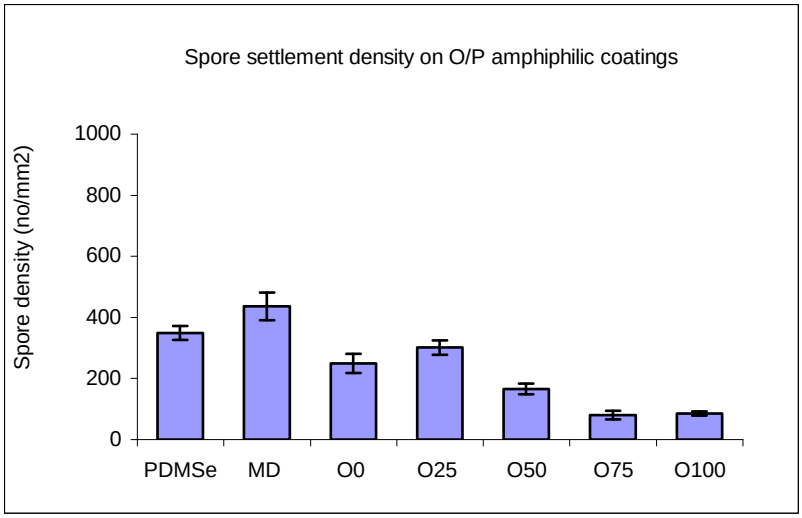

Figure 101. The density of attached *Ulva* spores on amphiphilic coatings after 1 hour settlement. Each point is the mean from 90 counts on 3 replicate slides. Bars show 95% confidence limits.

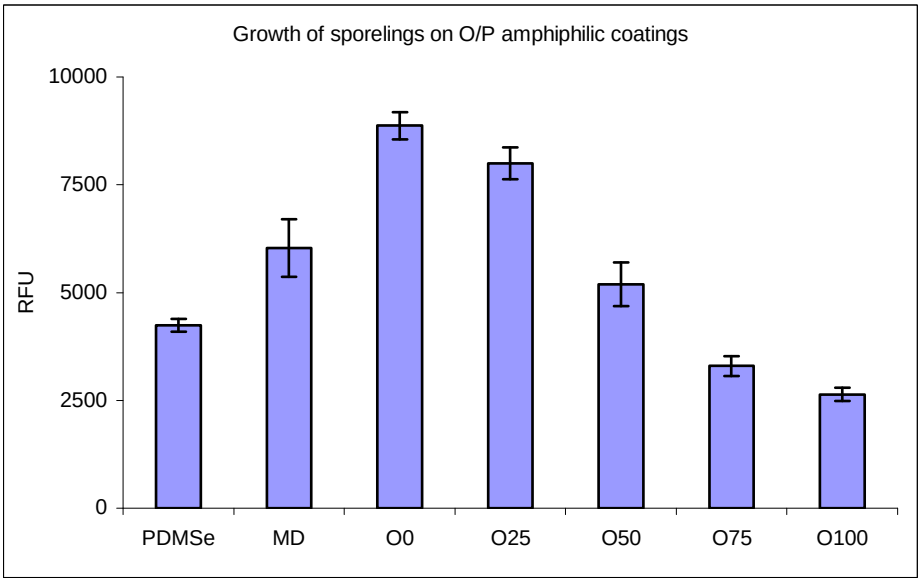

Figure 102. The growth of *Ulva* sporelings on amphiphilic coatings after 7 days. Each point is the mean biomass from 6 replicate slides measured using a fluorescence plate reader (RFU; relative fluorescence unit). Bars show standard error of the mean.

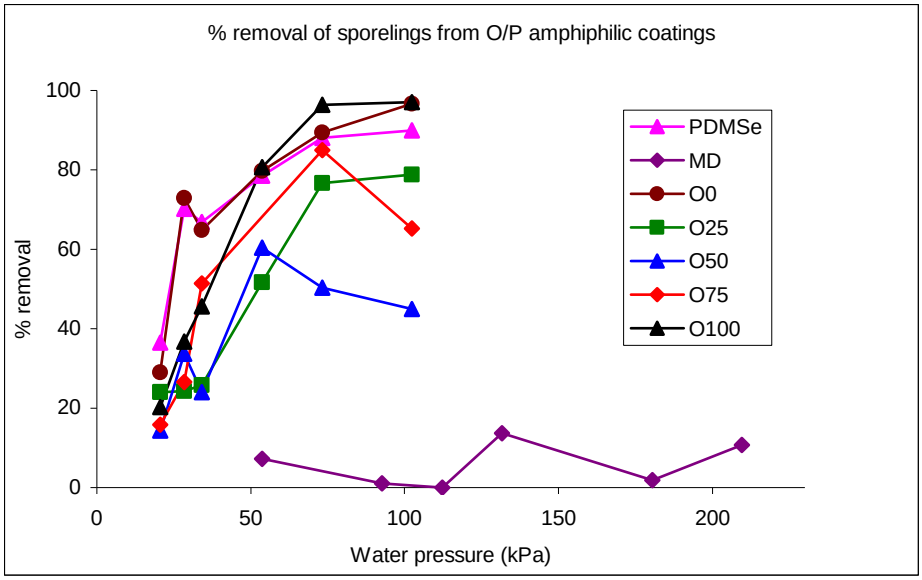

Figure 103. Percent removal of 7 day old sporelings from amphiphilic coatings plotted as a function of surface water pressure (kPa). Coatings were exposed to a range of different surface pressures from the water jet. PDMS is T2 Silastic.

Table 16 summarizes the estimated critical pressure to release 50% of the attached *Ulva* sporelings for both sets of coatings. The combination of the PS_{8K}-b-$P(E/B)_{25K}$-b-PI_{10K} derived SABCs with the MD6945 thermoplastic elastomer base layer led to a wide range of coatings that performed similarly the PDMS control.

Table 16. Critical surface pressures for 50% removal of sporeling biofilm derived from curves in figures 104. Samples listed in order of ease of removal.

Label	Critical water pressure (kPa)
PDMSe	24
O 0	24
O 75	34
O 100	36
O 50	48
O 25	52
MD	>200

Figure 104. Image of sporeling biofilms on Si coatings after 7 days growth (before exposure to water jet). From left: Glass, PDMSe, MD, O0, O25, O50, O75, O100.

6.0 Summary

At the beginning of this project a series of potential semifluorinated SABCs based on a SBS precursor were synthesized. This reaction was then successfully scaled up using the F8H2 semifluorinated side chain to produce enough SABC for small scale surface analysis and biofouling testing. Testing and characterization was performed, with somewhat mixed results. Surface characterization using NEXAFS and XPS suggested the presence of fluorine at the surface of multilayer coatings based on SBS-Br-F8H2, and biofouling assays showed some encouraging results—with lower settlement and growth of both barnacle larvae and *Ulva* spores and sporelings. Since quaternized polymers were used for many antibacterial applications it was also used for this project for biofouling applications. Although these polymers showed very good results for protein fouling resistance they did not show good results for biofouling tests with Ulva and Navicula.

Subsequently, SABCs based on perfluorinated alkyl and PEG groups attached to PS-*b*-PAA were synthesized. These materials show either hydrophobic or hydrophilic properties. Since PEG was used for many biofouling related applications to proteins it was selected as the hydrophilic component. Related work in our ONR project brought to our attention a commercially available amphiphilic surfactant, Zonyl® FSO-100 (registered trademark of E. I. du Pont de Nemours & Co., Inc.). This material consists of a hydrophilic polyethylene glycol (PEG) repeat group adjacent to a hydrophobic fluoroalkyl group. Block copolymers with ethoxylated fluoroalkyl side chains, prepared using Zonyl® FSO-100, have shown promise in resisting fouling by a wider ranger of marine organisms. This amphiphilic SABC was compared with the hydrophobic and hydrophilic diblock copolymers. The amphiphilic surface results in weak adhesion of both *Ulva* (which generally adheres strongly to hydrophilic surfaces) and also diatoms (which adhere strongly to hydrophobic surfaces, such as the commercially used PDMS surfaces, and also to copper based coatings).

It was later decided to use a soft triblock based SABC instead of the diblock copolymer to improve coating rebustness. These polymers showed really good results for all standard biofouling organisms including Ulva, Navicula and barnacles. These polymers covered the major part of this project. There were a series of materials synthesized from these polymers. These polymers included different functional side chains such as PEG, perfluoroalkyl groups, mixtures of PEG/perfluorinated segments, Brij, Pluronic and mixtures of hydrocarbon units with PEG attached to triblock copolymers. Many of these polymers showed excellent results against Ulva and Navicula. Especially the mixed amphiphilic polymers were of great interest because the ratio between hydrophilic/hydrophobic properties can be easily varied by synthetic methods. This is a great advantage over the commercially available amphiphilic chains such as Zonyl and Brij where we have no control over the hydrophilic/hydrophobic properties, and is the subject of scaleup and ongoing testing by NanoSurfaces, a startup company that has licensed this technology. All the synthesized SABCs have been summarized in figure 108.

All the materials produced have been characterized thoroughly for composition using techniques such as, NMR, IR and elemental analysis. The surface characterizations of these materials were performed using dynamic contact angle, XPS and NEXAFS. The surface properties of these materials showed good agreement with the observed

biofouling test results. All the surfaces showed rearrangement in water with the hydrophilic groups migrating to the surface over time. In general it was found that the amphiphilic and the "mixed" surfaces showed extremely good results for biofouling control (fouling release) as it appears that we can obtain desirable behaviors, that is, "the best of both worlds."

SABCs were applied to the surface using a simple spray coating technique and can certainly be applied to large surfaces in an industrial scale. Uniform surfaces were prepared by this method. The SABCs were spray coated on a soft SEBS layer. Initially G1652 was used as the base layer. Later another SEBS polymer, MD6945, was found to have the similar elastic modulus as that of PDMS and was used as the base layer. The biofouling release results showed that the softer base actually enhances the foul release properties of the surface. All the steps used in the preparation of multi layer coatings were repeated several times for reproducibility with different annealing conditions and solvents. Suitable surface preparation steps were identified with the sophisticated techniques such as, NEXAFS and XPS to make sure that the functional groups are on the surface.

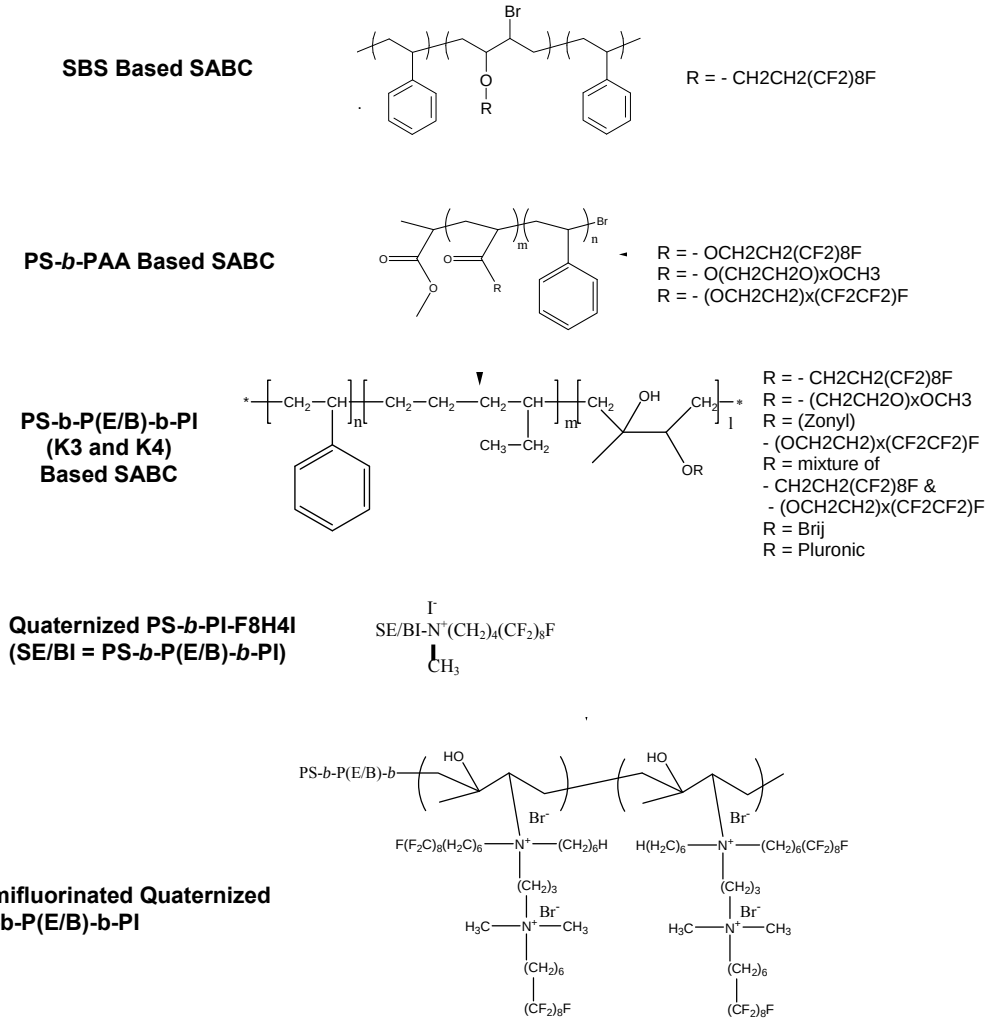

Figure 105. Summary of all the SABCs synthesized.

References:

1. Krishnan, S.; Weinman, C. J.; Ober, C. K. "Advances in polymers for anti-biofouling surfaces" *J. Mater. Chem.*, **2008**, 18, 3405—3413.

2. Magin1, C. M.; Cooper, S. P.; Brennan, A. B.; "Non-toxic antifouling strategies", *Materials Today*, 13, **2010**, 36-44.

3. Grozea, C. M.; Walker, G. C. "Approaches in designing non-toxic polymer surfaces to deter marine biofouling", *Soft Matter*, **2009**, 5, 4088–4100.

4. Townsin, R. L. "The ship hull fouling penalty", *Biofouling* **2003**, *19*, 9−15.

5. Yebra, D. M.; Kiil, S.; Johansen, K. D. "Antifouling technology—past, present and future steps towards efficient and environmentally friendly antifouling coatings" *Progress in Organic Coatings*, 50, **2004**, 75–104

6. Schiff, K.; Brown, J.; Diehl, D.; Greenstein, D. "Extent and magnitude of copper contamination in marinas of the San Diego region, California, USA" *Marine Pollution Bulletin*, 54, **2007**, 322–328.

7. Baier, R. E. "Influence of the initial surface condition of materials on bioadhesion" in *Proceedings of the Third International Congress on Marine Corrosion and Fouling*; Northwestern University Press: Evanston, Illinois, 1973; pp 633−639.

8. Baier, R. E. "Adhesion in the biological environment", *Biomater.,Med. Devices, Artif. Organs* **1984−85**, *12*, 133−159.

9. Hutter, J. L., Bechhoefer, J. "Calibration of Atomic-force Microscope Tips",*Rev. Sci. Instrum.* **1993**, *64*, 1868

10. Callow, M. E.; Callow, J. A.; Pickett-Heaps, J.; Wetherbee, R. "Primary adhesion of Enteromorpha (Chlorophyta, Ulvales) propagules: Quantitative settlement studies and video microscopy", *J. Phycol.* **1997**, *33*, 938−947.

11. Stanley, M. S.; Callow, M. E.; Callow, J. A. **"**Monoclonal antibodies to adhesive cell coat glycoproteins secreted by zoospores of the green alga *Enteromorpha*", *Planta*, **1999**, 210, 61−71.

12. Hoipkemeier-Wilson, L.; Schumacher, J. F.; Carman, M. L.; Gibson, A. L.; Feinberg, A. W.; Callow, M. E.; Finlay, J. A.; Callow, J. A.; Brennan, A. B. "Antifouling Potential of Lubricious, Micro-engineered, PDMS Elastomers against Zoospores of the Green Fouling Alga *Ulva (Enteromorpha)*", *Biofouling* **2004**, *20*, 53−63.

13. Chaudhury, M. K.; Finlay, J. A.; Chung, J. Y.; Callow, M. E.; Callow, J. A. "The Influence of Elastic Modulus and Thickness on the Release of the Soft-fouling Green

Alga *Ulva linza* (Syn. *Entermorpha linza*) from poly(dimethylsiloxane) PDMS Model Networks", *Biofouling*, **2005**, 21, 41-48.

Relevent Publications:

1. Lin, Q.; Krishnan, S.; Paik, M.; Busch, P.; Ober, C. K.; Hexemer, A.; Sohn, K. E.; Kramer, E. J.; Kowalke, G. L.; Wendt, D. E. **"Semifluorinated triblock copolymers as surface active components for multilayer marine antifouling coatings."** *Polymer Preprints*, **2005,** 46, 635-636.

2. Krishnan, Sitaraman; Ober, Christopher K.; Ayothi, Ramakrishnan; Lin, Qin; Paik, Marvin; Hexemer, Alexander; Kramer, Edward J.; Fischer, Daniel. "**Hydrophobic and hydrophilic fluoropolymers as non-adhesive interfaces in marine biofouling."** *Polymer Preprints*, **2005**, 46, 613-614.

3. Galli, G.; Martinelli, E.; Chiellini, E.; Ober, C. K.; Glisenti, A. **"Low Surface Energy Characteristics of Mesophase-Forming ABC and ACB Triblock Copolymers with Fluorinated B Blocks."** *Molecular Crystals and Liquid Crystals*, **2005**, 441, 211-226.

4. Krishnan, S.; Ayothi, R.; Hexemer, A.; Finlay, J. A.; Sohn, K. E.; Perry, R.; Ober, C. K.; Kramer, E. J.; Callow, M. E.; Callow, J. A.; Fischer, D. A. **"Anti-Biofouling Properties of Comblike Block Copolymers with Amphiphilic Side Chains."** *Langmuir* **2006**, 22, 5075-5086.

5. Krishnan, S.; Wang, N.; Ober, C. K.; Finlay, J. A.; Callow, M. E.; Callow, J. A.; Hexemer, A.; Sohn, K. E.; Kramer, E. J.; Fischer, D. A. **"Comparison of the Fouling Release Properties of Hydrophobic Fluorinated and Hydrophilic PEGylated Block Copolymer Surfaces: Attachment Strength of the Diatom *Navicula* and the Green Alga *Ulva*."** *Biomacromolecules* **2006**, *7*, 1449-1462.

6. C. J. Weinman, S. Krishnan, D. Park, M. Y. Paik, K. Wong, D. A. Fischer, D. A. Handlin, G. L. Kowalke, D. E. Wendt, K. E. Sohn, E. J. Kramer, C. K. Ober. "**Antifouling Block Copolymer Surfaces that Resist Settlement of Barnacle Larvae."** *PMSE Preprints,* **2007**, 96, 597-598.

7. S. Krishnan, J. A. Finlay, D. Park, C. J. Weinman, R. Dong, K. Wong, N. Asgill, M. E. Callow, J. A. Callow, D. L. Handlin, C. L. Willis, L. Brewer, D. E. Wendt, K. E. Sohn, E. J. Kramer, C. K. Ober. "**Ambiguous Polymeric Surfaces for Marine Antifouling Applications**." *PMSE Preprints*, **2008**, 98, 83-84.

8. S. Krishnan, C. J. Weinman, C. K. Ober. **"Advances in Polymers for Antibiofouling Surfaces."** *J. Mater. Chem.,* **2008**, 18, 3405 – 3413.

9. Weinman, C. J.; Finlay, J. A.; Park, D.; Paik, M. Y.; Krishnan, S.; Fletcher, B. R.; Callow, M. E.; Callow, J. A.; Handlin, D. L.; Willis, C. L., Fischer, D. A.; Sohn, K. E.; Kramer, E. J.; Ober, C. K. **"Antifouling ABC Triblock Copolymers with Grafted Functionality."** *PMSE Preprints*, **2008**, 98, 639-640.

10. Krishnan, S.; Weinman, C. J.; Ober, C. K. **"Advances in Polymers for Anti-Biofouling Surfaces."** *J. Mater. Chem.,* **2008**, 18, 3405-3413.

11. Weinman, C. J.; Finlay, J. A.; Park, D.; Paik, M. Y.; Krishnan, S.; Fletcher, B. R.; Callow, M. E.; Callow, J. A.; Handlin, D. L.; Willis, C. L., Fischer, D. A.; Sohn, K. E.; Kramer, E. J.; Ober, C. K. **"Antifouling ABC Triblock Copolymers with Grafted Functionality."** *PMSE Preprints*, **2008**, 98, 639-640.

12. Cho, Y. J.; Sundaram, H. S.; Gunari, N.; Weinman, C. J.; Paik, M. Y.; Dimitriou, M. D.; Finlay, J. A.; Callow, M. E.; Callow, J. A.; Walker, G. C.; Kramer, E. J.; Ober, C. K. **"Resistance of Triblock Copolymers with Grafted Amphiphilic Side Chains to Fouling by Protein and Algae"**, Polymer Preprints **2010**, 51, 386-387.

13. Sundaram, H. S.; Cho, Y. J.; Weinman, C. J.; Paik, M. Y.; Dimitriou, M. D.; Finlay, J. A.; Callow, M. E.; Callow, J. A.; Kramer, E. J.; Ober, C. K. **"Surface Active Zwitterionic Block Copolymer Synthesis for Antifouling Applications and Surface Characterization"** Polymer Preprints **2010**, 51, 384-385.

14. Sundaram, H. S.; Cho, Y. J.; Weinman, C. J.; Paik, M. Y.; Dimitriou, M. D.; Finlay, J. A.; Callow, M. E.; Callow, J. A.; Kramer, E. J.; Ober, C. K. "**Environmentally Friendly Non-ionic and Fluorine Free Surface Active Amphiphilic Block Copolymers for Fouling Release Applications",** *Polymeric Materials: Science & Engineering* **2010,** 103, 318-319.

15. Park, D.; Finlay, J. A.; Ward, R. J.; Weinman, C. J.; Krishnan, S.; Paik, M.; Sohn, K. E.; Callow, M. E.; Callow, J. A.; Handlin, D. L.; Willis, C. L.; Fischer, D. A.; Angert, E. R.; Kramer, E. J.; Ober, C. K. **"Antimicrobial behavior of semifluorinated-quaternized triblock copolymers against marine and airborne microorganisms."** *ACS Appl. Mater. Interfaces*, *ACS Appl. Mater. Interfaces*, **2010**, 2, 703–711.

16. Weinman, C. J.; Gunari, N.; Krishnan, S.; Dong, R.; Paik, M. Y.; Sohn, K. E.; Walker, G. C.; Kramer, E. J.; Fischer, D. A.; Ober, C. K. **"Protein adsorption resistance of anti-biofouling block copolymers containing amphiphilic side chains."** *Soft Matter*, **2010**, 6, 3237-3243.

17. Kristalyn, C. B. ; Lu, X.; Weinman, C. J.; Ober, C. K.; Kramer, E. J.; Chen, Z. **"Surface Structures of an Amphiphilic Tri-Block Copolymer in Air and in Water Probed Using Sum Frequency Generation Vibrational Spectroscopy"**, *Langmuir*, **2010**, 26, 11337–11343.

18. Krishnan, S.; Paik, M. Y.; Ober, C. K.; Martinelli, E.; Galli, G.; Sohn, K. E.; Kramer, E. J.; Fischer, D. A. "**NEXAFS Depth Profiling of Surface Segregation in Block Copolymer Thin Films"** *Macromolecules*, **2010**, 43, 4733–4743.